การสังเคราะห์อนุภาคคาร์บอนระดับนาโนเมตรที่มีสมบัติทางแม่เหล็กด้วยวิธีไพโรไลซิสของกลีเซอรอลและเฟอร์โรซีน เพื่อใช้กำจัดยาปฏิชีวนะ

นางสาวกรรัตน์ เกิดนาวี

วิทยานิพนธ์นี้เป็นส่วนหนึ่งของการศึกษาตามหลักสูตรปริญญาวิศวกรรมศาสตรดุษฎีบัณฑิต
สาขาวิชาวิศวกรรมเคมี ภาควิชาวิศวกรรมเคมี
คณะวิศวกรรมศาสตร์ จุฬาลงกรณ์มหาวิทยาลัย
ปีการศึกษา 2560

Synthesis of Magnetic Carbon Nanoparticles Using Pyrolysis of Glycerol and Ferrocene for Antibiotic Removal

Miss Konrat Kerdnawee

A Dissertation Submitted in Partial Fulfillment of the Requirements
for the Degree of Doctor of Engineering Program in Chemical Engineering
Department of Chemical Engineering
Faculty of Engineering
Chulalongkorn University
Academic Year 2017

Thesis Title	Synthesis of Magnetic Carbon Nanoparticles Using Pyrolysis of Glycerol and Ferrocene for Antibiotic Removal
By	Miss Konrat Kerdnawee
Field of Study	Chemical Engineering
Thesis Advisor	Associate Professor Tawatchai Charinpanitkul, D.Eng.
Thesis Co-Advisor	Professor Noriaki Sano, Ph.D.

Accepted by the Faculty of Engineering, Chulalongkorn University in Partial Fulfillment of the Requirements for the Doctoral Degree

.....Dean of the Faculty of Engineering

(Associate Professor Supot Teachavorasinskun, D.Eng.)

THESIS COMMITTEE

.....Chairman

(Professor Suttichai Assabumrungrat, Ph.D.)

.....Thesis Advisor

(Associate Professor Tawatchai Charinpanitkul, D.Eng.)

.....Thesis Co-Advisor

(Professor Noriaki Sano, Ph.D.)

.....Examiner

(Professor Pornpote Piumsomboon, Ph.D.)

.....Examiner

(Paravee Vas-Umnuay, Ph.D.)

.....External Examiner

(Weerawut Chaiwat, Ph.D.)

กรรัตน์ เกิดนาวี : การสังเคราะห์อนุภาคคาร์บอนระดับนาโนเมตรที่มีสมบัติทางแม่เหล็กด้วยวิธีไพโรไลซิสของกลีเซอรอลและเฟอร์โรซีน เพื่อใช้กำจัดยาปฏิชีวนะ (Synthesis of Magnetic Carbon Nanoparticles Using Pyrolysis of Glycerol and Ferrocene for Antibiotic Removal) อ.ที่ปรึกษาวิทยานิพนธ์หลัก: รศ. ดร. ธวัชชัย ชรินพาณิชกุล, อ.ที่ปรึกษาวิทยานิพนธ์ร่วม: ศ. ดร. โนริเอกิ ซะโน, หน้า.

การสังเคราะห์อนุภาคคาร์บอนระดับนาโนเมตรที่มีสมบัติทางแม่เหล็กสามารถสังเคราะห์ได้โดยวิธีการไพโรไลซิสระหว่างกลีเซอรอลและเฟอโรซีนที่ถูกป้อนแบบพ่นละอองภายใต้สภาวะเหนี่ยวนำด้วยแม่เหล็ก จากการทดลองเพื่อศึกษาผลกระทบอันเนื่องมาจากอุณหภูมิของการสังเคราะห์และสัดส่วนโดยน้ำหนักของกลีเซอรอลต่อเฟอโรซีนในการสังเคราะห์อนุภาคคาร์บอนระดับนาโนเมตรที่มีสมบัติทางแม่เหล็ก พบว่าที่อุณหภูมิการสังเคราะห์ 800 องศาเซลเซียส และ สัดส่วนโดยน้ำหนักของกลีเซอรอลต่อเฟอโรซีน 3 ต่อ 1 นั้นสามารถสังเคราะห์อนุภาคคาร์บอนระดับนาโนเมตรที่มีสมบัติทางแม่เหล็กโดยได้ร้อยละผลได้สูงที่สุดที่ 15.9 ซึ่งพบว่าการสังเคราะห์โดยมีการเหนี่ยวนำแม่เหล็กเป็นวิธีที่สามารถควบคุมการสังเคราะห์อนุภาคคาร์บอนระดับนาโนเมตรให้มีคุณภาพและร้อยละผลได้สูงขึ้น ออกซิเตตราไซคลีนถูกจัดให้เป็นสารปนเปื่อนทางสิ่งแวดล้อม เนื่องจากมีการนำมาใช้ในปริมาณมากและหลุดรอดออกมาจากกิจกรรมทางการเกษตรต่างๆ หลากหลายวิธีทางเลือกสำหรับการกำจัดยาปฏิชีวนะ ซึ่งวิธีการดูดซับและการย่อยสลายด้วยกระบวนการออกซิเดชั่นขั้นสูงด้วยการทำปฏิกิริยากับโอโซนเป็นวิธีที่เหมาะสมเนื่องจากเป็นวิธีที่ง่ายและมีประสิทธิภาพ ดังนั้นอนุภาคคาร์บอนระดับนาโนเมตรที่มีสมบัติทางแม่เหล็กที่สังเคราะห์ได้โดยวิธีการไพโรไลซิสระหว่างกลีเซอรอลและเฟอโรซีนที่ถูกป้อนแบบพ่นละอองจึงถูกนำมาใช้เป็นตัวดูดซับและตัวเร่งปฏิกิริยาสำหรับกำจัดออกซิเตตราไซคลีนจากน้ำเสียสังเคราะห์ ประสิทธิภาพการดูดซับด้วยอนุภาคคาร์บอนระดับนาโนเมตรที่มีสมบัติทางแม่เหล็กจะเพิ่มขึ้นเมื่ออยู่ในสภาวะพีเอชระหว่าง 3 ถึง 7 โดยสามารถอธิบายได้จากอิทธิพลการดูดซับด้วยแรงทางประจุไฟฟ้า การดูดซับออกซิเตตราไซคลีนด้วยอนุภาคคาร์บอนระดับนาโนเมตรที่มีสมบัติทางแม่เหล็กมีพฤติกรรมการดูดซับเป็นไปตามไอโซเทอมการดูดซับของแลงเมียร์ เมื่อผนวกอิทธิพลการดูดซับและการทำปฏิกิริยาด้วยโอโซนนั้นแสดงให้เห็นว่าอนุภาคคาร์บอนระดับนาโนเมตรที่สังเคราะห์ได้สามารถเพิ่มอัตราการกำจัดออกซิเตตราไซคลีนได้อย่างมีนัยสำคัญเมื่อเปรียบเทียบกับคาร์บอนแบล็ค, ผงกราไฟต์และการทำปฏิกิริยากับโอโซนเพียงอย่างเดียว นอกจากนี้อนุภาคคาร์บอนระดับนาโนเมตรที่มีสมบัติทางแม่เหล็กสามารถแยกออกจากน้ำเสียสังเคราะห์โดยใช้แท่งแม่เหล็กถาวร ท้ายที่สุดการนำอนุภาคคาร์บอนระดับนาโนเมตรที่มีสมบัติทางแม่เหล็กที่ถูกใช้แล้วนำกลับมาใช้ใหม่พบว่าสามารถนำกลับมาใช้ใหม่ได้อย่างมีประสิทธิภาพ

ภาควิชา	วิศวกรรมเคมี	ลายมือชื่อนิสิต	.....
สาขาวิชา	วิศวกรรมเคมี	ลายมือชื่อ อ.ที่ปรึกษาหลัก	.....
ปีการศึกษา	2560	ลายมือชื่อ อ.ที่ปรึกษาร่วม	.....

5571401521 : MAJOR CHEMICAL ENGINEERING
KEYWORDS: MAGNETIC CARBON NANOPARTICLE / GLYCEROL / FERROCENE / ANTIBIOTIC / OXY-TETRACYCLINE / ADSORPTION / OZONATION

KONRAT KERDNAWEE: Synthesis of Magnetic Carbon Nanoparticles Using Pyrolysis of Glycerol and Ferrocene for Antibiotic Removal. ADVISOR: ASSOC. PROF. TAWATCHAI CHARINPANITKUL, D.Eng., CO-ADVISOR: PROF. NORIAKI SANO, Ph.D., pp.

Synthesis of magnetic carbon nanoparticles (M-CNPs) via nebulizing co-pyrolysis of glycerol and ferrocene with magnetic induction was successfully conducted. Experimental investigation on influence of synthesizing temperature and ratio of glycerol to ferrocene suggested that at 800 °C of synthesizing temperature with an initial weight ratio of glycerol to ferrocene of 3:1, the highest M-CNP synthesizing yield of 15.9 % was achieved. With the presence of magnetic induction, controlled synthesis of M-CNPs could be anticipated as a promising method for producing M-CNPs with high quality and high yield. Oxy-tetracycline (OTC) has been recognized as environmental contamination due to its over-dosage and leakage from agricultural activities. Among various alternatives for removal antibiotic, adsorption and advance oxidation via ozonation are promising because of their simplicity and effectiveness. Therefore, M-CNPs synthesized by nebulizing pyrolysis of glycerol and ferrocene were employed as an adsorbent and catalyst for removal of OTC from simulated wastewater. Adsorption efficiency of synthesized M-CNPs could be promoted when pH was between 3 and 7. These results would be ascribed to the influence electrostatic adsorption. It was found that adsorption of OTC on the synthesized M-CNPs obeyed the Langmuir adsorption model. Synergetic effects of adsorption and ozonation revealed that synthesized M-CNPs could significantly enhance the removal rate of OTC when compared to those of carbon black, graphite powder and ozonation. Moreover, M-CNPs could be easily separated from simulated wastewater by permanent magnetic bar. Finally, regeneration of spent M-CNPs revealed that M-CNPs exhibited excellent reusability.

Department:	Chemical Engineering	Student's Signature	.....
Field of Study:	Chemical Engineering	Advisor's Signature	.....
Academic Year:	2017	Co-Advisor's Signature	.....

ACKNOWLEDGEMENTS

First and foremost, I would like to express my profound gratitude to my advisor, Associate Professor Dr. Tawatchai Charinpanitkul who has encouraged, advised useful guidance and always supported to me with his best wishes throughout my doctoral period. He also guides me about my daily life and my future plan. Furthermore, I also would like to express my sincere gratitude to my co-advisor, Professor Dr. Noriaki Sano who kindly supported and suggested me to do the experiment during my research in Kyoto university, Japan. I am also grateful to Professor Dr. suttichai Assabumrungrat, Professor Dr. Pornpote Piumsomboon, Dr. Paravee Vas-Umnuay and Dr. Weerawut Chaiwat for their useful comments and participation as the thesis committee. Furthermore, I would like to thank Ms. Pusanisa Patrachotesawate and all of my previous and present members of Center of Excellence in Particle Technology for their help, suggestion and warm collaborations. Most of all, I would like to express my greatest gratitude to my parent, Mr. Konrawut and Mrs. Rattana Kerdnawee, and my brother, Mr. Rattawoot Kednawee for their endless love and unconditionally support me since I was born.

CONTENTS

Page

Page

Page

Page

LIST OF TABLES

LIST OF FIGURES

Chapter I

Introduction

1.1 Motivation

Carbon nanoparticles (CNPs) have been recognized as a promising material which could be applied to many fields necessary for our daily life [1-3]. Among those CNPs, carbon nanotube (CNT) is a cylindrical nanostructure of carbon atoms with the diameter in a range of ten to hundred nanometers. It is recognized as a new type of carbon nanostructures found in 1991 by Iijima [2]. CNTs have attracted many researchers' interest due to their unique chemical, mechanical and electrical properties [4-6]. In general, CNTs can be classified into single-walled carbon nanotubes (SWCNTs) and multi-walled carbon nanotubes (MWCNTs) subject to the number of graphene layers constituting of their wall. Each type of CNT would exhibit advantages and drawbacks regarding to objectives of applications which be clearly identified [7].

There are many methods which have been applied for synthesis of CNPs, i.e. arc discharge, chemical vapor deposition and laser ablation [8]. Chemical vapor deposition is one of the most popular methods because of its scalability and applicability to use with various carbon sources [8]. With this method, raw material containing carbon atoms would be decomposed to vapor phase at a regulated temperature in prior to the self-assembly process of CNPs which would grow on the

surface of metal catalyst or some specific substrates [9, 10]. Pyrolysis is one of simple method which could be adapted for synthesizing magnetic carbon nanoparticles. Incorporation of metallocene with other carbon precursors could provide Fe-filled carbon nanoparticles which could exhibit magnetic property. In such simple method, many parameters, such as template, temperature, reaction time and pressure, have been regulated to control the formation process and structure of carbon nanoparticles [11-14]. However, based on a comprehensive literature survey, it is found that magnetic carbon nanoparticles under the influence of magnetic induction has been a few reports [15-17].

Glycerol is a major by-product of bio-diesel manufacturing process which has been of interest for renewable energy research worldwide. Meanwhile, the global supply of refined glycerol has been estimated to be higher than the global consumption [10]. As a result, oversupplied amount of glycerol derived from bio-diesel conversion has increased and leaded to its lower cost [18]. Therefore, it is of great importance for researching to find alternative means to utilize glycerol. So far, only few research works have been involved with direct utilization of glycerol as carbon source for synthesis of carbon nanoparticles [8-14, 19-29]. Therefore, this work seeks possibility to investigate alternative method for increasing value of glycerol as carbon source for carbon nanoparticle synthesis.

Among various applications, such as sensors, electronic devices, drug delivery and adsorbent, CNPs have been recognized as one of the most attractive candidates,

because of their highly porous and hollow structure, large specific surface area, light mass density and it should especially be noted that CNPs would be one of the most outstanding materials for the removal of various inorganic and organic pollutants [7, 30, 31]. Antibiotic is organic man-made compounds that have been developed for inhibiting the growth of unwanted microorganisms so that their application could be commonly found in a broad spectra of medical, industrial and agricultural fields [32, 33]. In aquaculture, an increase in antibiotic application leads to environmental problem because of its complex structure which could hardly be eliminated naturally. Therefore, it is necessary to develop an efficient technique to remove such antibiotic [32-38].

A wide range of chemical and physical methodologies for removal of organic compounds, which could pollute water resources, have been examined by taking adsorption,[39] liquid extraction, membrane separation [40], chemical oxidation [41-46] and biodegradation into account. As already mentioned above, M-CNPs are also recognized as a good alternative adsorbent to remove antibiotics [35-38]. In particular, when M-CNPs are used as an adsorbent for removing aqueous pollutants, it can be separated easily by using magnetic field. Meanwhile, magnetic separation technology has gradually attracted growing attention of many researchers as a rapid and effective technology for separating magnetic materials because of major advantages over other conventional separation techniques in terms of economy, high capacity, short operation time and no contamination. Meanwhile, ozone is a strong oxidant that is

widely used in wastewater treatment. Generally, the efficiency of ozone degradation for oxidizing pollutants largely depends on the oxidant concentrations (ozone and the OH radical produced during the decay of ozone) [19]. There are some previous works related to confirmation of utilizing metal-supported carbon materials to enhance oxidative degradation of organic compounds. It should be noted that M-CNPs (Fe-filled) could also enhance ozonation of organic compound pollutants because metal nanoparticles embedded in M-CNPs can promote oxidation by providing additional amount of OH radicals, which could also involve with oxidative degradation of organic pollutant [21, 47-49].

In this work, pyrolysis of glycerol with the presence of few ferrocene would be employed for synthesizing M-CNPs with magnetic field induction. In addition, an application of synthesized M-CNPs as adsorbent for adsorption and catalytic ozonation of antibiotic pollutant dispersed in water would also be experimentally examined.

1.2 Objective of the research

The objective of this research is to conduct experimental examinations on synthesis of M-CNPs using pyrolysis of glycerol and ferrocene with magnetic field induction. Utilizing as-synthesized and modified M-CNPs for removal of antibiotics from aqueous solution via catalytic ozonation in comparison with physical adsorption will also be experimentally investigated and discussed.

1.3 Scopes of the research

1.3.1 Synthesis of magnetic carbon nanoparticles using co-pyrolysis of glycerol and ferrocene.

1.3.1.1 Effect of magnetic field induction

1.3.1.2 Effect of synthesizing temperature

1.3.1.3 Effect of initial weight ratio of glycerol to ferrocene

All synthesized products were characterized by some necessary techniques as follows: morphology by scanning electron microscope SEM, and transmission electron microscope TEM, X-ray diffraction (XRD), specific surface area and pore structure by Brunauer-Emmett-Teller (BET), carbon atom arrangement by Raman spectroscopy.

1.3.2 Adsorption of antibiotics from aqueous solution by the synthesized Fe-filled MWCNTs.

1.3.2.1 Adsorption isotherm model related with behaviors of adsorptions. Therefore, adsorption isotherm of oxy-tetracycline on M-CNPs was investigated [35-38].

1.3.2.2 The adsorption efficiency of oxy-tetracycline depended on pKa and pH of solution. So, pH of solution was simulated condition which is acidic, neutral and alkaline.

All of these experiments will be conducted as batch adsorption experiment, which will be performed with UV-visible spectrophotometer (UV-Vis).

1.3.3 Degradation of antibiotics by the synthesized M-CNPs

The efficiency of ozone degradation for oxidizing pollutants largely depends on degradation conditions which are oxidant reagent (O_3, OH radical). metal nanoparticles can promote oxidation by increasing amount of OH radicals. M-CNPs could also involve with providing opportunities for reaction on their surface. The degradation of antibiotics was investigated by studying following effects [21, 46-49].

1.3.3.1 Effect of carbonaceous materials on OTC removal in catalytic ozonation

1.3.3.2 Influence concentration of ozone on OTC degradation

13.3.3 Influence of M-CNPs loading on OTC degradation

1.3.3.4 Influence initial concentration of oxy-tetracycline on OTC degradation

1.3.3.2 After the ozonation degradation of adsorbed oxy-tetracycline on M-CNPs, the M-CNPs s can be re-used. Therefore, the potential of recycling M-CNPs was investigated [49].

The resultant solutions from the degradation process was analyzed by a UV–Vis detector and a high-performance liquid chromatograph (HPLC).

1.4 Expected benefit

Expected benefits to be obtained from this research would be the knowledge in synthesis of M-CNPs by co-pyrolysis of glycerol and ferrocene in magnetic field.

Moreover, synthesized M-CNPs would be applied for treatment of water which is contaminated with antibiotics.

Chapter II
Fundamental knowledge

The fundamental knowledge related to glycerol, ferrocene, carbon nanotube, synthesis carbon nanotubes, antibiotic, removal of antibiotic, adsorption and ozonation were reviewed in this chapter.

2.1 Glycerol

Glycerol is the main component of triglycerides containing three hydrophilic hydroxyl groups, found in animal fat, vegetable oil, or crude oil. Glycerol is derived from biodiesel production [18,21]. Glycerol is an oily liquid which is viscous, odorless, colorless, and has a sweet taste [25,26]. Figure 2.1 shows the molecular structure of glycerol, made up of three hydroxyls. It is miscible in many substances such as acetone, ethyl acetate, dioxane and ethyl and partially insoluble in superior alcohol, fatty acids and hydrocarbonate such as hexane, benzene, and chloroform. Glycerol is very viscous at normal temperatures and It does not oxidize in the atmosphere in normal conditions, but can be easily oxidized by other oxidants. Properties of glycerol is shown in Table.2.1.

Glycerol solutions are exposed to heat and in contact with ferrous metal or copper since the salts contained in these materials can catalyze oxidation [31].

Glycerol has low volatility and low vapor pressure. Temperature changes have little effect on the vapor pressure of glycerol solutions.

Crude glycerol generated from biodiesel production and it is contaminated with impurities. It is a little economic value. Therefore, there have been many investigations into alternative uses of glycerol which are combustion, composting, animal-feeding, thermo-chemical conversions, and biological conversion methods for converting glycerol into valued-added products. Thermo-chemical method is an alternative for glycerol utilizing. It has been reported that glycerol can be thermochemically converted into other higher value products.

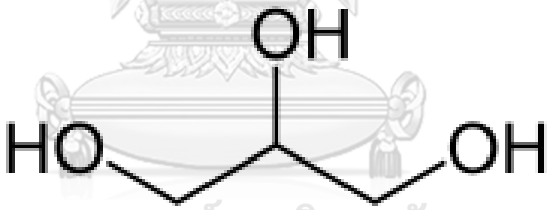

Figure 2.1 Chemical structure of glycerol

Table 2.1 Properties of glycerol (MSDS, ScienceLab.com)

Properties of glycerol	
Chemical formula	$C_3H_8O_3$
Molecular Weight	92.09 g·mol^{-1}
Appearance	colorless liquid
Odor	Mild
Density	1.26 g/cm^3
Melting point	19 °C
Boiling point	290 °C
Solubility in water	miscible
Vapor pressure	0 kPa (20°C)
Vapor density	3.17 (air=1)
Refractive index(n_D)	1.4746
Viscosity	1.412 Pa·s

2.2 Ferrocene

Ferrocene is a compound consisting of two cyclopentadienyl anions bound on opposite sides of a Fe center as shown in Figure 2.2. It is an organometallic

compound with the formula $Fe(C_5H_5)_2$. Their properties of ferrocene are shown in Table 2.2.

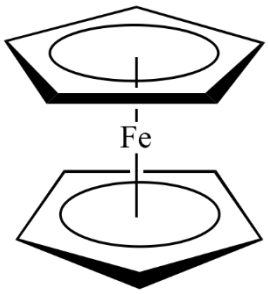

Figure 2.2 Chemical structure of ferrocene

Table 2.2 Properties of ferrocene (MSDS, ScienceLab.com)

Properties of ferrocene	
Chemical formula	$C_{10}H_{10}Fe$
Molar mass	186.04 g/mol
Appearance	light orange powder
Odor	camphor
Density	1.490 g/cm^3 (20 °C)
Melting point	173.5 °C
Boiling point	249 °C
Solubility in water	Insoluble in cold water, soluble in most organic solvents

2.3 Characteristics of carbon nanotubes (CNTs)

Carbon nanotube (CNT) is a one kind of carbon based materials which have been discovered by Ijima in 1991 [2]. They are allotropes of carbon with a cylindrical structure that are composed of sp^2 carbon bonding and consisted of honeycomb structure like a graphene sheet. Many researchers in science and engineering pay attention to CNTs because their unique properties (physical and chemical). The unique characteristics of CNT are the ultimate mechanical, superlative thermal and electronic properties. CNTs could be classified by number of wall-layer in single-wall, double-

walls or multi-walls. Single-walled nanotubes (SW-CNTs) are consisted of a single layer of graphene sheet rolled up for forming a cylindrical structure with a few nanometers of diameter while length up to micrometer. SW-CNTs have unique electronic and mechanical properties which could be applied in many fields, such as nanocomposite materials, field-emission materials and sensors. Therefore, SW-CNTs expected to play a important role in the next generation of utilized nano-electronic devises. Multi-walled carbon nanotubes (MW-CNTs) are consisted of multiple rolled layers of graphene sheet to form cylindrical structure with 0.3 nm of the distance between layers and 2-100 nm of diameters with up to millimeters lengths as shown in Figure 2.3 [32]. MW-CNTs are simpler to produce in large volume scale than SW-CNTs. However, the structure of MW-CNTs is complexity and variety. Both of SW-CNTs and MW-CNTs could be developed for highly specific applications and modification their mechanical and electrical properties.

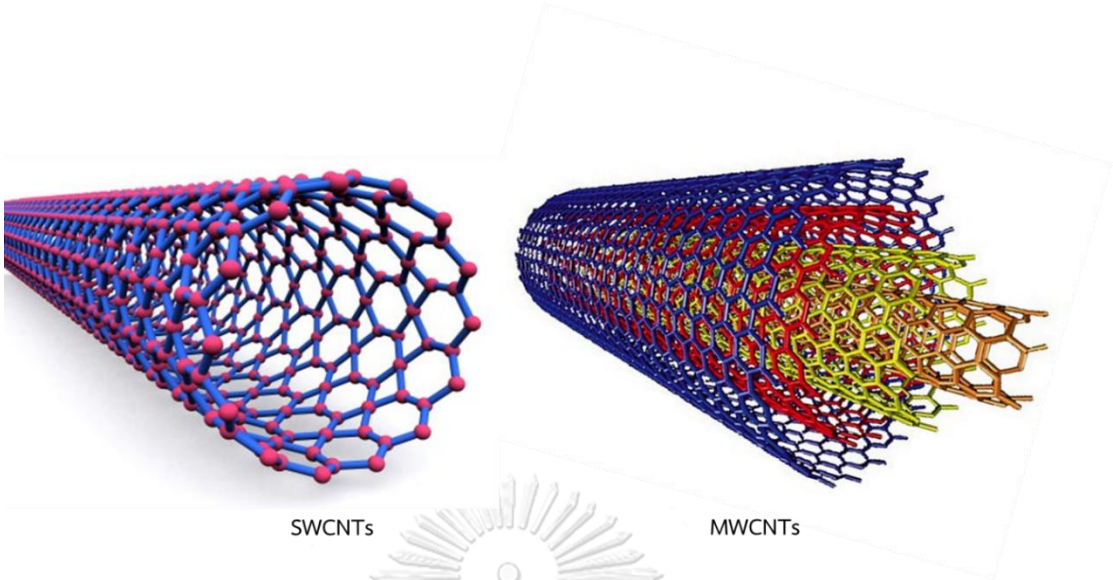

Figure 2.3 Configurations of carbon nanotubes which are single wall carbon nanotube and multiwall carbon nanotube

2.4 Synthesis of CNTs

There are several methods to produce CNTs such as chemical vapor deposition method of containing carbon molecules from carbon sources, including sublimation of graphite carbon by laser ablation and arc-discharge technique

Chemical vapor deposition is a thermal method by decomposition of carbon source in the gas phase at high temperature. It can be divided into several types by type of energy source such as plasma enhancement CVD from plasma source and thermal CVD from furnace or heating coil to supply energy. The supplied energy is used to decompose the molecule of precursors into a small radical or small hydrocarbon and then decompose to carbon atom. After that small molecule and carbon atom is decomposed into carbon cluster and diffuse and grow on catalyst

metal. CVD method could synthesize CNT in large scale and produce both SW-CNT and MW-CNT, depending on conditions of CNT-growth parameters such as synthesizing temperature, residence time, type of carbon sources and catalysts.

Laser ablation method is operated under laser source for synthesis CNTs with the high quality and purity of CNTs [8]. A graphite rod and metal catalyst mixture is ablated on their surface by laser at high temperature under inert atmosphere for generating vaporized carbon from a graphite rod. The vaporized carbon was condensed and formed CNT structure after cool down temperature. This method could have synthesized SW-CNTs with controllable size and high yield of synthesized CNTs.

Arc discharge method is conducted with high energy from electric current at high temperature. Anode and cathode electrodes which are made from graphite rods are placed in an inert gas, liquid nitrogen or water. An electric current transfer between anode and cathode electrodes. A graphite rod of anode was vaporized and forming a cluster of carbon after vaporized carbon was condensed. The synthesis of CNTs from arc discharge technique is simple step, but it requires high energy.

2.5 Antibiotic

Antibiotics are chemical compound which were derived from a microorganism such as bacteria, microbes or fungi via chemical method for pharmaceutical activity or synthesis drugs [32]. Antibiotic could destroy or kill for inhibiting the growth of

microorganism. However, some kind of antibiotic could accelerate growth rate of microorganism. In case of over usage of antibiotic, bacteria could be adapted themselves for acting as resistant of antibiotic. Antibiotics can be divided into several categories which are classify from chemical structure and action mechanism of antibiotic to target bacteria. Penicillins, monobactams group and cephalosporins are antibiotics with targets on bacterial on cell wall. Daptomycin, gramicidins, and polymixins group are antibiotics with targets on bacterial on cell membrane. Tetracyclines, macrolides and aminoglycosides group are essential group for attacking protein.These antibiotics are used for different applications and different target such as Tetracycline group were used in agriculture (aquaculture). Almost of antibiotics could not be digested and adsorbed well, it is generally released to the environment, leading to contaminate in water and soil which could affect on increasing of the resistance of adaptive microorganism and contaminate in environment [33].

Tetracyclines are a group of broad-spectrum antibiotics which perform in the ribosomal level for interrupting the process of protein synthesis of microorganisms. Tetracyclines group were discovered in 1948 by naturally fermentation products of a soil bacterium. The first type of tetracycline is chlortetracycline [50]. At present, tetracycline could be classified into three groups which are tetracycline natural products, tetracycline semi-synthetic compound and chemical modified tetracycline [51]. Chemical structures of tetracycline consisted of a tetracyclic naphtacene carboxamide ring structure with surrounding lower and upper peripheral zones.[51, 52]. Chemical

structures and pKa information of oxy-tetracyclines are showed in Figure 2.4 **[53]**.

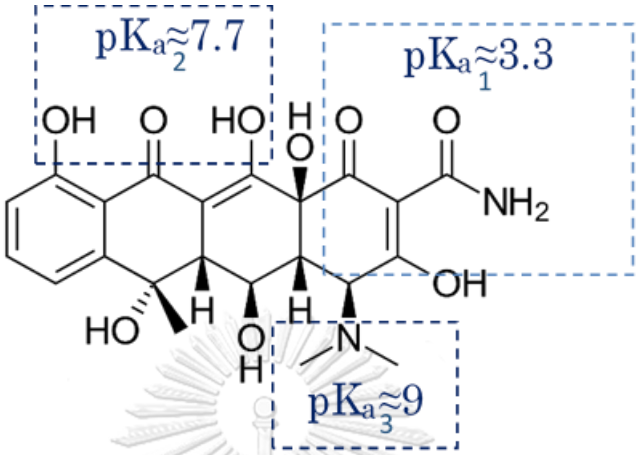

Figure 2.4 Structure of oxy-tetracyclines (OTC) and their pK_a

2.6 Methods of antibiotic Removal

A many of physical and chemical methodologies for organic compounds removal were investigated by many researchers. The methodologies could be classified into two types which are nondestructive and destructive processes. Adsorption, membrane techniques and liquid extraction are nondestructive processes. While biodegradation and chemical oxidation which are photolysis, electrochemical processes, chlorination, Fenton and photo-Fenton, semiconductor photocatalysis and ozonation are destructive methods. The different methods can be applied in suitable process, depending on the kind of pollutants and the operated cost of the process.

2.7 Adsorption processes

Adsorption process is a separation process on surface phenomenon. Commonly, adsorption is described in term of the molecules in fluid phase have to adsorb on solid surface. This process of adsorbate on the surface of adsorbent is called adsorption process. In term of high quality of absorption efficiency, the type of adsorbent should be having high specific surface area. Based on surface chemistry and forces involved in adsorption, there are three interfaces adsorption steps which are First, external diffusion step which is the molecules of the adsorbate in fluid moves to the outer surface of the adsorbent. Second, pore diffusion step which are the molecules of the adsorbate will diffuse into the pore of adsorbent. Finally, adsorption step that is the adhesion on porous surfaces between adsorbate and the surface of adsorbent. Type of adsorption depended on force involved and surface chemistry in each adsorption process which was can be divided into two types are physical adsorption or Phys sorption and chemical adsorption or chemisorption.

2.7.1 Physical adsorption

Physical adsorption occurs quickly with almost of monolayer adsorption. Physical adsorption is preserved by individuality of each of adsorbate and adsorbent. As physical adsorption takes place, First, it starts at a monolayer and then It could become to multi-layer until the pores are full filled with adsorbate. Therefore, the

maximum capacity of a adsorbent material could be more related to the pore volume [54].

2.7.2 Chemical adsorption

Chemical adsorption is the formation of chemical bonding between adsorbate and adsorbent. It is a reaction of transferring and sharing of electron including breakage of the adsorbate molecules into small molecules, atoms or some radicals that are bound separately. In naturally, chemical adsorption is limited to less than monolayer coverage on the surface of adsorbent [54].

Table 2.3 The kind of Interaction forces involved in adsorption process with three types of interfaces [17]

Interaction force	Approximate Energy of Interaction (kJ/mol)	Interface		
		Adsorbate/ Adsorbent	Adsorbates/ Water	Water/ Adsorbent
Electrostatic attraction	> 42	/	x	x
Electrostatic repulsion	> 42	/	x	x
Ionic species-neutral species attraction		/	x	x
Covalent bonding	> 42	/	x	x
Ionic species-dipole Attraction	< 8	/	/	/
Dipole-dipole attraction	< 8	/	/	/
Dipole-induced dipole Attraction	< 8	/	/	/
Hydrogen bonding	8 – 42	/	/	/
van der Waals attraction	8 – 42	/	/	/

2.7.3 Surface chemistry and forces involved in adsorption

Surface chemistry and forces involved in adsorption were investigated which there are three interfaces of interaction involved in adsorption including adsorbate-adsorbent, adsorbate-water and water-adsorbent. The interaction forces at different of interfaces were shown in Table 2.3. The forces of between adsorbent surface and adsorbates are shown in Figure 2.5 [17].

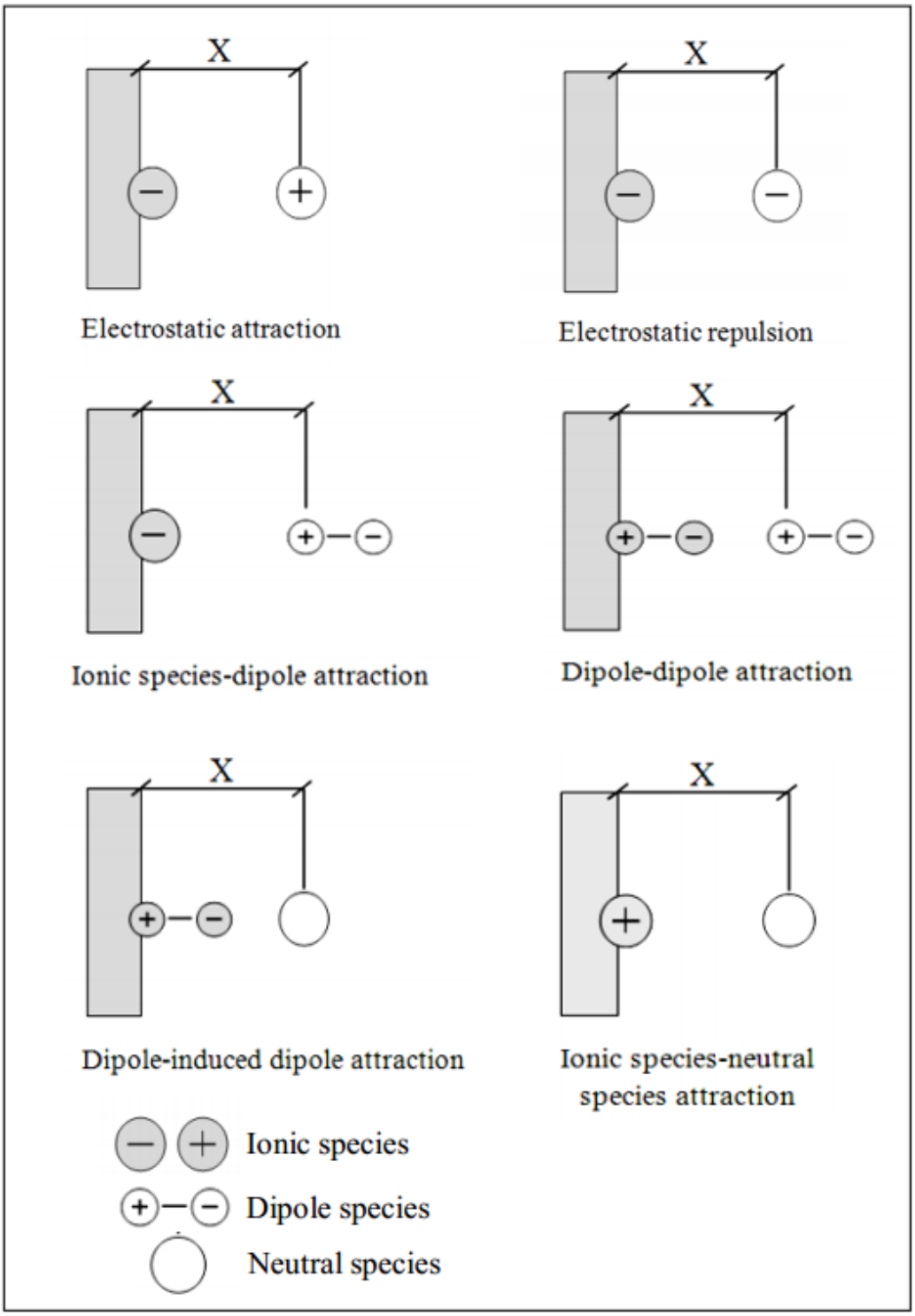

Figure 2.5 Attraction forces of functional groups on surface [17]

2.7.4 Adsorption isotherm

Adsorption isotherm is the relation of the amount of adsorbate absorbed on adsorbent at constant temperature at equilibrium condition [54]. Adsorption isotherm can be calculated by the ratio of the amount of adsorbate in term of concentration to the concentration of the solution at the equilibrium at any constant temperatures as equation 2.1. Adsorption isotherm could be classified into several types. The famous adsorption isotherms are the Langmuir and Freundlich isotherm.

$$Q_e = (\frac{C_o - C_e}{M}) \times V \quad (2.1)$$

Where Q_e is the amount of adsorbate adsorbed on adsorbent at equilibrium [mg/g]

C_0 is the concentration of adsorbate at initial [mg/L]

C_e is the concentration of adsorbate at equilibrium [mg/L]

V is the volume of solution [L]

M is the mass of the adsorbent [g]

Langmuir isotherm model is the most widely usage of the monolayer adsorption [54]. The important assumptions of Langmuir isotherm consisted of tree assumptions. First, the adsorbate in the solution contacted with strong attraction on the surface of the adsorbent. Second, the adsorbent has the specific surface for each specific molecules of adsorbent. Last, the adsorption is mono layer of adsorbate on the surface of adsorbent [39, 40]. A plot of ratio of the concentration of adsorbate at equilibrium (C_e) to the amount of adsorbate adsorbed at equilibrium (Q_e) against the concentration of adsorbate at equilibrium (C_e). A straight line with slope and intercept of the plot can be determined Q_m and K_L, respectively as shown in equation (2.2)

$$\frac{C_e}{Q_e} = \frac{C_e}{Q_m} + \frac{1}{K_L Q_m} \tag{2.2}$$

Where Ce is the concentration of adsorbate at equilibrium (mg/L),

Q_e is the amount of adsorbate adsorbed at equilibrium (mg/g),

Q_m is the maximum adsorption capacity (mg/g)

K_L is the Langmuir adsorption equilibrium constant (L/mg).

The essential feature of the Langmuir isotherm could be indicated by Langmuir adsorption equilibrium constant (R_L) parameter. R_L is a dimensionless constant related

to separation factor and equilibrium parameter. It can be indicated to predict favorable or unfavorable of adsorption. R_L can be calculated by using Eq. (2.3) [19].

$$R_L = \frac{1}{1+K_L C_0} \tag{2.3}$$

Where C_0 is the initial concentration of adsorbate (mg/L)

K_L is the Langmuir adsorption equilibrium constant (L/mg).

The meanings of RL are as follow:

$R_L = 0$ is irreversible adsorption process.

$R_L = 1$ is linear adsorption.

$R_L > 1$ is unfavorable adsorption.

$0 < R_L < 1$ is favorable adsorption.

Freundlich isotherm model could be described to the multi-layer of adsorption. This model related to the reversible process and non-ideal of adsorption [54]. Freundlich isotherm is wildly used in heterogeneous system with the organic compounds. The slope of Freundlich isotherm plotting can describes adsorption behavior if slop becomes close to 1, It was indicated that it is heterogeneous. K_F is an indicator of adsorption capacity. When, K_F is higher means that higher maximum capacity. The Freundlich equation is shown by equation. (2.4) and (2.5).

$$Q_e = K_F C_e{}^{1/n} \quad (2.4)$$

$$logQ_e = logK_F + \frac{1}{n} logC_e \quad (2.5)$$

Where C_e is the concentration of adsorbate at equilibrium (mg/L)

Q_e is the amount of adsorbate adsorbed at equilibrium (mg/g)

K_F is the Freundlich adsorption capacity parameter (mg/g (mg/L) 1/n)

n is the Freundlich adsorption intensity parameter

For the magnitude of n indicating the favorability of adsorption and the degree of heterogeneous of surface of adsorbate.

Where n=1 is the constant of adsorption

n<1 is the adsorption capability can be decreased by the concentration of solution is increased

2.8 Ozonation

Ozone is a strong oxidant agent to react both direct and indirect reaction. Direct ozonation is ozone molecule oxidized other compounds directly. Indirect ozone is disintegration of ozone in water and converted to OH radicals. OH radicals are very short time for living compounds but they have a stronger oxidation process than that of ozone. This is because the radicals have a high oxidation potential than ozone [46]. Redox potential of oxidizing agents was shown in Table 2.4 [19]. The process of

oxidation when the number of OH-radicals in a solution rises, It is called advanced oxidation process or AOP.

Table 2.4 Redox potential of oxidizing agents [19]

oxidizing agents	redox potential of oxidizing agents(V)
Fluorine (F)	2.87
Hydroxyl radical (OH)	2.86
Oxygen atom (O)	2.42
Ozone molecule (O_3)	2.07
Hydrogen peroxide (H_2O_2)	1.78
Chlorine (Cl)	1.36
Chlorine dioxide (ClO_2)	1.27
Oxygen molecule (O_2)	1.23

Therefore, ozonation process can be produced by both ozone (direct) and OH-radicals (indirect). The ozone oxidation process is represented schematically in Figure 2.6. This Figure shows that ozone oxidation consists of direct reactions and indirect reactions [19].

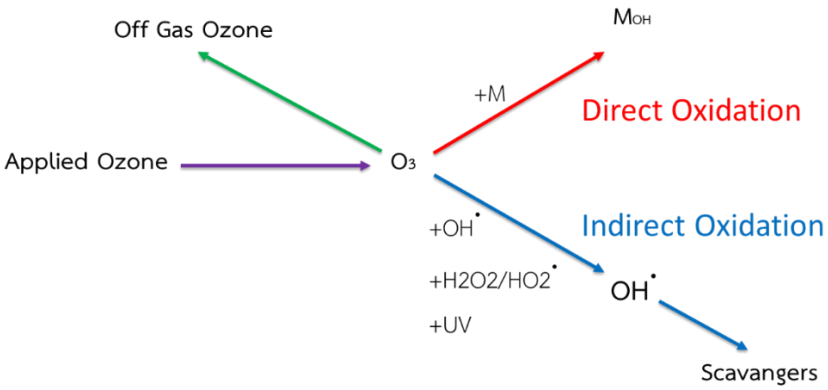

Figure 2.6 Reactions of ozone [19]

Chapter III
Literature reviews

The literature reviews are separated in 4 parts; I. utilization of glycerol II. utilization of industrial waste for carbon nanoparticles production III. synthesis of magnetic carbon nanotube IV. carbon nanoparticle applications.

3.1 Utilization of glycerol

Glycerol or glycerin is a major byproduct of biodiesel manufacturing process with approximately 10% of biodiesel produced is crude glycerol as by product. Nowadays biodiesel process is wildly expanding in term of alternative fuel. Crude glycerol is being produced. However, glycerol is high operating cost of purification for using in pharmaceutical, cosmetics and food industry. Therefore, many researchers try to find alternative methods to use this disposal. Many methods to apply for using crude glycerol have been investigated such as thermochemical/biological conversions, combustion and composting to produce other value-added products. Thermo-chemical methods is one of the popular alternative methods for increasing it's value-added of crude glycerol. It has been reported that glycerol could be converted to high value added such as propylene glycol, acetal, or variety of other products by thermochemically [14, 55-57].

3.2 Utilization of industrial waste for carbon nanoparticles production

High purity carbon sources with purity which are hydrocarbon group (methane, ethylene, acetylene, butane, hexane, benzene, toluene, etc.) and other carbon sources such as carbon dioxide and carbon monoxide were used for CNTs synthesis. The optimum conditions of synthesizing CNTs depended on synthesizing temperature, reaction time, pressure of system, type and ratio of carbon source and catalyst. However, High purity carbon sources from hydrocarbon are limited to supply and high cost, so It is interesting to study for using alternative carbon sources from industrial wastes, municipal wastes or plastics wastes, and by product from industrial such as red oil, glycerol or slop oil). Therefore, wastes and by-product from industry have been considered as one of good alternatives carbon source for synthesis carbonaceous nanomaterials as summarized in Table 3.1 [56]. Kerdnawee et.al (2017) summarized previous works related with using waste and by product from industry as carbon source for synthesizing CNTs [19, 23, 24, 26, 29, 56, 58-64] . It was also clearly observed that type of feed and catalysts, synthesizing temperature, type and flow rate of carrier gas are importance parameter for synthesizing CNT with different morphology, size and length. Moreover, synthesizing temperature are a importance parameter for converting all precursors into small clusters to form CNTs structure by self-assembly process [65]. Carbon black or amorphous carbon could be formed by synthesis without catalysts instead of forming of CNTs [19, 26, 29]. In addition, the compositions of carbon precursors are different in term of type, properties or impurities affected to generate

poisoning and corrosion in the synthesis system. The essential synthesizing parameters, such as ratio of carbon source to catalyst, types of catalysts and carbon sources, reaction temperature, were examined for improving the synthesis of CNTs. The various kinds of carbon source from gas, liquid or solid with various types of catalysts can be used as source of carbon for forming CNT [14, 19, 21, 25, 26, 29, 66]. As mentioned information would be implied that utilizing catalytic pyrolysis or chemical vapor deposition with catalyst is a promising method for synthesis CNTs because of its practical on handling and scalability [20].

Table 3.1 Summarized previous works involving with synthesis of carbon nanotube using wastes from industrial [56]

	Synthesizing parameters							Characteristics	
	Source	Feed	Catalyst	Reactor Type	Temperature (°C)	Carrier Gas	Reaction Time	Length	Diameter
Afre et al., 2006	Chemical process waste	Turpentine Oil	Co and Fe	Quartz Tube	500–900	N_2		NR	2.5 nm
Liu et al., 2006	Petroleum refining process waste	Deoiled Asphalt	Ferrocene	Quartz Tube	700–1200	Ar	20–50 min	NR	180 nm
Bajad et al., 2015	Plastic waste	Polypropylene	Ni/Mo/MgO	Muffle Furnace	700–900		10 min	NR	2–25 nm
Charinpanitkul et al., 2009	Chemical process waste	Naphthalene	Ferrocene	Quartz Tube	600–1000	N_2	15 min	Several Microns	> 100 nm
Zhuo et al., 2010	Plastic waste	HDPE	304 Stainless steel with Co, Ni or No	Quartz Tube	800		1 min	1–5 µm	15–84 nm
Sano et al., 2012	Petroleum refining process waste	Ethylene	316 Stainless Steel	Quartz Tube	700	H_2	30 min	5–80 µm	3–10 nm
Li et al., 2012	Petroleum refining process waste	Heavy Oil Residue	Fe, Co, Ni, Au and Pt	Quartz Tube	900	H_2	20 min	NR	0.89–1.19 nm
Yang et al., 2012	Automobile waste	Scrap Tyre Rubber	Co, Mg, Mn, Al	Quartz Tube	650	H_2	60 min	NR	30–50 nm
Morales et al., 2013	Petroleum refining process waste	Acetylene	$FeAl_2O_4$	Quartz Tube	730	H_2/N_2	60 min	NR	2–45 nm

Note: NR represents "not reported"

3.3 Synthesis of magnetic carbon nanotube

Since Kroto discovered fullerene structure (C60) in 1985 [1] and carbon nanotubes (CNTs) structure was reported by Ijima (1991) [2], considerable research and development have been developed for synthesis and applications of carbonaceous nanomaterials. After that, carbon nanohorns, carbon nanocapsules, carbon nanoonions, carbon nanofibers and so on were discovered [1, 2, 7, 67, 68]. Such carbonaceous nanomaterial has become of interest for many researchers because of its unique and outstanding properties. Some of previous works of synthesis of carbon nanoparticle was reviewed and summarized by Kerdnawee, et.al. (2017) as shown in Table 3.*2* [56]. Table 3.*2* show an overall of methods for CNTs synthesis which provided difference carbonaceous structure [20, 56, 69].

Table 3.2 Comparison of synthesis techniques for synthesis single wall and multiwalled carbon nanotube, fullerene, carbon nanohorn and graphene [56]

Structure / Technique	SWCNT	MWCNT	Fullerene	CNH	Graphene
Arc discharge	x	/	/	/	x
Arc discharge with catalyst	/	/	/	x	x
Laser deposition	x	x	/	/	x
Laser deposition with catalyst	/	/	/	x	x
CVD (Pyrolysis)	/	/	x	x	x
CVD with catalyst	/	/	x	x	/
CVD (Plasma with catalyst)	/	/	/	x	/

Each synthesizing technique would provide varied carbonaceous nanomaterials with different in term of purity, production yield and handling. For example, arc discharge method would be appropriate for production of SW-CNTs, MW-CNTs and fullerenes but difficult for scale-up. While, chemical vapor deposition is a flexible technique to produce various kind of carbonaceous nanomaterials. In term of synthesized products, besides SW-CNTs and MW-CNTs, graphene and carbon nanohorns have been interacted

attention from researchers. While the details of growth mechanism has not been fully understood so research and development of formation mechanism have been interested [7, 55, 57, 63, 70-74]. Therefore, development of synthesis carbonaceous nanomaterial from cheaper and stable raw materials have been interested. A remarkable amount of research goals have been comprised in term of purity, yield of product, cost, and scalability [4, 14, 60, 67-69, 75, 76]. Normally, all of synthesis methods of CNT would require similar conditions, such as optimum temperature for preparing all of precursors from decomposition of carbon sources via the self-assembly processes. While different controlling conditions, different types of CNTs such as SW-CNTs and MW-CNTs, could be synthesized [62, 77, 78].

3.3.1 Chemical vapor deposition (CVD)

Among various synthesizing methodologies, as compared in Table 3.*2*, chemical vapor deposition (CVD) or thermal pyrolysis is recognized as an efficient method because of its advantages in low operating costs in large-scale production with excellent controllability in growth steps such as purity, length, alignment, orientation, diameter and yield of CNTs. Many research have indicated that the pyrolysis of organometallic compounds, such as ferrocene, nickel phthalocyanine, and iron phthalocyanine could be employed as reactants and catalysts for synthesis of carbon nanostructures [19, 21, 23-26, 29, 79]. In case of thermal pyrolysis, some metal cluster, such as Fe, Co or Ni, are play an important role in term of catalyst for M-CNPs growth

[66, 80]. Meanwhile, many methods with catalysts and various carbon sources are also the on-going work which have been reported by many researchers around the world. One of the most concentrating topics for research for tuning of synthesizing parameters to optimize productions of carbonaceous nanomaterials has been investigated in many countries. Nowadays, it has been accepted that utilization of alternative carbon sources by using catalytic would possibly increase in production yield and also improve quality of CNT, including minimize the amount of expensive catalyst usage by supplying low cost of carbon sources [24, 26, 64, 81-83].

Sano et al. (2006) proposed to separate Fe-included carbon nanocapsules (CNCs) and multi-wall nanotubes (MWCNTs) using a "fall-to-stop-reactor". The temperature was controlled in the range of 600-1000 °C and the flow rate of H_2 was 100 cm^3/min. The solid products would deposit consisting of Fe included CNTs and CNCs. The products were obtained from different zone of the reactor that divided into five zones containing 500-600°C, 600-700 °C, 700-800 °C, 800-900 °C and 900-1000 °C. It was found that at temperature higher than 900 °C, the high yield of Fe-included CNTs and CNCs was obtained and at 1000 °C. It was the optimized temperature to achieve the separated synthesis of CNTs and CNCs [13].

Charinpanitkul et al. (2009) proposed that carbon nanoparticles can be synthesized by co-pyrolysis of naphthalene and ferrocene with 1:1 of weight ratio. Various kinds of structure were founded which are carbon nanotubes (CNTs) and carbon nanocapsules

(CNCs). The effect of synthesizing temperatures was investigated in the range of 800 – 1050 °C. It was found that morphology, size of CNT and total yield of products depend on the increased synthesizing temperature. When increasing synthesizing temperature, formation of CNCs with some CNTs was synthesized. [14].

3.3.2 Synthesis of nanomaterials under magnetic fields

Hybridized carbon and magnetic materials can be controlled by induction of magnetic field. Base on literature reviews, magnetic force could control the growth direction of carbonaceous nanomaterial, metal nanoparticles and carbonaceous nanomaterial with embedded metal [84, 85].

3.4 Carbon nanoparticle applications

Applications of carbon nanoparticles has been interesting due to their unique properties which are mechanical, electrical, thermal and optical [7, 86] and some previous works were reviewed and reported by Kerdnawee, et.al (2017) [56]. Owing to those advantages, CNTs is great promise as material for nanoelectronics, energy storage devices, drug delivery, sensors system and emitters. Broad of promising applications of carbon nanoparticles have been interested by many researchers around the world. Therefore, a lot of works done for studying what is the important characteristics of carbon nanomaterials for each specific requirement applications. Using a data base

information of literatures, founded that their applications such as antibiotic removal, pollutant gas detection and handling of spilled oil were studied by many researchers.

3.4.1 Adsorption of antibiotic

Leakage of some chemicals or pollutants were employed from dairy life activities including agricultures and industries have been recognized as one of importance issue. Among those chemical and pollutants, it was founded that antibiotics is a large serious affects to environment [87]. Normally, commercial conventional adsorbents (zeolite or activated carbon) are available but there is some weak point about handling of adsorbent after adsorption so It interacted the attention of researcher to seek other alternative adsorbent for removal pollutant. Therefore, some special properties of carbonaceous nanomaterials have been developed to solve their weak point.

From a viewpoint of adsorption process, CNTs with mesoporous structure leading to diffusion of small pollutants to adsorbent sites was easier when compared to zeolite or activated carbon which have randomly pore structure with micropore. It should be implied that carbonaceous nanomaterials are available for the access of small molecule of pollutant but zeolite and activated carbons normally contain some micropores, which are available for the access of large molecule of pollutant.

Lu et al. (2005) studied the adsorption of trihalomethanes on CNTs and powdered activated carbon. They reported that adsorption of trihalomethanes with CNTs reached adsorption equilibrium faster than powdered activated carbons, which would be

described by the different porous structures of CNTs and powdered activated carbons. The uniform pore of CNTs were useful for the diffusion of pollutants into the pores of carbon material.

Ji et. al. (2009) studied on investigation of adsorption of tetracycline on CNTs, graphite and activated carbon. The adsorption efficiency of tetracycline based on adsorbent surface area in the order of graphene and single wall CNTs > multiwalled CNTs >> activated carbon. It was found that adsorption of tetracycline to graphite and single wall CNTs and graphene was better when compared to other carbon adsorbents because of the available adsorption sites. The interaction between molecule of tetracycline and surface of adsorbent interacted with van der Waals forces, **π**-**π** EDA interactions and cation-**π** bonding [87].

Ehsan et al. (2013) studied on adsorption and desorption process of tetracycline on surface of graphene oxide. It was investigated by studying effect of pH of solution, adsorption equilibrium time and adsorption temperature. They found that tetracycline strongly adsorbs on the surface of graphene oxide surface with **π**-**π** interaction and cation–**π** bonding. About kinetic of adsorption, It was found that adsorption of tetracycline on graphene oxide reached adsorption equilibrium within 15 min with the pseudo second order model with rate constants in the range of 0.2742–0.5362 g/mg min [38].

Jafari et al. (2011) studied by using multiwall carbon nanotubes as adsorbent for adsorption of two cephalosporins antibiotics which are cephalexin and cefixime. They studied the influence of pH, sample volume, adsorbate and adsorbent concentration and temperature. The isotherm models were fitted with Langmuir isotherm for cephalexin and Freundlich model for cefixime. The kinetics model was well fitted of pseudo-first order that showed higher statistic value (R^2). The maximum adsorption capacity of MW-CNTs for adsorption of cephalexin and cefixime was 1,100 and 820 mg/g, respectively. The adsorption temperature did not have any effect on adsorption in this study [36].

3.4.2 Degradation of antibiotic (Oxy-tetracycline)

Generally chemical reaction for degrading pollutant with advance oxidation process requires specific catalysts which was contained some metal or embedded metal on the support materials. Among various supporting materials, carbon is one of excellent candidate due to its large specific surface area and stability. Therefore, the supporting catalysts would interact the researcher attended to seek other new candidates with specific for each reactions [20, 80].

Sano et al. (2012) synthesized aligned multi-walled carbon nanotubes directly on a stainless-steel surface. It was found that when control oxidation steps the length of MW-CNT can reach 80 μm. It was implied that synthesized MW-CNTs on stainless steel

meshes can be applied as a catalyst support for using in reaction of ozonation to enhance removal efficiency of phenol in water [21].

Sano et al. (2009) prepared porous carbon-gel for catalyst supporting of cobalt or nickel for enhancing decomposition of phenol by using ozonation. Results revealed that decomposing of phenol with carbon-gels supporting cobalt or nickel were better than that with only pristine carbon-gel and without carbon-gel supporting. In term of comparison between cobalt and nickel, cobalt exerted better catalyst for enhancing ozonation of phenol than nickel catalyst. [47].

Zhang et al. (2013) developed composite heterogeneous catalyst by combining of CNTs and zero valent iron (Fe^0) for using in ozonation. This hybrid material was synthesized by electrophoresis deposition of oxidized MW-CNTs on the surface of Fe^0 substrate after that it was calcined at high temperature. The hybrid Fe^0-CNTs could be used as catalyst for catalytic in oxidation with ozone for removal methylene blue. Moreover, effect of pH of the solution of methylene blue on catalytic ozonation efficiency was studied as a function of pH [48].

Chapter IV
Synthesis of M-CNPs

Controlled synthesis of magnetic carbon nanoparticles (M-CNPs) via co-pyrolysis of glycerol and ferrocene with magnetic induction was successfully conducted. In comparison to synthesizing condition without of magnetic induction, synthesis of M-CNPs with magnetic induction could be controlled as a promising method for synthesizing M-CNPs with high quality and high yield. Optimum conditions for synthesizing M-CNTs were investigated on influence of synthesizing temperature in a range of 700 to 1000 °C and influence of weigh ratio of glycerol to ferrocene suggested that optimum condition for M-CNPs synthesis was conducted with weight ratio of glycerol to ferrocene of 3:1, the highest yield of M-CNPs was achieved at 800 °C. Characteristics of M-CNPs were conducted, morphology of the synthesized M-CNPs was confirmed by transmission electron microscopy (TEM) while thermogravimetric analysis (TGA) was investigated for analyzing carbon and Fe contents. The M-CNPs could respond to magnetic force due to embedded Fe content were also analyzed by AC-magnetic susceptibility analyzer.

4.1 Research background

As mentioned in chapter of introduction, carbon nanoparticles or CNPs have been recognized as a promising material which could be applied to many fields necessary for our daily life [1-3]. Among those CNPs, carbon nanotubes (CNTs) have

been recognized as a new type of carbon nanostructures which are a cylindrical nanostructure of carbon atoms with the diameter in a range of ten to hundred nanometers and it was reported in 1991 by Iijima [2]. CNTs have attracted many researchers' interest due to their unique chemical, mechanical and electrical properties [4, 5, 88]. In general, CNTs can be classified into single-walled carbon nanotubes (SWCNTs) and multi-walled carbon nanotubes (MW-CNTs) subject to the number of graphene layers constituting of their wall. Each type of CNTs would exhibit advantages and drawbacks regarding to objectives of targeted applications which have been examined by many research teams [7]. There are many methods which have been proposed and developed for synthesis of CNPs, i.e. arc discharge, chemical vapor deposition and laser ablation. Chemical vapor deposition is one of the most popular methods because of its scalability and applicability to usage of various carbon sources, which can be decomposed in vapor phase at a regulated temperature in prior to the self-assembly process of CNPs. Such CNPs would grow on the surface of metal catalyst or some specific substrates [9, 10]. Meanwhile, pyrolysis, which is recognized as one of simple CVD methods, could be adapted for mass production of CNPs. Recently, it is reported that co-pyrolysis of metallocene with carbon precursors would be a promising strategy to produce Fe-filled carbon nanoparticles which could exhibit magnetic property [56, 89, 90]. Some experimental variables, such as ratio of metallocene to carbon precursor, temperature, reaction time and pressure, have been regulated to control the formation and structure of carbon nanoparticles via such co-

pyrolysis method [91, 92]. However, based on a comprehensive literature survey, it is found that formation of CNPs under the influence of magnetic induction has not been thoroughly examined [23]. Meanwhile, it should be noted that glycerol is a major by-product of bio-diesel manufacturing process which has been of interest for renewable energy research worldwide. However, the global supply of refined glycerol has been estimated to be lower than the global consumption. As a result, oversupplied amount of glycerol derived from bio-diesel conversion arouses increasing research interest to find alternative means for its effective utilization. To the best of our knowledge, only few research works have been involved with direct utilization of glycerol as carbon source for synthesis of carbon nanoparticles [56]. Therefore, this work seeks possibility to investigate alternative method for producing value-added products from glycerol as carbon source by synthesis of CNPs. In this work, pyrolysis of glycerol with the presence of few ferrocene would be employed for synthesizing M-CNPs with magnetic field induction with an aim to increase yield and quality of the resultant M-CNPs. Based on experimental investigation with the synthesizing temperature in a range of 700 to 1000 °C with an initial weight ratio of glycerol to ferrocene in the range of 3:1 – 7:1 were investigated. In addition, AC-magnetic susceptibility analyzer could also confirm the strong response of M-CNPs with respect to magnetic induction.

4.2 Research methodology

4.2.1 Synthesis of M-CNPs with magnetic induction

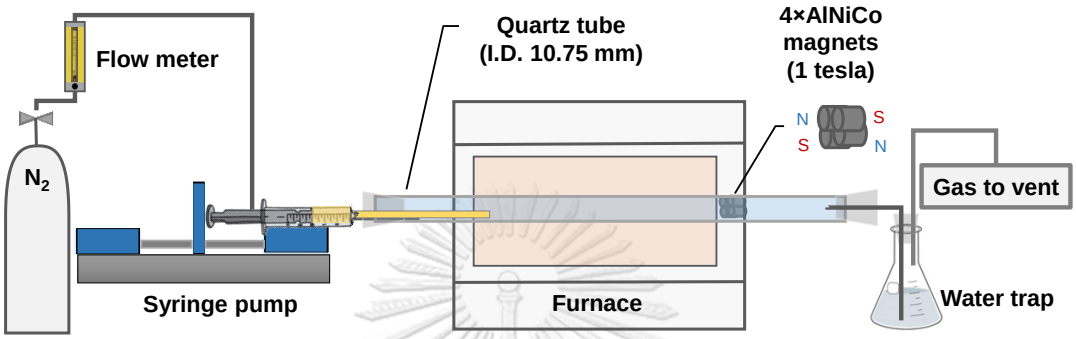

Figure 4.1 Experimental schematic for synthesis M-CNPs with magnetic collector

M-CNPs were synthesized in an experimental set-up consisting of electrical furnace and quartz tube (10.75 mm in I.D., 570 mm in length). Glycerol (Qrex, 99.5% purity) and Ferrocene (Sigma-Aldrich, 98% purity) have been used as precursor and source of carbon and Fe catalyst, respectively. 2 ml of glycerol and ferrocene mixture was fed into the quartz tube reactor with the flow rate of 0.003 ml/min by a syringe pump where the regulated temperature was high enough for decomposing all precursors. After the electrical furnace was employed to regulate the quartz tube reactor temperature to a designated set point, a nitrogen flow rate of 30 ml/min was introduced for conveying the resultant M-CNPs which was generated by the self-assembly reaction to the outlet. The magnetic collector was applied at downstream

zone for collecting the remaining products which were not deposited on the quartz tube as shown in Figure 4.1. The synthesizing process was controlled for 66 min, afterwards the reactor was cool down to room temperature. Substantial amount of the synthesized products was collected from the deposit on the inner wall of the reactor while another portion was trapped on the surface of the magnetic collector due to the magnetic induction. It should be noted that the magnetic collector was made of Al-Ni-Co magnet, which is more stable at high temperature than any other typical magnet bar. Based on our measurement the surface magnetic flux on the magnetic collector was 0.85×10^{-3} T. Designated experiments were conducted for investigating the effect of magnetic field induction and two main variables being explored were temperature and weight ratio of glycerol to ferrocene. To examine the effect of magnetic induction, synthesizing experiments were conducted using magnetic rod collectors in comparison to those using stainless steel rods as non-magnetic collectors of the same dimensions. For looking into the influence of the synthesizing temperature on the yield of the synthesized M-CNPs, the reactor temperature was varied in a range of 700 to 1000 °C while the weight ratio of glycerol to ferrocene was kept constant at 3:1. Finally, experiments with different initial weight ratio of glycerol to ferrocene varied in a range from 1:1, 3:1, 5:1 to 7:1 with the constant reactor temperature of 800 °C were conducted for figuring out the effect of an increase in carbon content on the yield of the synthesized M-CNPs.

4.2.2 Analysis

Microscopic structure and morphology of all synthesized products were characterized by a transmission electron microscope (TEM) (JEOL, JEM 1010). For evaluating thermal stability and compositions in terms of carbon and Fe contents within synthesized products, thermogravimetric analysis (TGA) (Shimadzu, TGA-50) with a ramping rate of 10 °C/min from room temperature to 900 °C was carried out. For confirming graphitic carbon and disorder carbon structure, Raman spectroscopy (Lamda Vision, MicroRAM-3000L) were employed for analyzing all synthesized products. AC magnetic susceptibility of synthesized products was also monitored by a magnetometer (Magqu Co., XacQuan-II), with maximum magnetic flux of 15 mG and varied frequencies in a range of 11 to 24901 Hz.

4.3 Effect of magnetic field induction

Within each typical experiment, typical synthesized products could be collected from thick layer of black particulate deposit on the inner wall of the quartz tube reactor and loose layer of black deposit on the external surface of magnetic rod collectors which were equipped at the exit of the reactor. However, when the stainless rod collectors were employed instead of the magnetic rod collectors, most of synthesized product was collected from the deposit on the inner wall of the quartz tube reactor with only few amounts of deposit on the external surface of the stainless

rod collectors. Based on TEM analyses shown in Figure 4.2 (a) and (b), most of typical products synthesized with the glycerol to ferrocene weight ratio of 3:1 and synthesizing temperature of 800 °C was composed of magnetic carbon nanoparticles (M-CNPs) and clusters of Fe nanoparticles. Most of Fe nanoparticles were encapsulated within the carbonaceous layers of carbon nanotubes (CNTs) or carbon nanoparticles (CNPs).

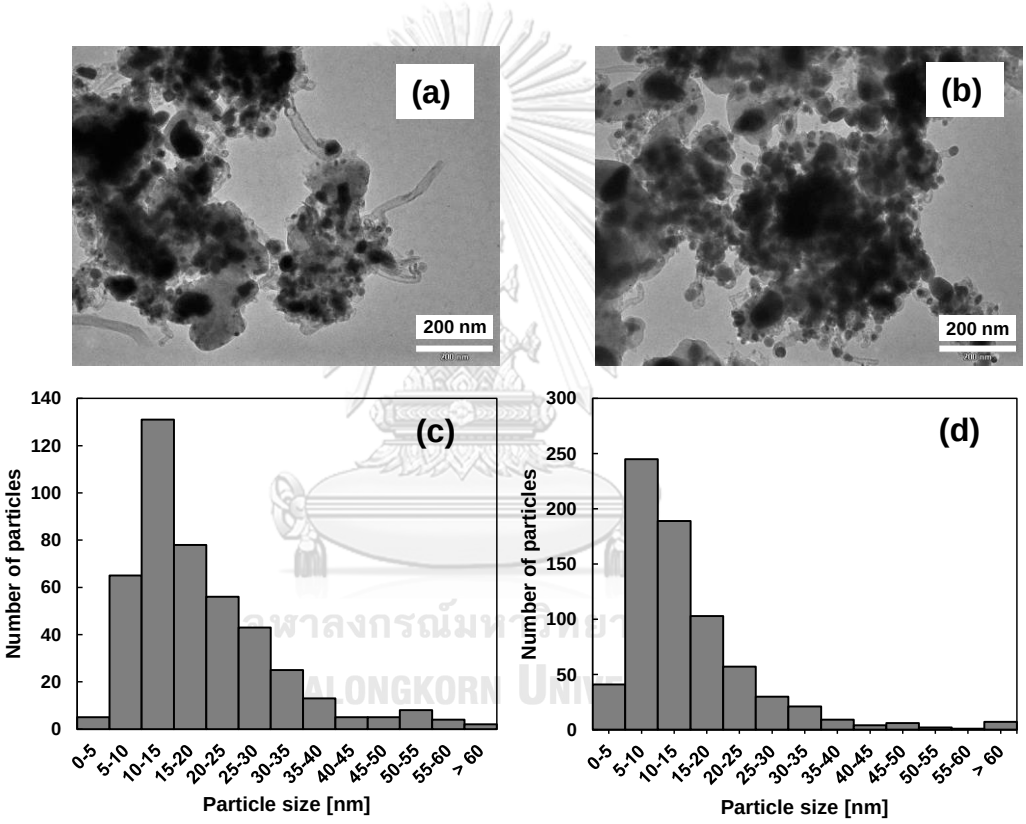

Figure 4.2 (a) TEM images of typical sample collected (a) from the surface of the inner wall of the quartz tube reactor, and (b) TEM image of atypical sample collected from the surface of the magnetic collectors; with being particle size distribution (PSD) of embedded Fe nanoparticles in sample (a) from the surface of the inner wall of the quartz tube reactor, and (d) from the surface of the magnetic collectors

A substantial number of TEM micrographs were employed for determining nominal size of M-CNPs and Fe nanoparticles based on an image processing method. As shown in Figure 4.2 (a), a typical sample of deposit collected from the inner wall of the quartz tube reactor contained M-CNPs with diameter in a range of 20-60 nm together with Fe nanoparticles with a rather broad size distribution in a range of 5 to 60 nm. Meanwhile, the synthesized product collected from the external surface of magnetic rod was mainly composed of M-CNPs with diameter in a range of 10-30 nm and encapsulated Fe nanoparticles with small diameter in a range of 5 - 45 nm as could be observed in Figure 4.2 (b). It is worth noting that the synthesized products collected from different location exhibited distinctive characteristics. For further comparison, particle size distribution (PSD) of Fe nanoparticles encapsulated within the synthesized products shown in Figure 4.2 (a) and (b) was statistically analyzed and depicted in Figure 4.2 (c) and (d), respectively. The Fe nanoparticles encapsulated in M-CNPs collected from the inner wall of the quartz tube reactor possessed a broader size distribution with an average size of 19.2 nm. On the other hand, the Fe nanoparticles encapsulated in M-CNPs which were collected from the external surface of the magnetic rod exhibited a narrower size distribution with an average size of 15.9 nm. It is well recognized that self-assembly process of CNTs or CNPs could be stimulated with the presence of catalytic Fe nanoparticles [91]. Because of higher condensing temperature, Fe nanoparticles which were generated from decomposition of ferrocene would tend to precipitate and glow on the inner surface of the quartz

tube reactor. Consequently, atomic carbon clusters which were generated from decomposition of glycerol and ferrocene would undergo the self-assembly process to form M-CNPs and CNTs growing on the surface of the quartz tube reactor. Meanwhile, some Fe nanoparticles with smaller size would be entrained by the convective flow of the carrier gas. Interaction among Fe nanoparticles and carbon clusters would also lead to formation of M-CNPs due to the self-assembly process [91].

After the self-assembly reaction, such resultant products would be entrained by the carrier gas flow and then be collected by the magnetic field induction around the magnetic rod collector, resulting in formation of loose deposit on the external surface of the magnetic rod collector. However, when the stainless-steel rod collector was employed instead of the magnetic rod collector, the stainless-steel rod would hinder the total flow of gas stream, leading to back-mixing of the entrained products which attributed to additional amount of deposit on the inner surface of the quartz tube reactor. For confirmation, amount of C and Fe in synthesized products were conducted using TGA analyses and then yield of C, Fe and M-CNPs was determined using equations (4.1) -(4.3).

$$\text{Yield of C (\%)} = \frac{\text{Weight of C within the synthesized M-CNPs (g)}}{\text{Weight of C in feed (g)}} \times 100 \quad (4.1)$$

$$\text{Yield of Fe (\%)} = \frac{\text{Weight of Fe within the synthesized M-CNPs (g)}}{\text{Weight of Fe in feed (g)}} \times 100 \quad (4.2)$$

$$\text{Yield of M-CNPs (\%)} = \frac{\text{Weight of the synthesized M-CNPs (g)}}{\text{Weight of Glycerol + Ferrocene (g)}} \times 100 \quad (4.3)$$

Figure 4.*3* reveals that with the presence of the magnetic rod collector both C yield and Fe yield were higher than those when the stainless-steel rod collector was employed for collecting the synthesized M-CNPs. With the average particle size below 100 nm, motion of the synthesized M-CNPs could be dominated by the inertial and diffusional mechanisms. However, because of the magnetic field induction around the magnetic rods, the attractive force acting on the M-CNPs could overcome the inertial and diffusional forces, resulting in an increase in deposit of M-CNPs on the surface of the magnetic collector. These results could suggest that the inductive magnetic field emerging from the magnetic collector could enhance the yield of M-CNPs synthesized from co-pyrolysis of glycerol and ferrocene.

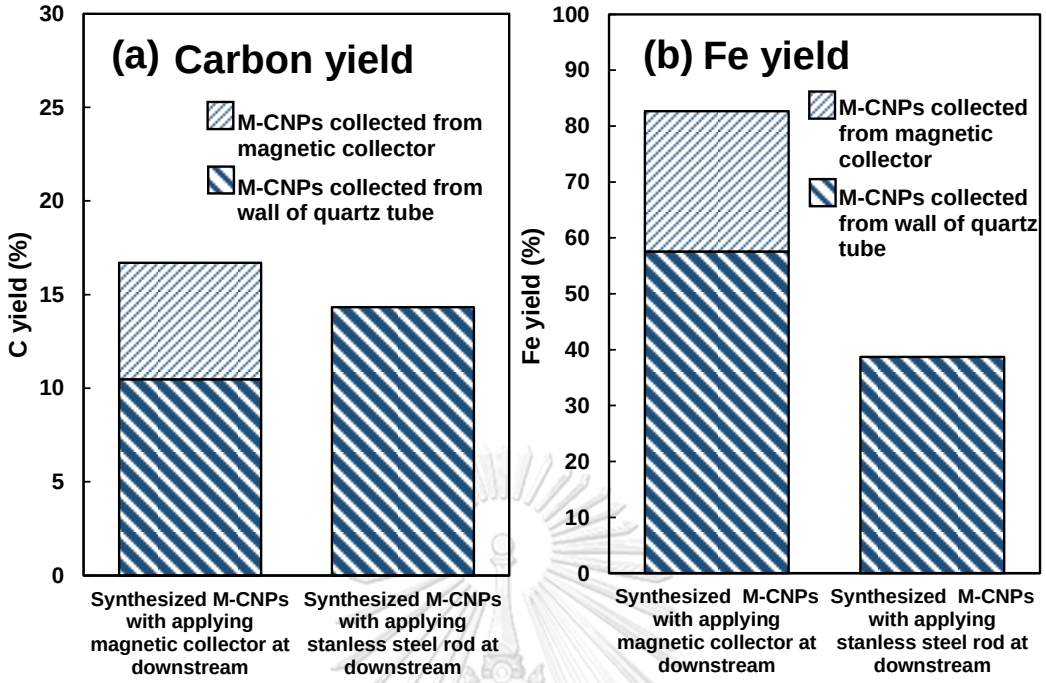

Figure 4.3 Comparison of yields of (a) Carbon and (b) Fe within the sample of M-CNPs collected from the inner wall of the quartz tube reactor and from the surface of the collector

4.4 Effect of synthesizing temperature

4.4.1 Morphology of M-CNPs

The morphology and structure of depositing M-CNPs on inner wall of reactor with varied synthesizing temperature and keeping constant weight ratio of glycerol to ferrocene 3:1 and 30 ml/min of N_2 flow rate were examined by TEM as shown in Figure 4.4. The synthesized products which were synthesized at 700 °C mainly consisted of amorphous carbon with the as-grown CNTs exhibited nominal diameter of 10-20 nm. These results would be ascribed to incomplete self-assembly of carbon

precursor at low temperature. When synthesizing temperature was increased to 800-900°C, it exerted insignificant effect on morphology and size of the synthesized products. It could be observed that the synthesized products consist of a large amount of carbon nanotubes (CNTs) with a little agglomeration of amorphous carbon nanoparticles. With the increasing in the synthesizing temperature to 800 and 900°C, a gradual increase in the diameter of as-grown CNTs up to 40 nm could be observed. When the synthesized temperature reached 1000 ℃, it could be observed that outer diameter of synthesized CNTs also remains nearly the particles at 800 and 900 ℃, whereas the inner diameter was decreased. It could be implied that synthesized M-CNPs was thickened by increasing number of their wall thickness at 1000 °C [93, 94].

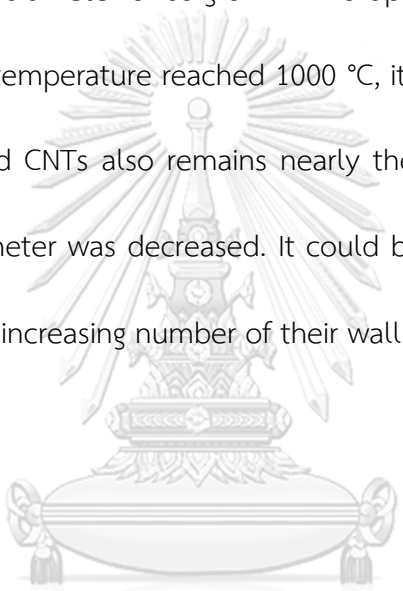

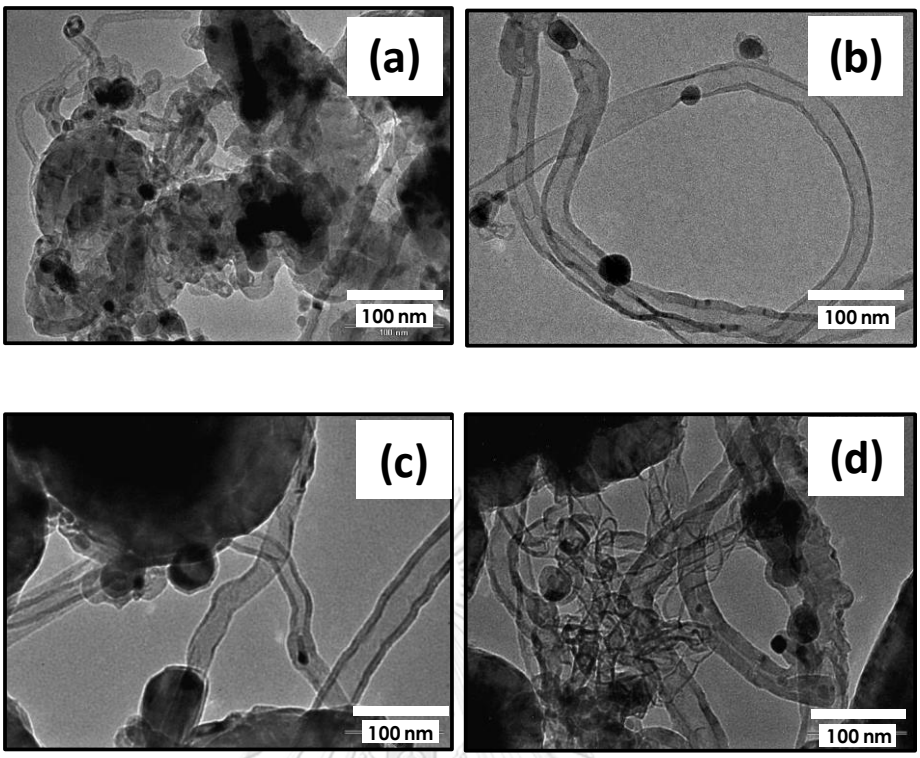

Figure 4.4 TEM image of synthesized M-CNPs from 3:1 of weight ratio of glycerol to ferrocene ratio at different synthesizing temperature at (a) 700 °C, (b) 800 °C, (c) 900 °C and (d) 1000 °C

4.4.2 Thermal stability of synthesized M-CNPs

To investigate the compositions of as grown M-CNPs, TGA was used for the thermogram of the weight percentage analysis. For TGA analysis, the heating temperature was increased up to 900°C to evaluate thermal stability of synthesized M-CNPs. Different plots of TGA curves in Figure 4.5 corresponded to different synthesized temperatures. For analysis thermal stability of M-CNPs, other forms of carbon and defected forms of M-CNPs are oxidized at lower temperatures in comparison with non-defected M-CNPs structure. Therefore, the temperature at the

first point of dropped weight of M-CNPs is starting point of oxidation. in TGA could be described the presence of impurities in as-grown M-CNPs. At synthesized temperature of 700 ℃, the first point temperature of oxidation process of particles was lower when compared with high synthesized temperature [95]. Therefore, it could be implied that carbon which was synthesized at 700 ℃ consisted of other forms of carbon such as amorphous or defected carbon. This was supported by TEM image shown in Figure 4.4. At synthesized temperatures above 700 ℃, the first point of starting oxidation temperature was same and could be implied that structure of products not be changed. Furthermore, carbon content from synthesized particles which were trapped on magnetic collector was higher than the one collected from inner wall of reactor products. In addition, weight percent of carbon and iron content of M-CNPs which were collected from inner wall of reactor and was trapped on magnetic were shown in Table 4.1.

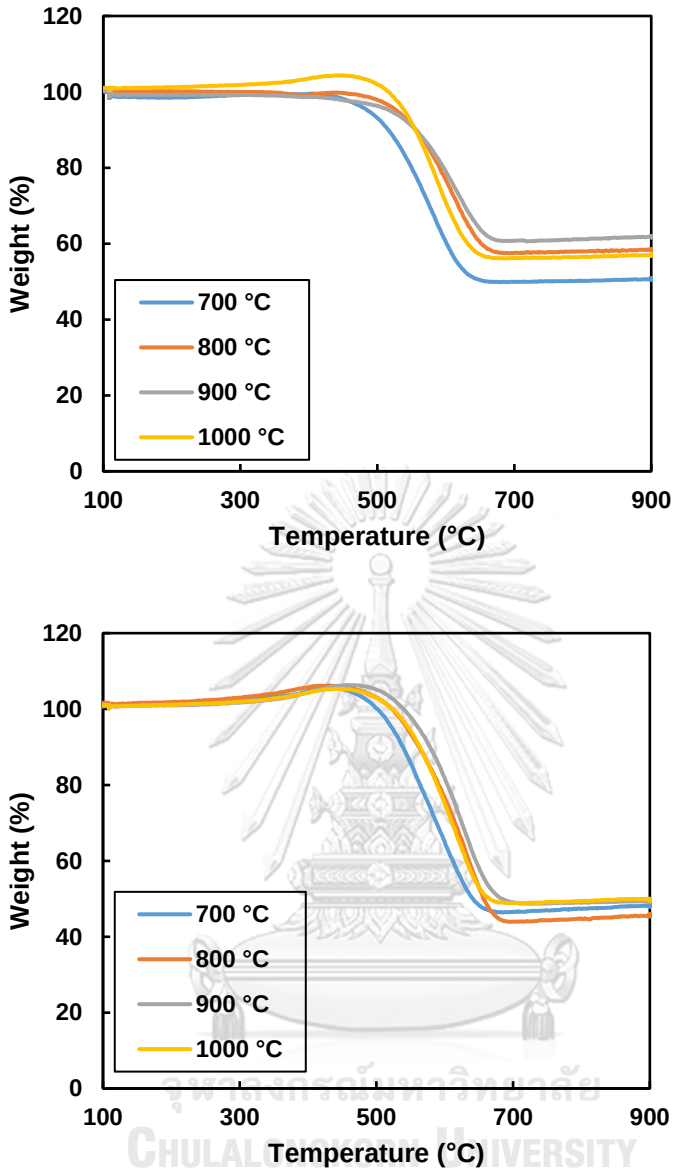

Figure 4.5 Thermal stability of M-CNPs synthesized at different temperature of (a) M-CNPs collected from inner wall of reactor and (b) M-CNPs collected from magnetic collector

Table 4.1. Thermal degradation data of different M-CNPs varied synthesizing temperatures at 3:1 weight ratio of glycerol to ferrocene

Synthesizing temperature (°C)	on quartz tube (reaction zone)		on magnetic (downstream zone)	
	Carbon (Wt%)	Fe (Wt%)	Carbon (Wt%)	Fe (Wt%)
700	58.0	42.0	60.5	39.5
800	50.6	49.4	58.24	41.8
900	46.9	53.1	59.6	40.4
1000	51.7	48.3	65.8	34.2

4.4.3 Magnetic susceptibility

AC magnetic susceptibility in term of complex number of M-CNPs which was synthesized with 3:1 weight ratio of glycerol to ferrocene at 800 °C as a function of frequency was investigated. X_r and X_i as shown in Figure 4.6 (a) are real and imaginary numbers of AC magnetic susceptibility respectively [96]. AC magnetic susceptibility of M-CNPs which was collected from both inner wall of reactor and magnetic collector was investigated in term of $X_{r,0}$ as a function of synthesized temperature, as shown in Figure 4.6 $X_{r,0}$ is the extrapolated value of X_r curve at frequency 0 Hz. $X_{r,0}$ magnetic susceptibility of M-CNPs which was collected from inner wall of reactor was higher than M-CNPs from magnetic collector in every synthesized temperature. This cloud explained by crystal size of Fe clusters as shown in nanoparticles size distribution

histograms in Figure 4.2. Because large grain size of Fe cluster in the as-grown was more responsive than small grain size of Fe cluster in the as-grown M-CNPs [90]. At synthesized temperature 700 ℃, $X_{r,0}$ value of magnetic susceptibility of M-CNPs which was collected from inner wall of reactor and from magnetic collector are lower than at other temperatures. It could be seen that $X_{r,0}$ is related with amount of carbon around Fe. From Figure 4.4, synthesized particles at synthesized temperature 700 ℃ mainly consisted of thickness layer of covering-carbon amorphous on Fe cluster leading to M-CNPs which was synthesized at 700 ℃ was not good responsibility with magnetic force. Furthermore, M-CNPs with synthesized temperature of 700 ℃ contained less amount of metallic Fe, as shown in Table 4.1 causing low magnetic property responsive. $X_{r,0}$ value of magnetic susceptibility apparently rises with synthesized temperature reach to 800 ℃ due to as-grown M-CNPs contained high percentage of Fe with 40.76%. Then $X_{r,0}$ tended to decrease in the synthesized temperature at 900 ℃ up to 1000 ℃. It could be noted that magnetic susceptibility is low response because when increased synthesized temperature, wall thickness of M-CNPs was increased as supported by Figure 4.4. It was directly affected to reduce magnetic susceptibility because the obstruction between magnetic force and Fe cluster was increased by number of carbon wall.

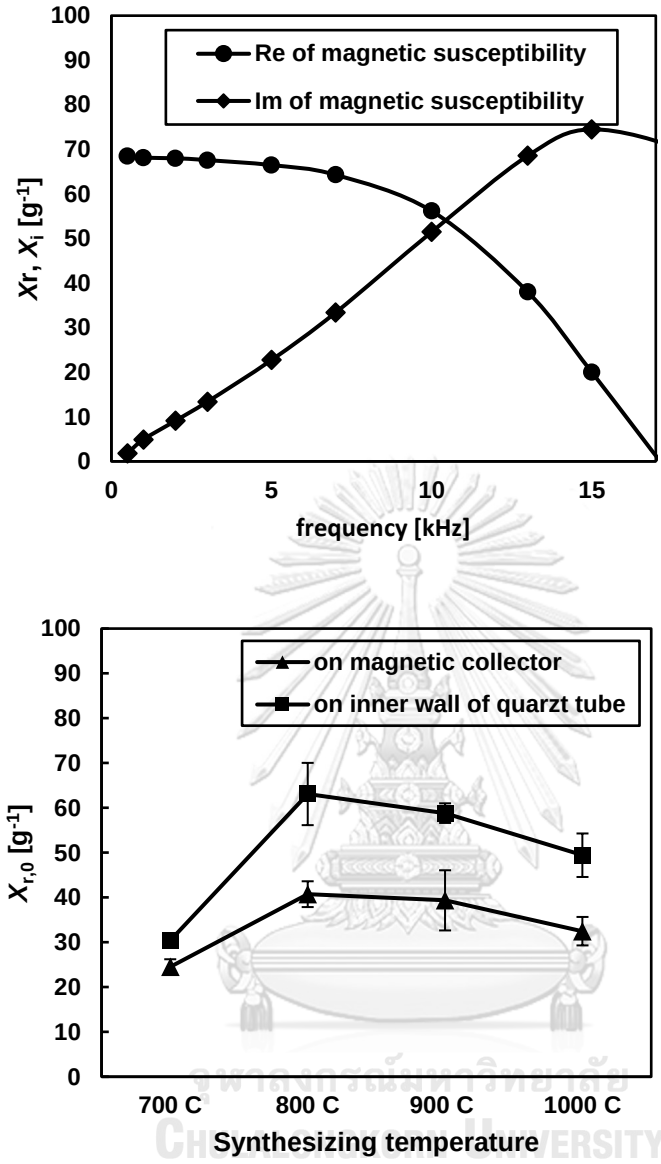

Figure 4.6 (a) AC magnetic susceptibility of synthesized M-CNPs which was synthesized at glycerol to ferrocene weight ratio 3:1 at 800 °C as function of frequency, and (b) magnetic susceptibility of M-CNPs which was collected from inner wall of reactor and from magnetic collector at 0 Hz as function of synthesizing temperature

4.4.4 Yield

Figure 4.7 illustrates the yield of C, Fe and M-CNPs synthesized from the mixture of glycerol and ferrocene with weight ratio of 3:1 at different synthesizing temperatures as determined by equation (4.1) -(4.3) respectively. Interestingly the synthesizing temperature exerts detectable effect on both C and Fe yields. It could be experimentally confirmed that C and Fe yields within the synthesized M-CNPs collected from the surface of the inner wall of the reactor were higher than those of M-CNPs deposit on the magnetic collector. In general, ultrafine particles, such as M-CNPs with nominal size below 100 nm would prefer to deposit on the wall of obstacles due to their collision, which is recognized as inertial impaction. However, with an elevated temperature, motion of such particles would also be accelerated by their diffusion. As depicted in Figure 4.7 (a), with an increase in the synthesizing temperature, the C yield within the M-CNPs collected from the surface of the inner wall of the reactor gradually declined from 13.40 to 10.31 % while the C yield within the M-CNPs collected from the surface of the magnetic collector was rather stable. However, the Fe yield within the M-CNPs collected from both the surface of the inner wall of the reactor and the surface of the magnetic collector were rather stable as could be observed in Figure 4.7 (b). In addition, the Fe yield within the M-CNPs collected from the surface of the inner wall of the reactor were almost 3-4 folds of those in the M-CNPs collected from the surface of the magnetic collector. An increase

in the synthesizing temperature from 700 °C to 1,000 °C would enhance the diffusion of carbon because of its lower atomic weight, resulting in a higher loss of carbon clusters which could engage with oxygen to generate CO and CO_2.

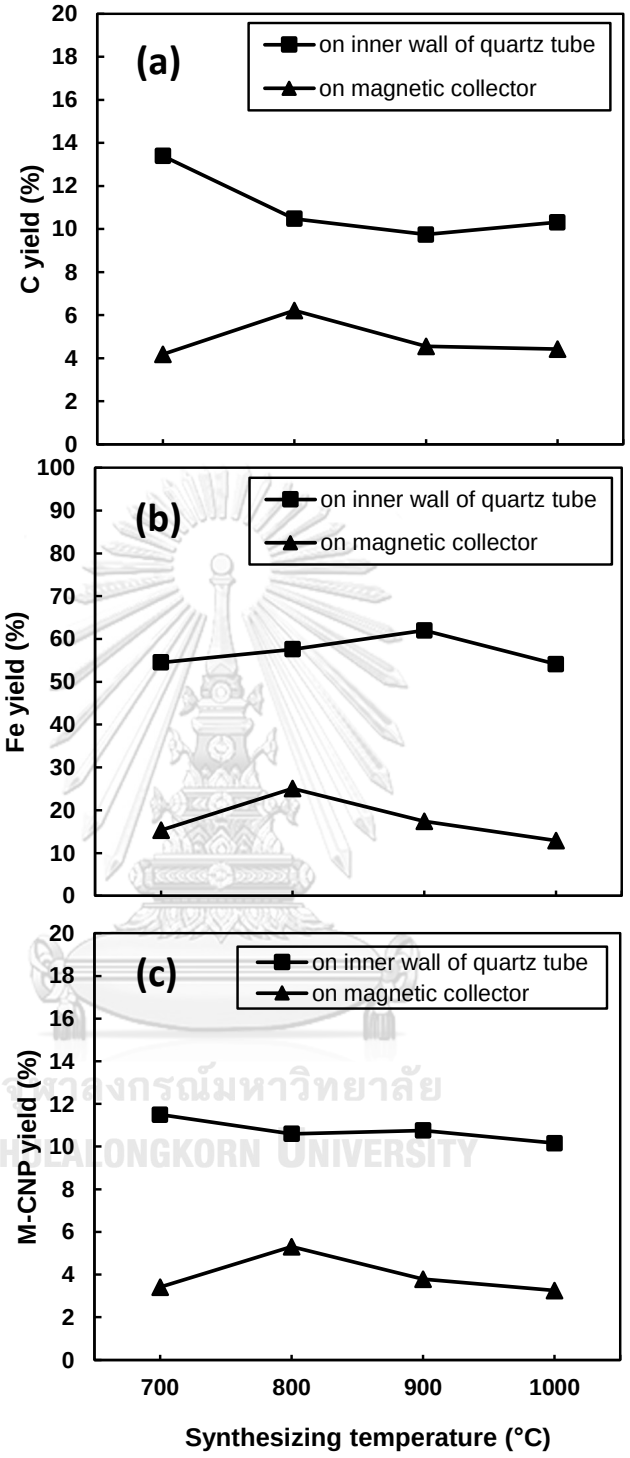

Figure 4.7 Effect of synthesizing temperature on (a) carbon yield, (b) Fe yield and (c) yield of synthesized M-CNPs which were collected from the inner wall of the quartz tube reactor and on the magnetic collector

The stable Fe yield would be ascribed to the fact that Fe clusters which could rapidly precipitate to form Fe nanoparticles would deposit onto the surface of the inner wall of the reactor and the surface of the magnetic collector. In Figure 4.7 (c), determination of the M-CNP yield which could represent total amount of valuable products with respect to the total consumption of raw materials suggests that the highest yield was achieved at 800 °C. In general, an increase in temperature could generally enhance the diffusion of C and Fe atoms together with an increase in volumetric gas flow rate. However, it should be noted that the diffusional term is an exponential function of temperature while the volumetric gas flow rate would be a linear function of temperature. Therefore, it is reasonably implied that the higher synthesizing temperature would result in the higher loss of M-CNPs entraining with the carrier gas. These experimental results would suggest that the main mechanism of deposition of M-CNPs synthesized from co-pyrolysis of glycerol and ferrocene under different synthesizing temperature were composed on the inertial-diffusional impaction on the surface of the inner wall of the reactor and the magnetic inductive impaction on the surface of the magnetic collector. Meanwhile, entrainment with diffusion of the synthesized M-CNPs with the main flow of carrier gas would also lead to their loss. Based on our experimental results, it is reasonable to imply that 800 °C would be the most promising temperature for synthesizing M-CNPs from co-pyrolysis of glycerol and ferrocene.

4.5 Effect of initial weight ratio of glycerol to ferrocene

In general, amount of raw material supplied to the reactor would be another important parameter which could affect the process of product formation. Ferrocene was used as a supplied of carbon sources and iron atom which could behave as catalyst. Meanwhile glycerol which was employed as main carbon source is much cheaper because it is by-product of bio-diesel production [5]. Therefore, an increase in the weight ratio of glycerol to ferrocene is taken into account with an expectation to reduce the synthesizing cost of M-CNPs. Figure 4.8 reveals dependence of C, Fe and M-CNP yields on the initial weight ratio of glycerol to ferrocene with a constant synthesizing temperature of 800 ℃. Both C and Fe yields in products collected on the surface of the inner wall of the reactor tended to increase when the initial weight ratio of glycerol to ferrocene was increased from 1:1 to 7:1 (Figure 4.8 (a-b)) but C and Fe yields of products collected on the magnetic collector were rather stable when the initial weight ratio of glycerol to ferrocene was varied in the same range.

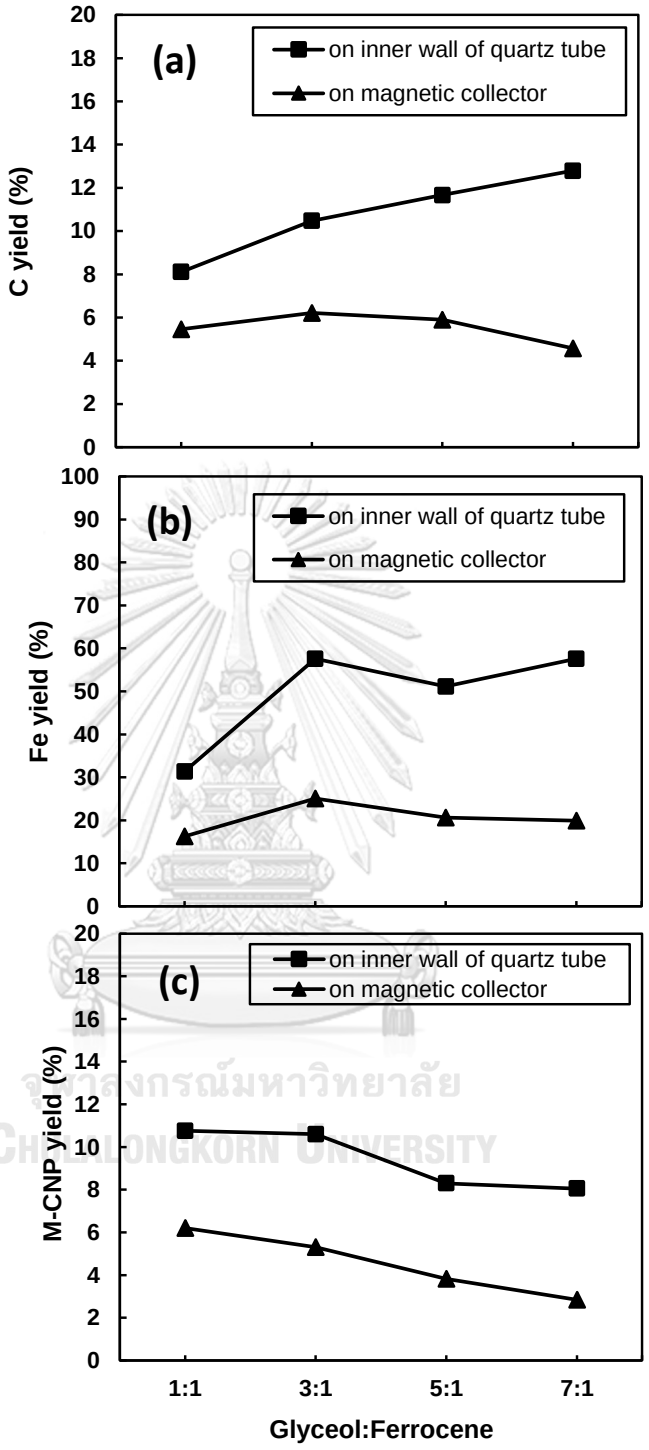

Figure 4.8 Initial weight ratio glycerol to ferrocene dependence of (a) carbon yield, (b) Fe yield and (c) yield of synthesized M-CNPs collected from the surface of the inner wall of the quartz tube reactor and from the magnetic collector

Nevertheless, total product yield analyses shown in Figure 4.8 (c) suggest that yields of M-CNPs which were collected as products depositing on the surface of the inner wall of the reactor were gradually decreased from 10.76 to 8.05 wt% with an increase in the initial weight ratio of glycerol to ferrocene. Similar trend was also observed from the M-CNP yield in the synthesized products trapped by the magnetic collector In general, sufficient amount of catalyst nanoparticles would promote the interaction of carbon clusters, resulting in a high yield of CNPs [91].

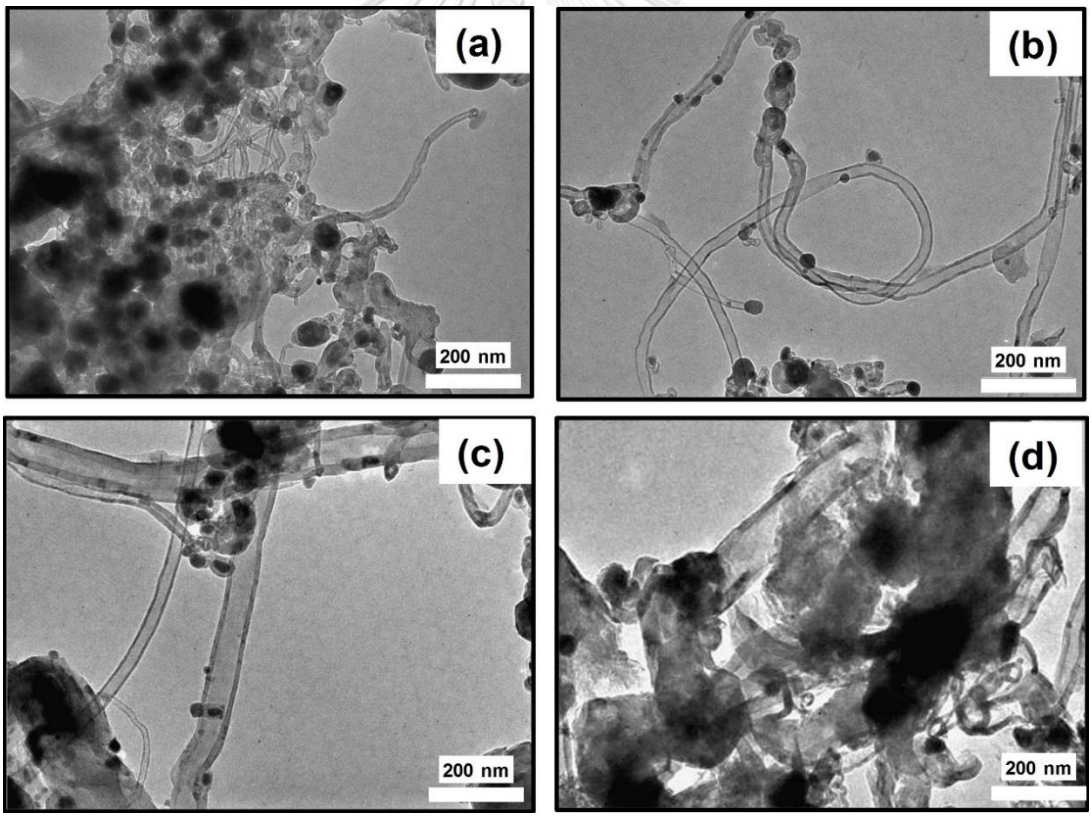

Figure 4.9 TEM image of synthesized M-CNPs which was synthesizing at 800 °C with different weight ratio of glycerol to ferrocene, (a) 1:1, (b) 3:1, (c) 5:1 and (d) 7:1

In this work, the catalyst is iron nanoparticles which were supplied from ferrocene only. Therefore, it is undoubted that the increases in the initial weight ratio of glycerol to ferrocene would inevitably subdue the role of iron nanoparticle catalyst, resulting in the decreased yield of synthesized product or M-CNPs. At the same time, TEM was also conducted for microscopic analyses of the synthesized products under the influence of the initial weight ratio of glycerol to ferrocene as depicted in Figure 4.9. It could be clearly observed that with the initial weight ratio of 1:1, the synthesized products contain a tremendous amount of small dark particles, which were iron nanoparticles, with an amount of dispersed M-CNPs, which are multi-walled carbon nanotubes (MW-CNTs). When the initial weight ratio was further increased from 3:1 to 7:1, well dispersed MW-CNTs with significantly smaller iron nanoparticles were observed by TEM analyses. It could be expected that the smaller iron nanoparticles would enhance the more uniformly grown and dispersed MW-CNTs [9, 96].

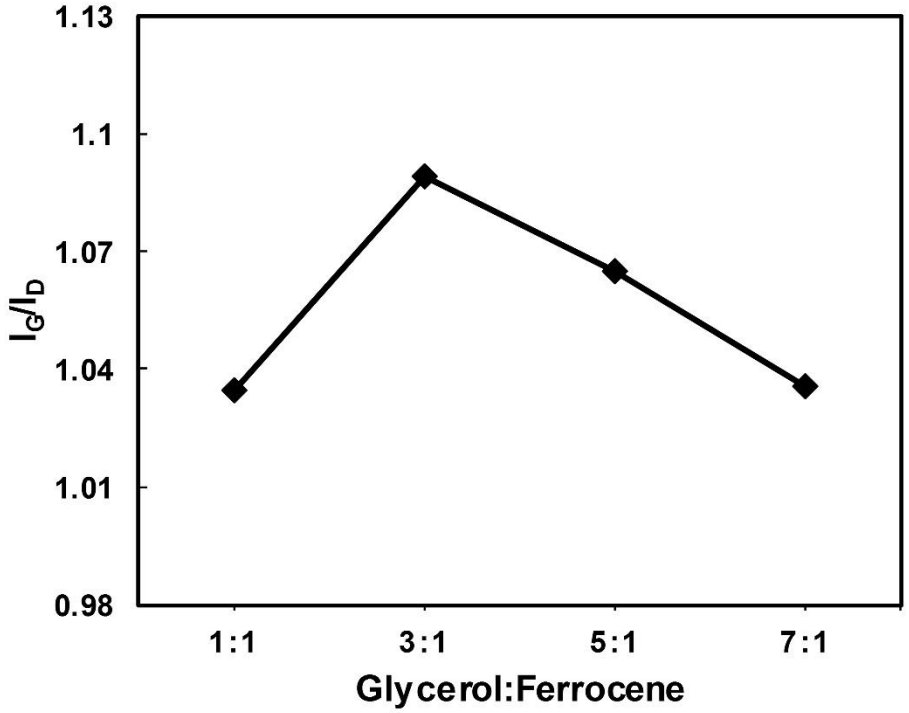

Figure 4.10 Raman spectroscopic analyses of M-CNPs synthesized from glycerol and ferrocene with different initial weight ratio in the range of 1:1 -7:1

Meanwhile, Figure 4.10 reveals Raman spectroscopic results of the synthesized products under the influence of the initial weight ratio of glycerol to ferrocene. The intensity ratio of graphite-related peak to disorder-related peak, I_G/I_D of each synthesized samples, which could represent the relative amount of graphitic carbon to disorder graphitic structure, suggested that with the initial weight ratio of 1:1, The initial weight ratio of 1:1, the amount of graphitic carbon structure within the synthesized sample was rather low because of the excessive amount of iron nanoparticles. When the initial weight ratio was increased from 3:1 to 7:1, the ratio of

graphitic carbon to disorder graphitic structure achieved a maximum at 1.09 and then decreased to 1.03. These analytical results reveal that the excessively low weight ratio of glycerol to ferrocene would result in the presence of excessive amount of iron nanoparticles and a small amount of MW-CNTs with lower IG/ID. Insufficient carbon contents would result in lower yield of the synthesized MW-CNTs [92]. Nevertheless, it should be noted that 3:1 would be the optimal value of the initial weight ratio of glycerol to ferrocene which could provide the most promising synthesized products which contain the highest graphitic carbon structure.

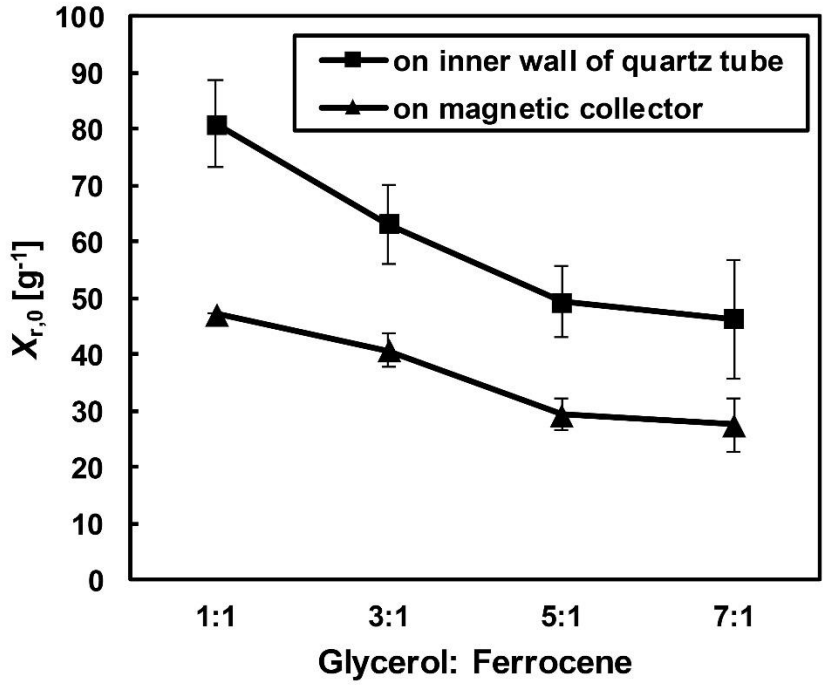

Figure 4.11 Effect of initial weight ratio of glycerol to ferrocene on magnetic susceptibility of M-CNPs

For verification of magnetic response, magnetic susceptibility at 0 Hz, $X_{r,0}$, was estimated by extrapolating the real number in the complex number of AC magnetic

susceptibility. The values of $X_{r,0}$ of M-CNPs collected from the inner wall of the reactor and on the collector, was analyzed are shown in Figure 4.11 with respect to the initial weight ratio of glycerol to ferrocene. The results show that magnetic susceptibility of synthesized M-CNPs was significantly high due to the presence of iron nanoparticles embedded inside M-CNPs [12, 96]. As expected, $X_{r,0}$ of M-CNPs collected from the inner wall of the reactor was higher than that of M-CNPs collected on the collector due to the influence of iron nanoparticle with larger nominal size. This result would be ascribed that the magnetic collector could help inducing iron nanoparticles even with smaller nominal size which could also be detected by TEM analyses [13]. Moreover, integrating results of TGA, TEM and $X_{r,0}$ analyses would suggest that the magnetic induction due to the magnetic collector placed at the exit of the reactor would lead to controlled synthesis of M-CNPs with different yield and characteristics. With an increase in the initial weigh ratio of glycerol to ferrocene, a few amounts of iron relative to that of carbon clusters was decreased as shown in
Table 4.2, resulting in lower proportion of magnetic responsive portion in the synthesized M-CNPs. It should be noted that with a lower initial weigh ratio of glycerol to ferrocene a narrow error bar of $X_{r,0}$ values could be obtained. This observation could confirm again that an increase in the initial weigh ratio of glycerol to ferrocene would result in a decrease in amount of Fe content in the M-CNPs, leading to higher deviation of measurement of $X_{r,0}$ values.

Table 4.2. Thermal degradation data of different M-CNPs varied weight ratio of glycerol to ferrocene at synthesizing temperature 800 °C

Glycerol: ferrocene (Weight ratio)	on quartz tube (reaction zone)	on magnetic (downstream zone)

	Carbon (Wt%)	Fe (Wt%)	Carbon (Wt%)	Fe (Wt%)
1:1	46.1	53.8	52.69	47.4
3:1	50.6	49.4	58.2	41.8
5:1	64.5	35.5	69.5	30.5
7:1	69.2	30.8	70.1	29.9

Based on above mentioned results and discussion, controlled synthesis of magnetic carbon nanoparticles (M-CNPs) via co-pyrolysis of glycerol and ferrocene with magnetic field induction was confirmed. The influence of synthesizing temperature in a range 700 to 1000 °C suggested that with an initial weight ratio of glycerol to ferrocene of 3:1, the highest yield of M-CNPs could be achieved at 800 °C. Experimental results suggest that controlled synthesis of M-CNPs with magnetic induction could be anticipated as a promising method for producing M-CNPs with high quality and high yield when compared to the condition with the absences of magnetic induction.

4.6. Conclusion

In this study, the morphology, yield and magnetic susceptibility of M-CNPs synthesized from co-pyrolysis of glycerol and ferrocene were strongly influenced by the synthesizing temperature and initial weight ratio of glycerol to ferrocene. TEM, TGA and magnetic susceptibility analyses were employed for confirming that the resultant products mainly consisted of M-CNPs with carbon and Fe contents.

Integration of all experimental confirmation suggests that the synthesizing temperature of 800 °C and initial weight ratio of glycerol to ferrocene at 3:1 was the optimum condition for synthesizing M-CNPs. Under the influence of magnetic induction due to the usage magnetic collectors, M-CNPs with much enhanced yield, higher graphic carbon structure and remarkable magnetic susceptibility could be controlled synthesized.

Chapter V

Adsorption of oxy-tetracycline antibiotic on synthesized M-CNPs

Synthesized magnetic carbon nanoparticles (M-CNPs) by nebulizing pyrolysis of glycerol and ferrocene has been investigated for an application as an adsorbent for removal of oxy-tetracycline (OTC) from wastewater. Based on substantial experimental results, it is found that the adsorption of OTC on synthesized M-CNPs would obey the Langmuir model much better than the Freundlich model. The essential feature of the Langmuir isotherms is indicated by the maximum adsorption capacity (Qm) and the adsorption equilibrium constant (KL), which were 266.4 mg/g and 0.38 L/mg, respectively. These results suggest that the synthesized M-CNPs exhibited good potential for the adsorption of OTC. The OTC adsorption efficiency was increased from 54.6 to 84.2 when the initial pH of the OTC solution was respectively increased from 1 to 5 because OTC was ionized into cationic species at low pH of solution. While M-CNPs surface was negatively charged at pH higher than pH_{pzc} leading to promoted attraction between negative and positive charge of M-CNPs and OTC, respectively. However, a further increase in the initial pH higher than 5 would result in the hindered adsorption. These results would be ascribed that when the pH was increased above 5, the OTC would occupy negative charge because OTC is dissociated to release proton, resulting in less attraction to the surface of M-CNPs which is preferable to cationic specie.

5.1 Research background

Among various novel adsorbents, carbon nanoparticles would be one of the most outstanding alternatives selective to organic pollutants because of their highly porous and large specific surface area [97]. It is well recognized that glycerol is a major by-product of bio-diesel manufacturing process which could be converted to other high value-added products, including magnetic carbon nanoparticles (M-CNPs). Meanwhile, an increase in antibiotic application leads to environmental problem. Antibiotic is synthetic chemical with complex structure which is hardly eliminated naturally and exerts undesired consequence. Therefore, it is necessary to develop an efficient technique to remove antibiotic. Among various antibiotics, OTC is one of the most wildly used in agricultural activities. Therefore, it would be a synergetic work which could transform abundant glycerol into M-CNPs which could also be employed to tackle a serious problem of antibiotic pollutant.

5.2 Research methodology

Nebulization of glycerol (Qrex, 99.5% purity) and ferrocene (Sigma-Aldrich, 98% purity) mixture with a weight ratio of 3:1 is employed to supply a stream of carbon and catalyst precursor into a tubular reactor. M-CNPs were synthesized by an experimental set-up consisting of electrical furnaces and quartz tube (10.75 mm in I.D., 570 mm in length) and carrier gas flow instrument. The quartz tube reactor

temperature was regulated by the electrical furnace for heating up the reactor to 800 °C. 2 ml of glycerol and ferrocene mixture was fed into the tubular reactor with a regulated flow rate of 0.003 ml/min by syringe pump to a designated position in the quartz tube reactor, where the regulated temperature was high enough for decomposing all precursors. A nitrogen flow rate of 30 ml/min was introduced for conveying the resultant M-CNPs generated by the self-assembly of carbon clusters to the outlet. After a period of designated holding time, the reactor was cool down to room temperature and the resultant M-CNPs were collected from deposit on the inner wall of the reactor.

Adsorption of OTC using the synthesized M-CNPs was conducted in a batch system consisting of 1000 mL OTC solution. Under the room temperature initial concentration and pH of the OTC solution were adjusted in a range of 10 – 100 ppm and 1-11, respectively. 0.08 - 0.48 mg of M-CNPs was added into the OTC solution and then 4 mL of liquid samples was taken at different time until reaching equilibrium for OTC concentration analyses using UV-Vis spectroscopy (UV-1700, Shimadzu) as shown in Figure 5.1.

.

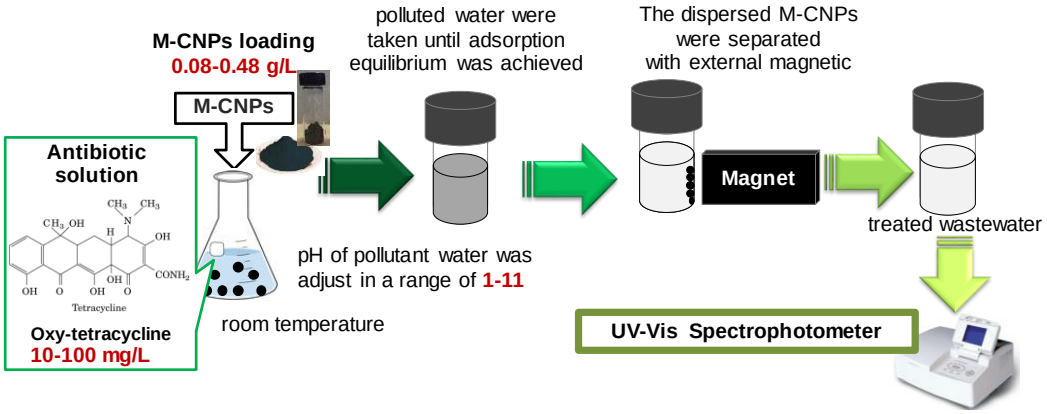

Figure 5.1 Experimental setup of M-CNPs adsorption

5.3 Effect of M-CNP loading on OTC adsorption

Effect of M-CNP loading on the OTC adsorption was experimentally investigated under a designated condition. Adsorption efficiency is defined as equation (5.1).

$$Adsorption\ efficiency = \frac{(C_0 - C_t)}{C_0} x100 \quad (5.1)$$

Where C_0 is initial concentration of antibiotics (mg/L) and Ct is concentration of antibiotics at any time t (mg/L).

Dependence of adsorption efficiency on M-CNPs loading is shown in Figure 5.2. The adsorption efficiency was gradually improved with an increase in the M-CNP loading but it was only slightly increased when the loading exceeded 8 mg. It could be implied that an equilibrium of OTC adsorption and desorption onto the

surface of M-CNPs would achieve under the investigating condition. Therefore, 0.32 g/L of M-CNP loading was designated as a basis for further investigation on effect of other experimental variables.

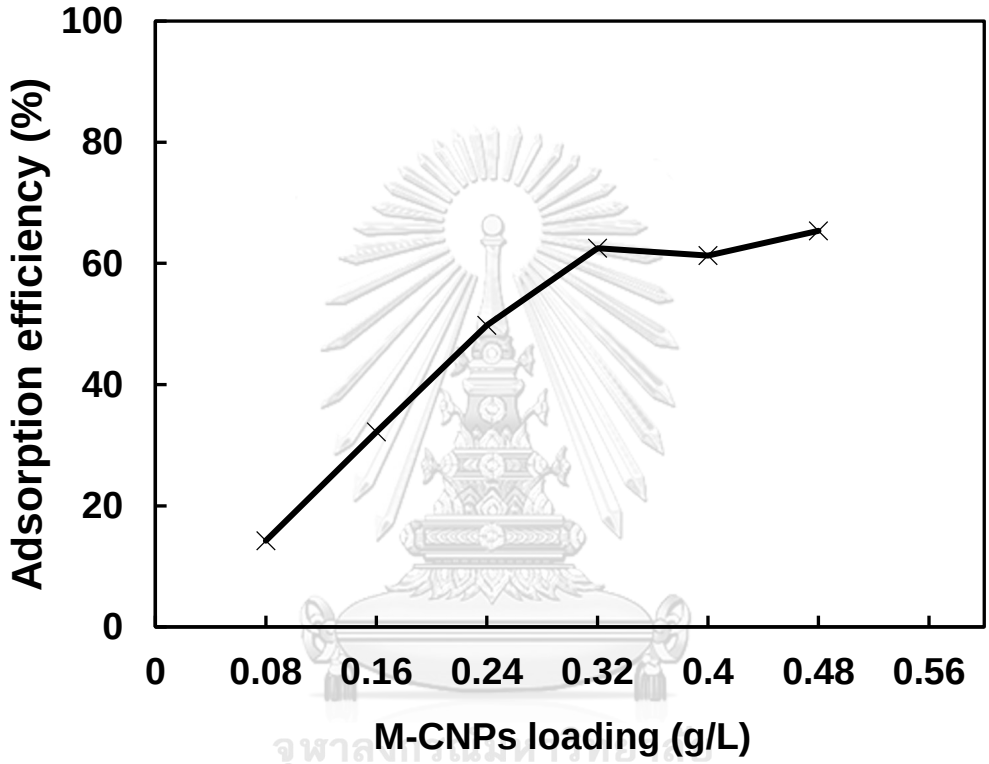

Figure 5.2 Effect of synthesized M-CNPs loading on the adsorption efficiency of OTC

5.4 Effect of initial pH of OTC solution on M-CNPs adsorption

Effect of initial pH of OTC solution on adsorption is shown in Figure 5.3. It could be clearly observed that with the initial pH in a range of 1 to 11 the adsorption efficiency was gradually elevated. Then the adsorption efficiency became lower with a further increase in the initial pH up to 11.

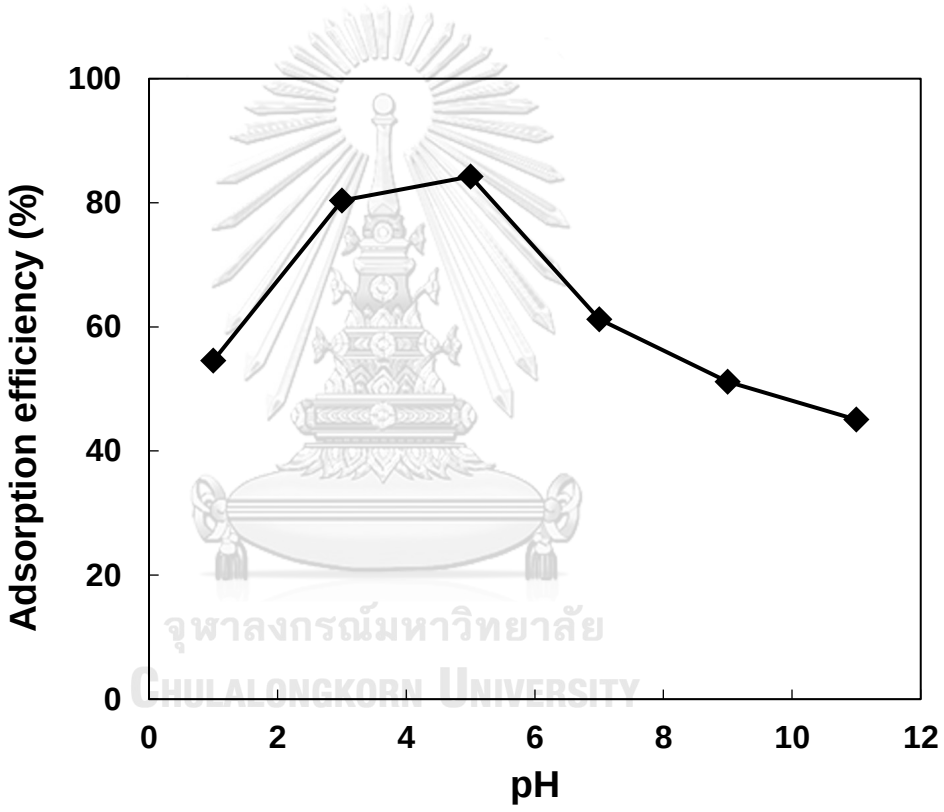

Figure 5.3 Effect of initial pH on adsorption of OTC on synthesized M-CNPs

These results would be attributed to the ionization on the surface of both the OTC molecule and synthesized M-CNPs [87]. Base on experiment, M-CNPs surfaces exert negative charge when pH of their suspension is controlled above 2.5 which is point of

zero charge (pH_{PZC}) of M-CNPs. In addition, each branch within the molecule of OTC could exert different influence on its electrochemical property based on pKa as shown in Figure 5.4. There are pKa_1, pKa_2 and pKa_3 which is equal to 3.3, 7.7 and 9.7, respectively [98].

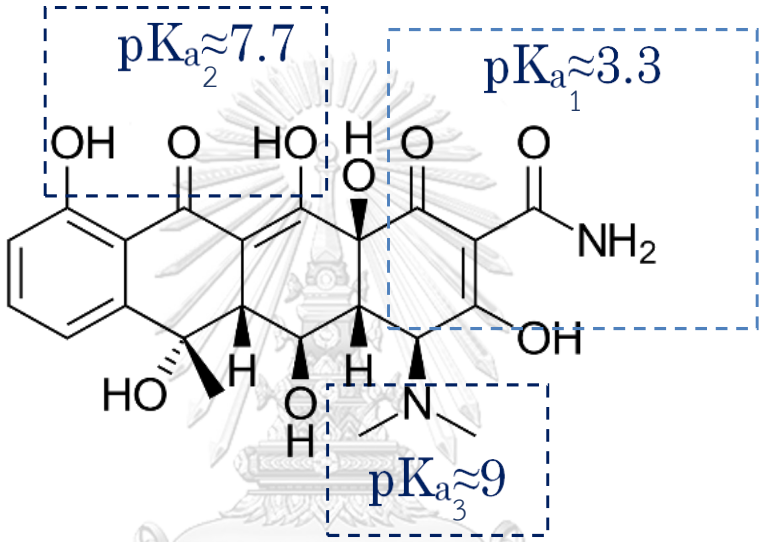

Figure 5.4 Typical key components in OTC molecule and their pKa

When pH of OTC solution was adjusted below 3.3, OTC molecules would behave as a cation because of the protonation of dimethyl-ammonium group. Therefore, electrostatic repulsion between positive charges was occurred, as shown in case 1 of Figure 5.5. Under the condition with pH of between 3.3 and 7.7, OTC molecules would become a zwitterion because of loss of proton from the tri-carbonyl system, so OTC molecule could be interacted with negative charge of M-CNPs by electrostatic force, as shown in case 2. However, when pH of OTC solution is controlled above 7.7, they

would oppositely behave as anion due to the loss of a proton from phenolic diketone moiety and the tri-carbonyl system as shown in case 3 and behave as fully deprotonated form when pH above 9.7. Thus, electrostatic repulsion between negative charge of OTC and M-CNPs was occurred, as mentioned in case 4. The protonation of OTC and deprotonation of synthesized M-CNPs would be affected by variation in pH [99].

Case 1 : pH of solution < < pK_{a3} of OTC and pH_{pzc} of M-CNPs

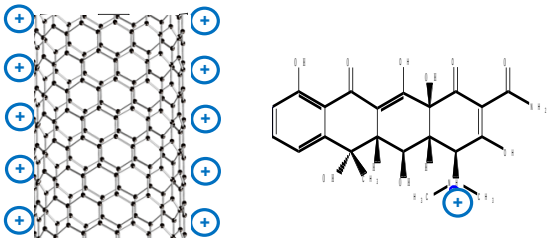

Case 2 : pK_{a2} > pH of solution > pK_{a1} of OTC and pH_{pzc} of M-CNPs

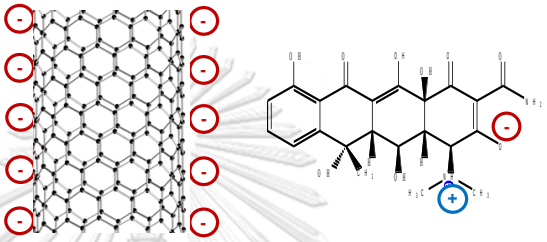

Case 3 : pK_{a3} > pH of solution > pK_{a2} of OTC and pH_{pzc} of M-CNPs

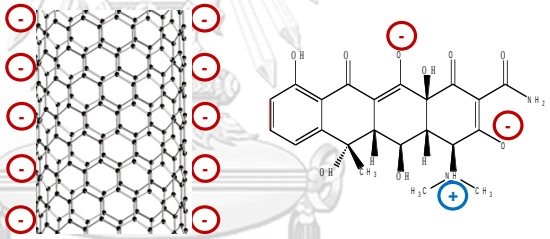

Case 4 pH of solution > pK_{a3} of OTC and pH_{pzc} of M-CNPs

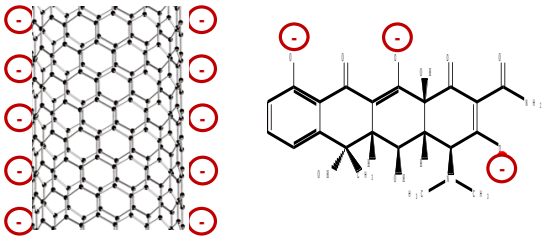

Figure 5.5 Schematic of simplified electrostatic adsorption between a surface of M-CNP and OTC molecules at difference pH conditions

5.5 Adsorption isotherm of OTC on M-CNPs

Examination on adsorption isotherm of OTC could be employed for understanding interaction of OTC onto the surface of M-CNPs. All repeated experimental data were analyzed based on both Langmuir and Freundlich isotherm models which are defined by equation 5.2 and 5.3.

$$\frac{C_e}{Q_e} = \frac{C_e}{Q_m} + \frac{1}{K_L Q_m} \tag{5.2}$$

Where C_e is the concentration of adsorbate at equilibrium (mg/L)

Q_e is the amount of adsorbate adsorbed at equilibrium (mg/g)

Q_m is the maximum adsorption capacity (mg/g)

K_L is the Langmuir adsorption equilibrium constant (L/mg)

$$Q_e = K_F C_e^{\frac{1}{n}} \quad (5.3)$$

Where C_e is the concentration of adsorbate at equilibrium (mg/L)

Q_e is the amount of adsorbate adsorbed at equilibrium (mg/g)

K_F is the Freundlich adsorption capacity parameter (mg/g(mg/L)1/n) and

n is the Freundlich adsorption intensity parameter.

Table 5.1 Key parameters of Langmuir and Freundlich isotherms for adsorption of OTC on synthesized M-CNPs

Langmuir			Freundlich		
Qm (mg/g)	**K_L**	**R^2**	**K_F**	**n**	**R^2**
135.135	0.077	0.999	25.154	2.664	0.965

The constant values of Langmuir and Freundlich isotherm models obtained from our experimental data analyses are summarized in Table 5.1. Based on statistical consideration, it is found that the adsorption of OTC on synthesized M-CNPs would obey the Langmuir model much better than the Freundlich model (R^2_{Lang} = 0.9988 > R^2_{Freu} = 0.9654) as shown in Figure 5.6. The essential feature of the Langmuir isotherms can be indicated by 266.382 mg/g of Q_m and 0.378 of K_L, which could suggest that the synthesized M-CNPs exhibited a good potential for the dsorption of OTC [100].

Figure 5.7 showed Langmuir isotherm fitting between experiment and calculation base on Langmuir isotherm. It was implied that OTC adsorption on M-CNPs fitted with Langmuir isotherm model.

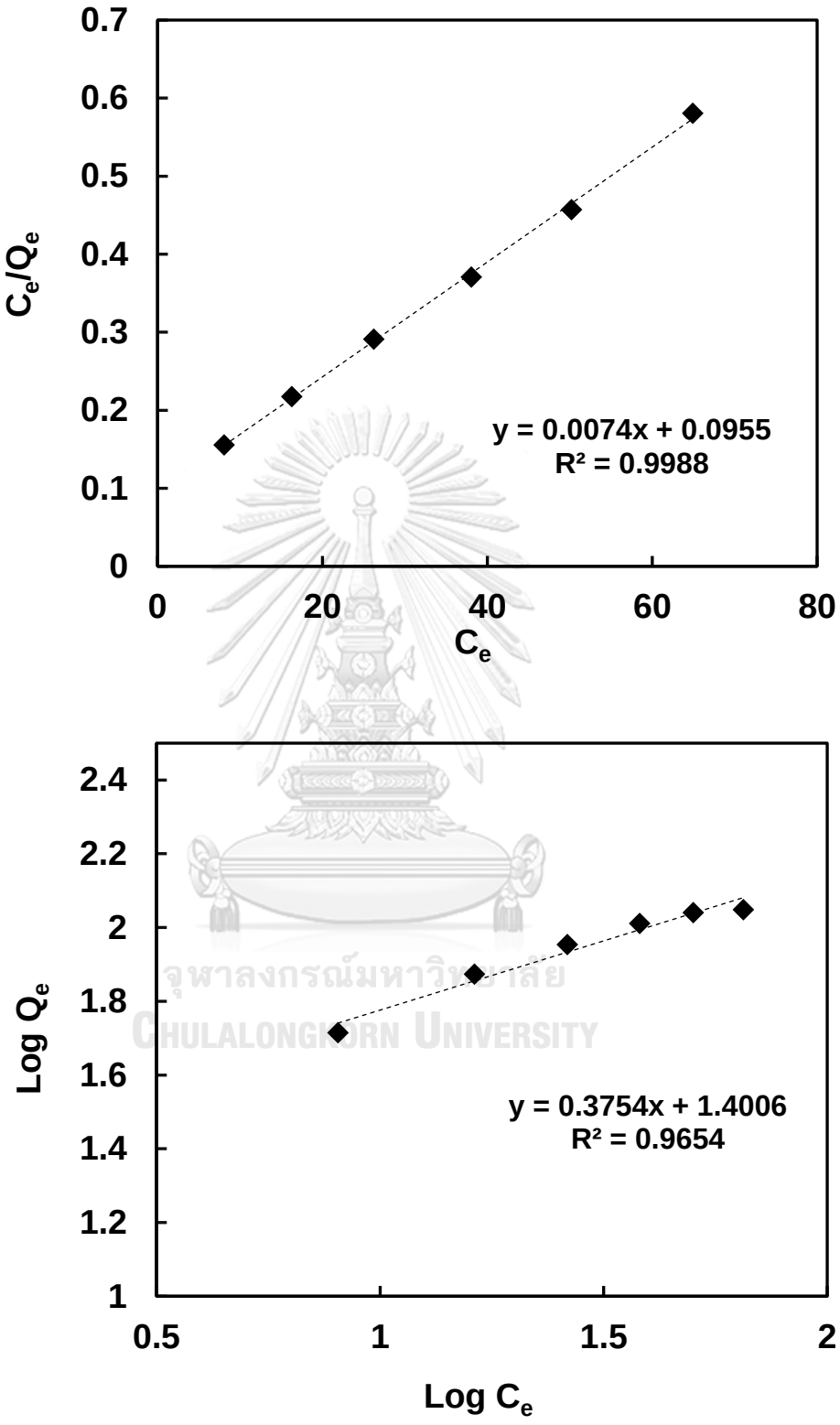

Figure 5.6 Isotherm plots for the adsorption of OTC on synthesized M-CNPs (a) Langmuir isotherm (b) Freundlich isotherm plots

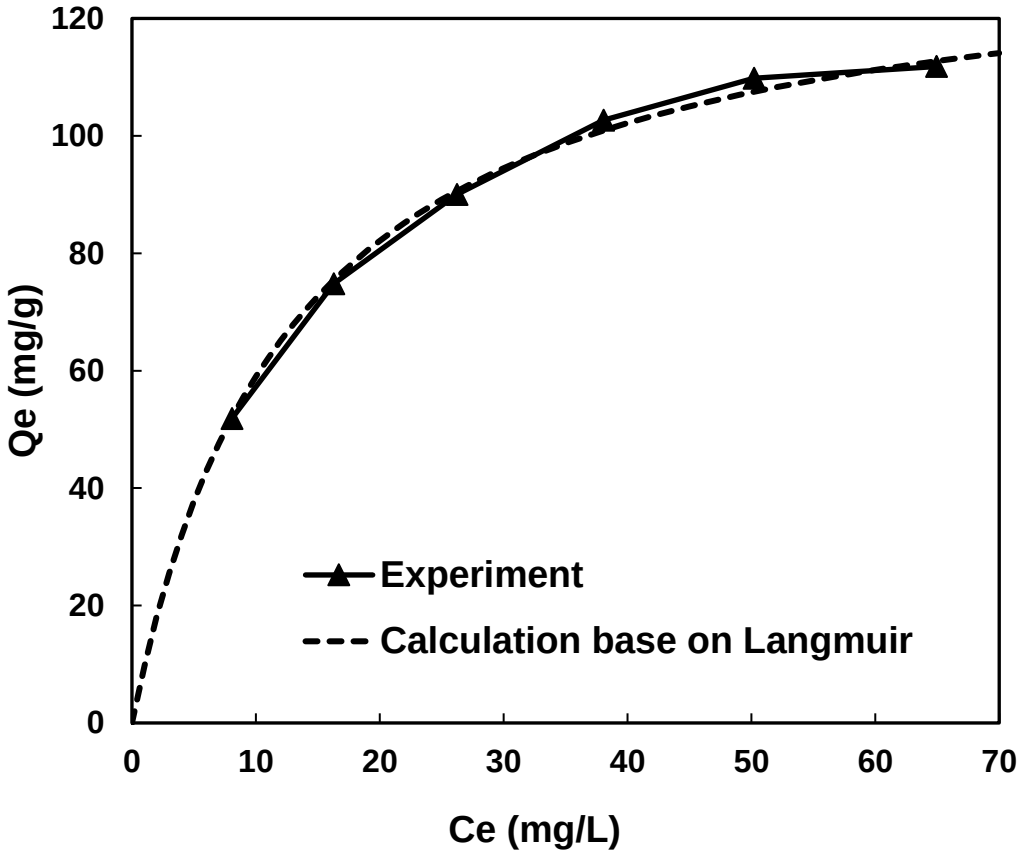

Figure 5.7 Langmuir isotherm fitting plots for the adsorption of OTC on synthesized M-CNPs

5.6 Conclusion

M-CNPs could be synthesized via co-pyrolysis of nebulized glycerol/ferrocene mixture. The OTC adsorption efficiency of synthesized M-CNPs was clearly influenced by the initial pH of OTC solution due to the interaction between OTC molecules and the surface of M-CNPs. Therefore, the adsorption could be promoted under pH in the

range of 3-7. The adsorption of OTC on the synthesized M-CNPs preferably obeyed the Langmuir isotherm model.

Chapter VI

Magnetic carbon nanoparticle for catalytic ozonation on oxy-tetracycline

Oxy-tetracycline (OTC) has been recognized as not only a good antibiotic but also environmental contamination resulted from over-dosage and leakage from agricultural activities. Among various alternatives, catalytic ozonation is a promising method because of its simplicity and effectiveness. In this work, magnetic carbon nanoparticles (M-CNPs) synthesized by nebulizing pyrolysis of glycerol and ferrocene has been applied as a catalyst for enhancing ozonation of OTC. Effects of catalyst loading and initial concentration of OTC on degradation have been experimentally examined in comparison with other typical carbonaceous powders which are carbon black and graphite. While the change of OTC concentration were analyzed using high performance liquid chromatography (HPLC) analyzer for examining its characteristics, fresh and spent carbonaceous catalysts were also characterized using electron microscopy, surface area and porosity analyzer, and x-ray diffraction (XRD) analyzer.

6.1 Research background

In aquaculture, antibiotic usage tends to increase and leads to environmental problem. Among various antibiotics, OTC is the most wildly used in agricultural activities for antibiotic application to enhance survival rate of embryo meanwhile it

normally decays very slowly in nature due to its complex chemical structure. As a result, there are many research teams have tried to develop efficient technique to remove OTC [101]. Catalytic ozonation is a promising method for the removal of various inorganic and organic pollutants contaminated in water owing to its simplicity and effectiveness [102, 103]. Carbon nanoparticle (CNP) is one of outstanding carbonaceous materials regarding to its high porosity, hierarchical porous structure and large specific surface area, which are beneficial to the removal of various inorganic and organic pollutants[48, 96, 103]. Based on some previous investigation CNPs can be used to remove several kinds of pollution including heavy metals, organic and inorganic compounds that are in gas, liquid, and solid phase. Adsorption capacity of CNPs would be varied depending upon different types of adsorbate, i.e. polarity and molecular size [104]. Meanwhile, pollutant adsorption capacity of CNPs would be better understood by investigating effects of properties of CNPs as well as relevant variables and parameters of adsorption. To achieve scalable production of such CNPs, many methods, i.e. arc discharge, pyrolysis and laser ablation, have been developed. Pyrolysis is one of the most promising methods because of its flexibility with regard to various raw materials to be supplied. In general, raw material containing carbon atoms would be decomposed to atomic carbon clusters at a regulated temperature in prior to the self-assembly process of CNPs. Such carbon clusters would preferably grow on the surface of metal catalyst which should be introduced into the reactor together with carbon source. Meanwhile, it should be noted glycerol is a major by-product of

bio-diesel manufacturing process which has been of interest for increasing its value-added. Therefore, this work seeks possibility to investigate an alternative method for increasing value-added of glycerol as carbon source for synthesizing CNPs. Based on previous works, CNPs synthesized from pyrolysis of carbon source and ferrocene could exert response to magnetic field [76]. Such magnetic property of CNPs would provide not only catalytic activity but also capability to be separated from water by applying magnetic field. As a result, a combination between magnetic separation and catalytic ozonation would provide a great potential interest for novel purification applications. In this work, pyrolysis of glycerol with ferrocene was employed for synthesizing magnetic carbon nanoparticles (M-CNPs) then an application of M-CNPs as a catalyst for enhancing ozonation of OTC as antibiotic pollutant in water was also experimentally examined.

6.2. Research methodology

M-CNPs could be synthesized using an experimental set-up consisting of an electrical furnaces and a quartz tube (10.75 mm in I.D., 570 mm in length). Glycerol (Qrex, 99.5% purity) and ferrocene (Sigma-Aldrich, 98% purity) have been used as source of carbon and Fe catalyst, respectively. 2 ml of glycerol and ferrocene mixture was fed into the tubular quartz tube reactor with a flow rate of 0.003 ml/min by a syringe pump. Based on our previous investigation, an appropriate condition which

could provide an optimal yield of synthesized M-CNPs was already reported in chapther 4. In short, for ensuring the complete decomposition of both compounds, temperature at the feeding position was set at 305 °C, which was sufficiently higher than the boiling temperature of glycerol (290 °C). To stimulate the self-assembly reaction of CNPs, temperature in the reaction zone of the reactor was regulated at 800 °C while nitrogen gas with a flow rate of 30 ml/min was introduced for conveying continuously the resultant M-CNPs to the outlet. In each repeated experiment the CNP synthesis was carried out for 66 min then the reactor was cooled down to the room temperature before the collection of the resultant products.

Ozonation of OTC dissolved in water was conducted in a semi-batch reactor to investigate performance of each carbonaceous material as shown in Figure 6.1. Ozone was generated from oxygen gas using corona-discharge equipment with a regulated concentration of 0.5 g/m^3 confirmed by an ozone meter. Ozone with a flow rate of 20 mL/min was introduced through a sintered glass filter to the reactor containing 200 mL of 100 ppm OTC solution. 10 mg of each carbonaceous material, which was M-CNPs, carbon black and graphite powder, could be dispersed in the OTC solution by bubbling due to the gas flow which could ensure complete mixing of carbonaceous material suspension. Change of OTC concentration could be determined by analyzing liquid sample collected at designated time with HPLC (SPD-20A, Shimadzu Corp.). After terminating the ozonation, M-CNPs were separated from the liquid samples using a permanent magnetic for further characterization.

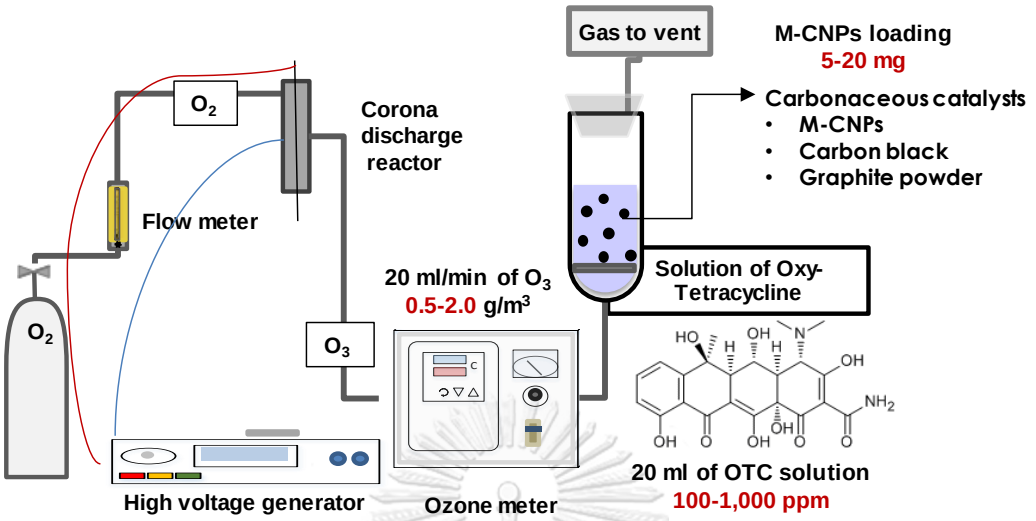

Figure 6.1 Schematic diagram of experimental set-up for catalytic ozonation of OTC

6.3 Characteristic of magnetic carbon nanoparticles in ozonation process

Morphology of synthesized CNPs could be confirmed by TEM and SEM. It could be obviously observed that typical sample of CNPs synthesized from co-pyrolysis of glycerol and ferrocene consists of multi-walled carbon nanotubes and metal nanoparticles. The synthesized CNPs exhibit high BET surface of 22.3 m^2/g, with high graphitic carbon content and high AC-magnetic susceptibility while the average size of metal nanoparticles is approximately 19.2 nm. Ratio of Raman spectral intensity (I_G/I_D), which was employed for determining a relative amount of graphitic carbon nanostructures to disorder carbon structure within the synthesized CNP sample, suggested that the synthesized CNPs contained higher content of graphitic carbon nanostructure [48]. Meanwhile, the AC magnetic susceptibility ($X_{r,0}$) of CNPs which could be characterized by complex number (X_r and X_i) as a function of frequency [21].

$X_{r,0}$ with a value of 68.0 g^{-1} suggests that the synthesized CNPs could strongly interact with magnetic field, which would be useful for its separation using magnetic field application. As a result, it is reasonably implied that the synthesized CNPs could exhibit magnetic response or could be recognized as magnetic carbon nanoparticles or M-CNPs.

6.4 Catalytic ozonation of OTC

OTC removal within our designated experimental set-up could be considered as a combination of adsorption onto the carbonaceous surface of CNPs and oxidation by ozoneExperimental results shown in Figure 6.2 reveal that the removal rate of OTC was much enhanced when M-CNPs were employed as catalyst when compared to the ozonation alone. Regarding to the fact that each carbonaceous material mainly consists of the same carbon constituent, the same mechanism of OTC adsorption would be implied because OTC is a macromolecular organic compound with molecular weight of 460.44, which would be adsorbed on carbon surface. For comparison of performance of each carbonaceous material, the decrease in OTC concentration with the presence of graphite powder, carbon black and M-CNPs was taken into account for discussion.

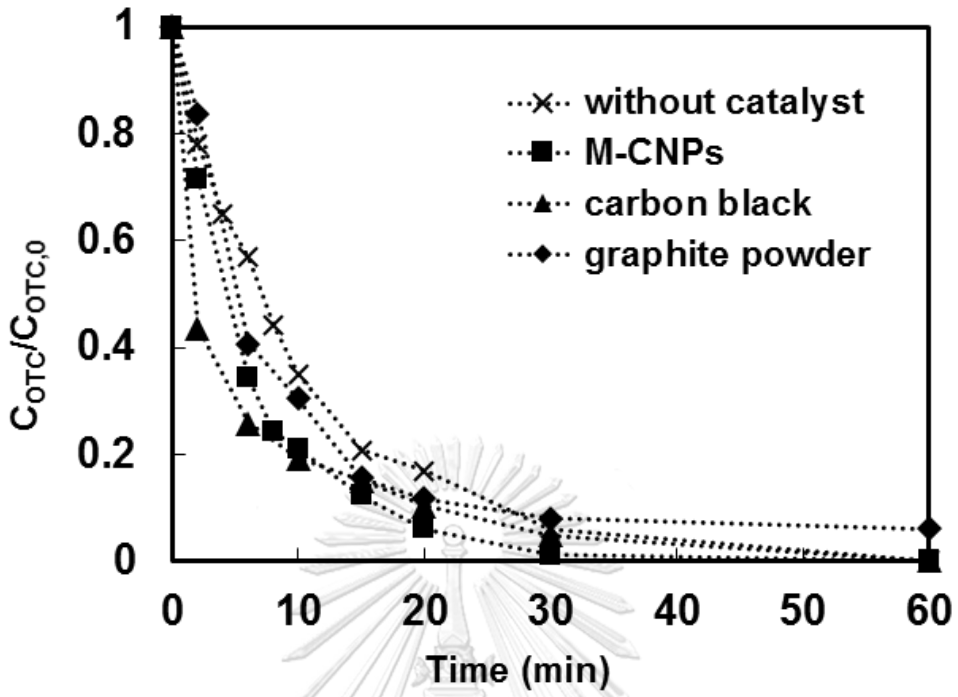

Figure 6.2 Effect of types of carbonaceous material on removal of OTC with ozonation

Interestingly, our experimental results reveal that at the beginning the decrease in the OTC concentration with the presence of carbon black was faster than those with the presence of M-CNPs and graphite powder. This would be ascribed to an advantage of carbon black which contains higher specific surface area (102.1 m^2/g) when compared to those of 22.3 m^2/g of M-CNPs and 9.4 m^2/g of graphite powder. However, with sufficient removal time, it could be clearly observed that completion of OTC removal with the presence of M-CNPs could be achieved within 30 min while the completion with the presence of carbon black or graphite powder would require 60 min. These

results would further suggest M-CNPs would exert superior OTC removal due to additional mechanism which would be catalytic decomposition of OTC owing to catalytic role of Fe nanoparticles embedded within M-CNPs.

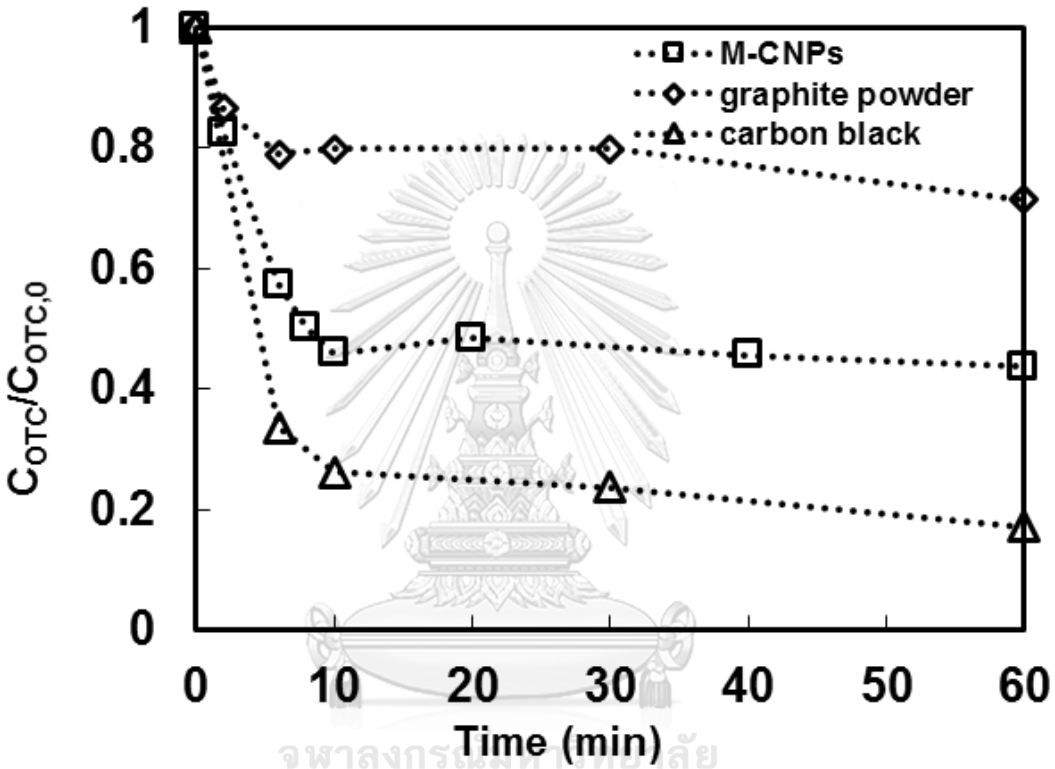

Figure 6.3 Effect of types of carbonaceous material on removal of OTC with adsorption

Based on all of our experimental results, removal mechanism of OTC via ozonation in the presence of M-CNPs is a combination of homogeneous and heterogeneous reactions. The ozonation reaction of OTC could be considered in two parallel pathways, which are direct and indirect ozonation. On one hand, a part of OTC could

be directly oxidized by contacting with dissolved ozone molecules and some hydroxyl radicals which could also be generated by hydration [105]. On the other hand, with the presence of carbonaceous materials, i.e. carbon black, graphite powder and synthesized M-CNPs, the other part of OTC could also be physically adsorbed onto the surface of those materials which mainly consist of carbonaceous constituents. However, with the presence of M-CNPs embedded with Fe nanoparticles which would behave as catalyst for converting ozone to hydroxyl radical. Hence, M-CNPs could exert superior performance in OTC removal when compared to other carbonaceous adsorbents or ozonation alone [49, 105, 106]. For confirmation of catalytic enhancement effect of Fe nanoparticles, additional experiments of OTC removal using only carbonaceous materials without introduction of ozone were also conducted. Experimental results shown in Figure 6.3 clearly reveal that removal of OTC by each carbonaceous material could exert only a certain contribution due to adsorption which would be limited by its adsorption equilibrium.

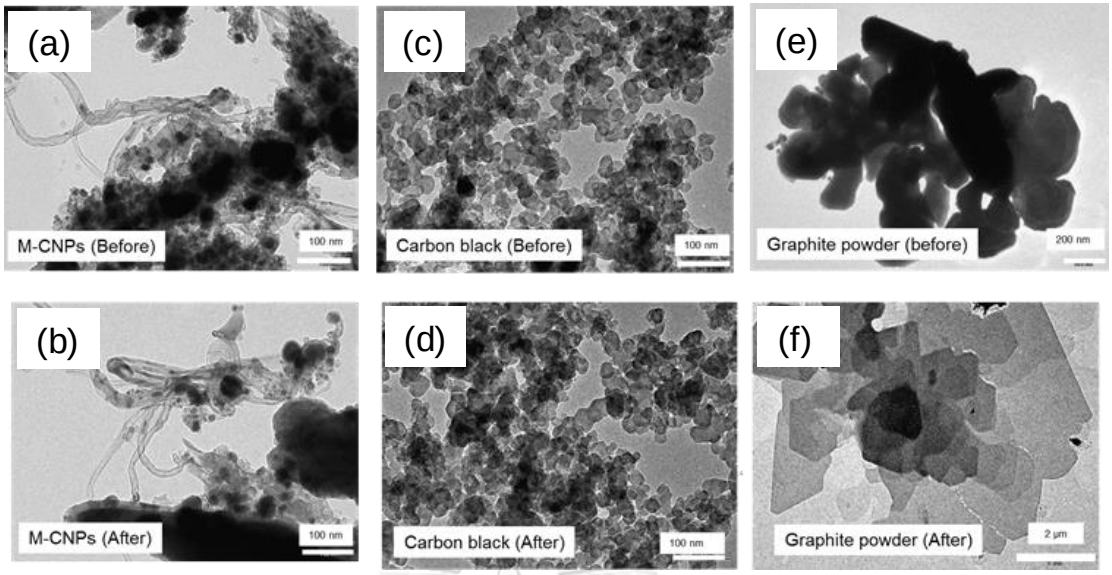

Figure 6.4 TEM images of before and after ozonation of (a-b) M-CNPs (c-d) carbon black (d-e) graphite powder, respectively

An integration of all experimental results discussed above would suggest that the superior performance of M-CNPs for OTC removal would be attributed to the co-existence of carbonaceous and Fe constituents, which could exert both adsorption and catalytic ozonation [49, 105-107]. Meanwhile, investigation on transformation of carbonaceous materials after subject to the ozonation would also be necessary for their reutilization. TEM micrographs depicted in Figure 6.*4* reveal the surface morphology of each carbonaceous material before and after ozonation. Figure 6.*4* (a), (c) and (e) represent fresh M-CNPs, carbon-black, and graphite powder, respectively while Figure 6.*4* (b), (d) and (f) are spent M-CNPs, carbon-black, and graphite powder, respectively. It should be noted that there is no significant change in surface

morphology of M-CNPs, suggesting that they could persist reactive interaction with ozone. Similar result could also be observed in the case of carbon black. However, comparison of surface morphology of fresh and spent graphite powder reveals distinguishable difference. Thin and separated layers of graphene sheets could be observed in typical TEM micrograph of spent graphite powder, suggesting that ozone would play a certain role in peeling graphene sheets from the graphite powder [108]. Emergence of additional carbonaceous derivatives would provide some contributions depending upon their contact with OTC. For confirmation, analyses of specific surface of carbon black and graphite powder, which would exhibit a decreasing trend caused by damage of their structure due to ozonation, would be further reported in the future. Finally, confirmation of simplicity in separation of dispersed M-CNPs using an external permanent magnet was also confirmed as illustrated in Figure 6.5.

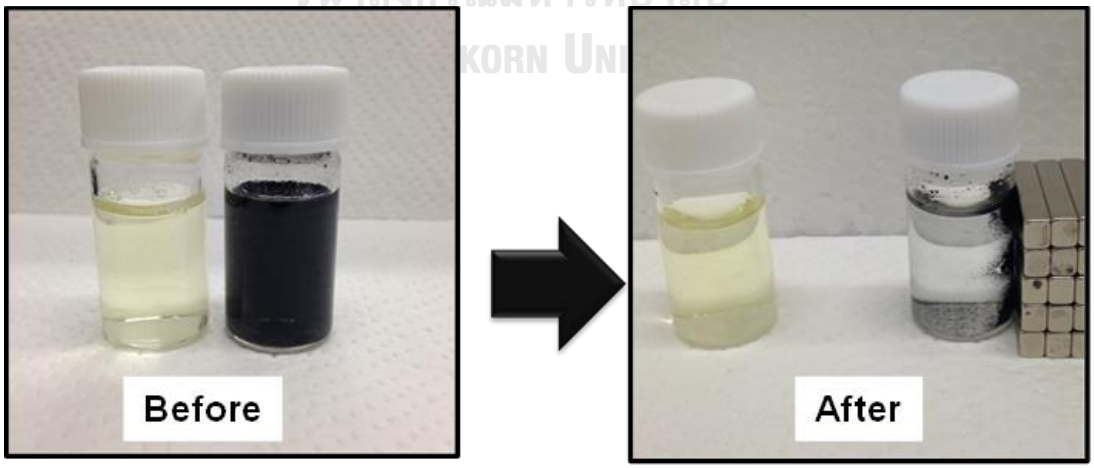

Figure 6.5 Separation of M-CNPs from OTC wastewater by using force of permanent magnetic

The separation could be completed within 10 sec. It should be further noted that at first the simulated wastewater containing OTC exhibited a yellowish color but after the M-CNPs loading the resultant liquid turned black. After separation by the magnetic bars, color of the resultant liquid became transparent while all of M-CNPs were collected on the wall of the container nearby the magnetic bars. Nevertheless, it should be noted that the intensity of OTC in the simulated wastewater is not linearly proportional to its concentration. This result would also confirm that M-CNPs would be a promising material for removal of water pollutants with a simple separation burden.

6.5 Optimum conditions on OTC degradation

6.5.1 Influence concentration of ozone on OTC degradation

The degradation of OTC by ozone was investigated at difference ozone concentrations in a range of 0.5 – 2 g/m^3 with constant feed flow rate of ozone at 20 ml/min. In generally ozone act as oxidizing agent and it can oxidize molecule of OTC for degradation and remove OTC molecule. Based on exerimental data, it was found that high efficiency of OTC degradation was observed when using high concentration of ozone concentration, as illustrated in Figure 6.6. The ozone concentration at equilibrium in solution was also incresed following the Henry's raw when increses ozone concentration in feeding of ozone gas at the inlet. The increasing ozone concentration at equilibrium in solution resulted in increasing of mass transfer driving

force in system. Therefor the increasing volumetric mass transfer coefficient of ozone from gas phase to liquid phase [103, 109]. Thus, the removal rate was increased with the increasing concentration of ozone. The rate constant of the OTC removal with M-CNPs was apparent in pseudo-first-order kinetics which was $(4.7\pm0.2)\times10^{-3}$ s^{-1} according to the following equation (6.1) and (6.2). R^2 ranged from 0.985 to 0.991. Calculated data base on pseudofirst-order kinetics was well fitting with experimental results [21]

$$-\frac{d[OTC]}{dt} = k[O_3][OTC] \qquad (6.1)$$

$$-\frac{d[OTC]}{dt} = k'[OTC], \quad k' = k[O_3] \qquad (6.2)$$

where [OTC] is OTC concentration at time t

k' is the pseudo-first-order rate constant. The high correlation coefficients

.

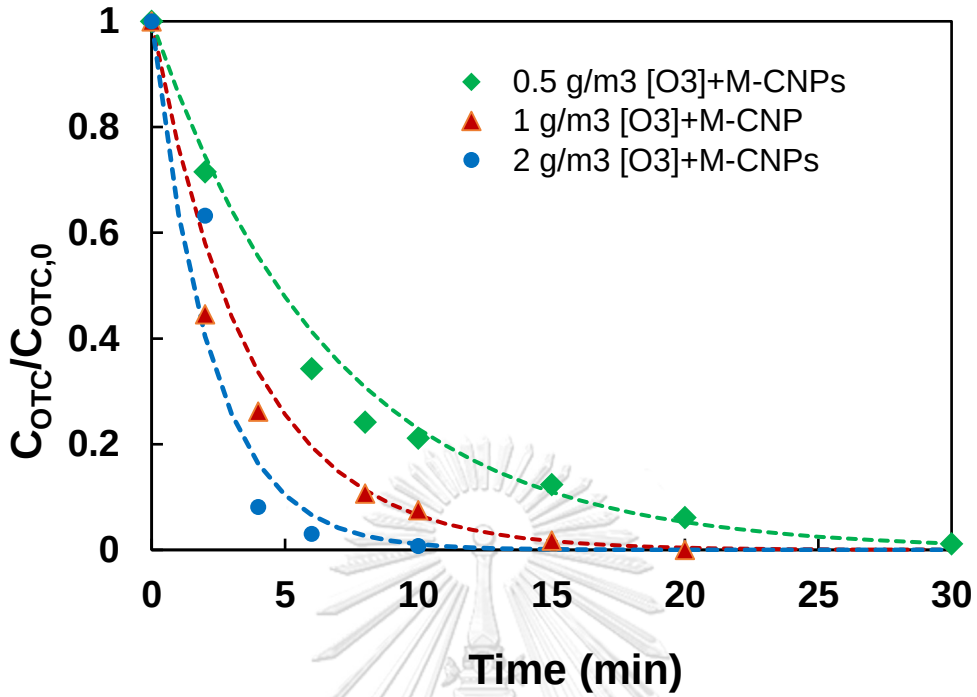

Figure 6.6 Influence concentration of ozone on OTC degradation

6.5.2 Influence of M-CNPs loading on OTC degradation

As shown in Figure 6.7 the degradation rate increased with the increasing amout of M-CNPs loading, when amout of M-CNPs loading were increased from 5 to 10 and 20 mg per 20 ml of OTC solution, respectively. Degradation of OTC by ozonation can be regarded as a mass transfer process combiled with chemical reactions. Ozone was dissolved into the aqueous phase and oxidized OTC compound on surface of M-CNPs. It is generally well accepted that the ozone reaction can occur on M-CNPs catalyst depending upon the relative rates of mass transfer and chemical reaction involved [109, 110]. The embeded Iron on M-CNPs in aqueous solotion is able to convert ozone to hydroxyl radicals. It is implied that more adding of M-CNPs could improveirates of mass transfer and chemical reaction of OTC removal.

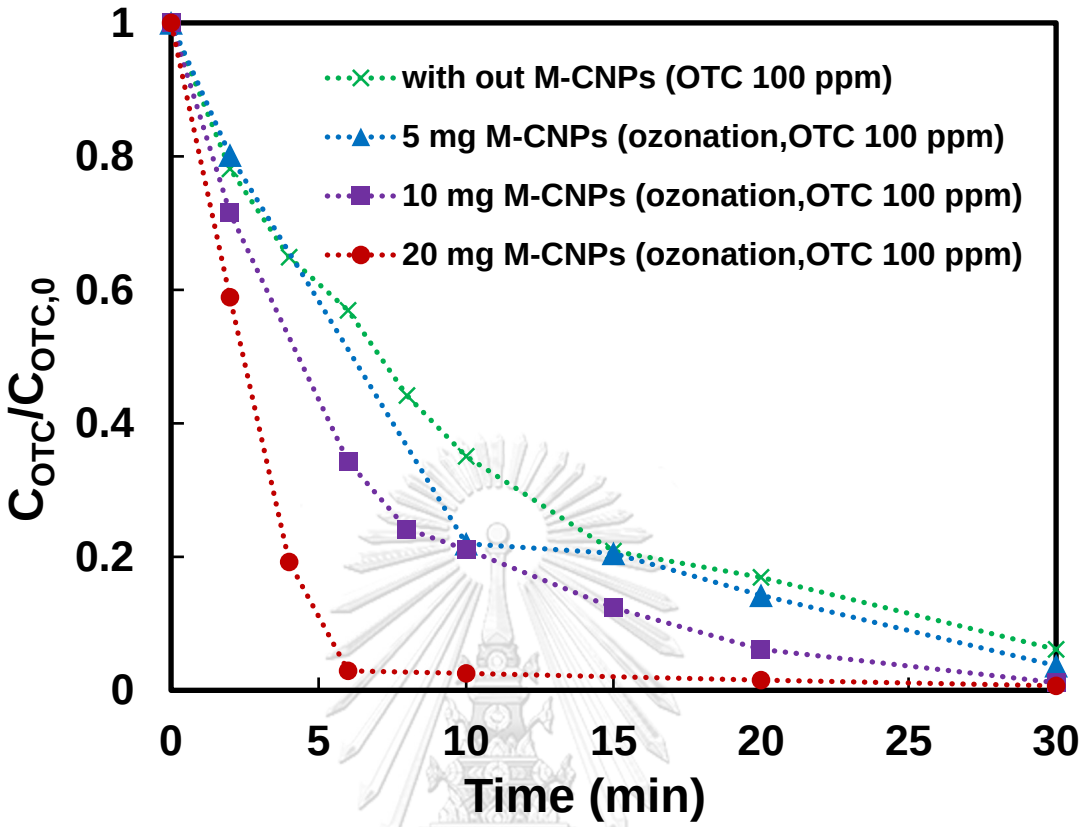

Figure 6.7 Influence of M-CNPs loading on OTC degradation

6.5.3 Influence of initial concentration of OTC on degradation degradation

Invastigation the effect of initial concentration of OTC on degradation were studied by varying initial OTC concentrations in the range of 100-1,000 ppm and keeping constant amout of M-CNPS at 10 mg. Figure 6.8 shows the effect of the initial OTC concentration on M-CNPs catalytic degradation efficiency. A trend of OTC degradation was observed that when increasing initial OTC concentration, the time for completed OTC removal was longer. When the initial OTC concentration was increased

from 100 to 500 and 1000 ppm, completed OTC degradation would require reaction duration at 30, 60 and 120 min, respectively.

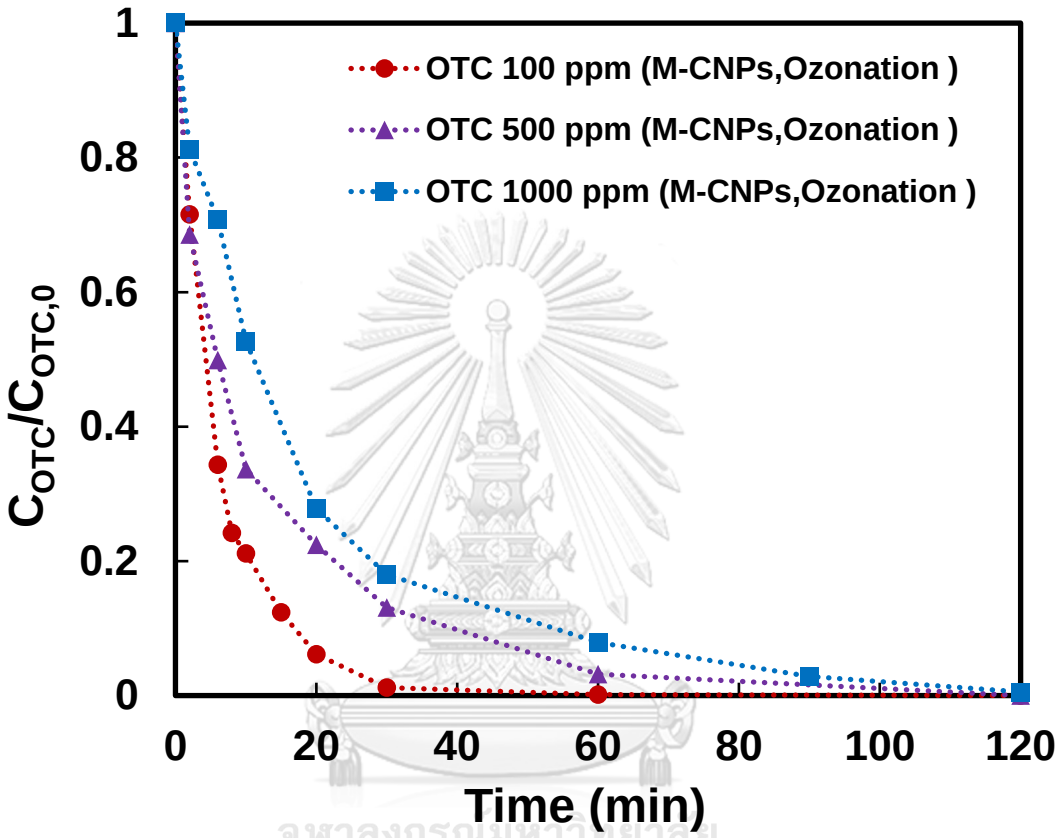

Figure 6.8 Influence initial concentration of OTC on degradation

6.6 Recyclic ability of M-CNPs on OTC degradation

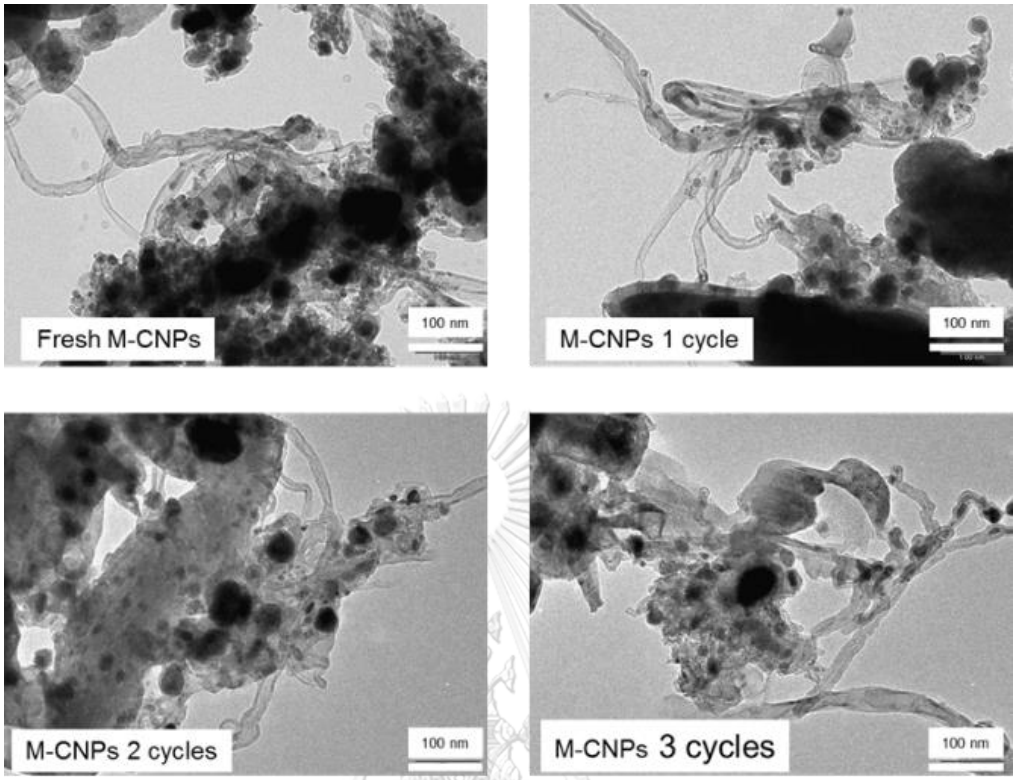

Figure 6.9 TEM images of fresh M-CNPs and M-CNPs used for 3 cycles

Figure 6.9 show morphology of M-CNPs that is fresh and spent for one to three cycles respectively. These could be observed that the morphology trend to change more clearly when M-CNPs were spent more often. Therefor, It could be implied that structure of M-CNPs was damaged by oxidation of ozone.

Table 6.1 Comparison of M-CNPs properties before and after used.

	BET surface ($m^2.g^{-1}$)	$X_{r,0}$ (g^{-1})
Fresh M-CNPs	22.3	56.1
M-CNPs 1 cycle	27.2	39.9
M-CNPs 2 cycles	22.1	34.0
M-CNPs 3 cycles	13.6	31.4

Table 6.1 shows specific surface area and AC-magnetic susceptibility of fresh M-CNPs and spent M-CNPs for one to three cycles. It was found that specific surface area of M-CNPs trends to decrease relatively to numbers of cycle. Results of morphology changing and specific surface area decreasing cause by ozone damage on M-CNPs structure [107]. Table 6.*1* also shows that AC-magnetic susceptibility trend to decrease relatedly to the increasing of numbers of cycle. The decreasing of AC-magnetic susceptibility could occur because embedded Fe in M-CNPs was oxidized by ozonation and then converted to iron oxide when M-CNPs was used several time in ozonation process. The results were supported by XRD results. When M-CNPs were used in several time, peak of Fe was decrease because Fe was oxidized and form other structures as shown in Figure 6.10.

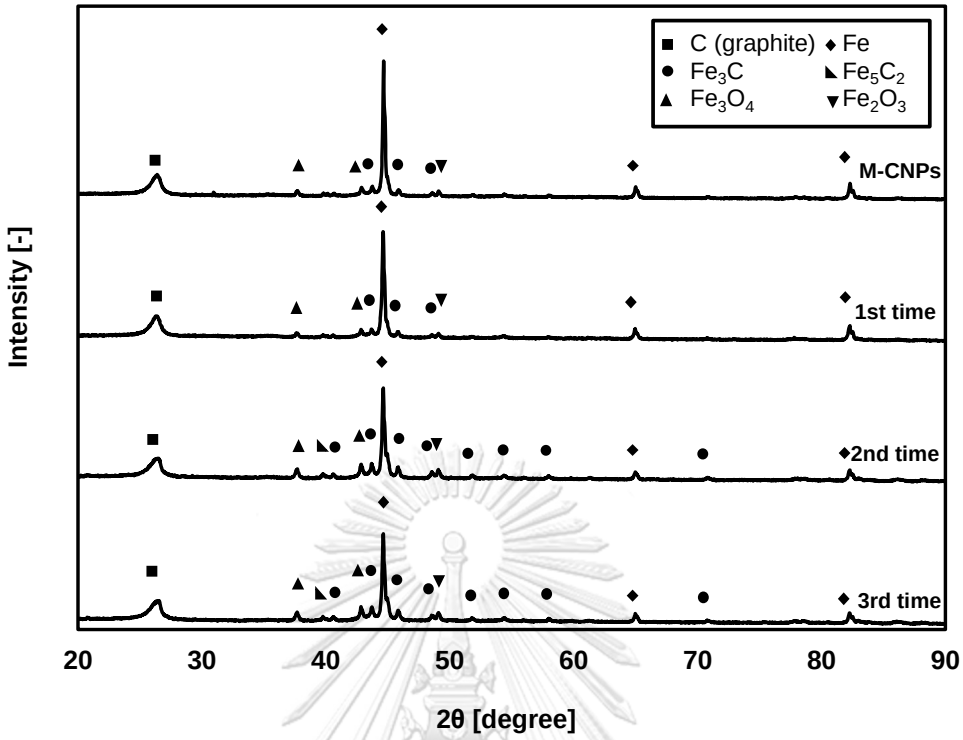

Figure 6.10 XRD pattern of recycles M-CMPS after ozonation process

Figure 6.11 (a-b) shows degradation and adsorption profile of OTC using fresh and spent M-CNPs. It was found that degradation and adsorption profile of OTC are not significantly difference between M-CNPs that is fresh and reused three times through a series of consecutive experiments. The results could be implied to the reusability of M-CNPs owing to the no loss of catalytic activity.

Although specific surface area and AC-magnetic susceptibility which stated in Table 6.1 after three times usage decrease tentatively which could represent the deactivation of catalyst, degradation and adsorption profile seem not to be effect from several times used. These could be suggested that catalyst deactivation has no effect on degradation and adsorption profile of OTC using M-CNPs for three cycles.

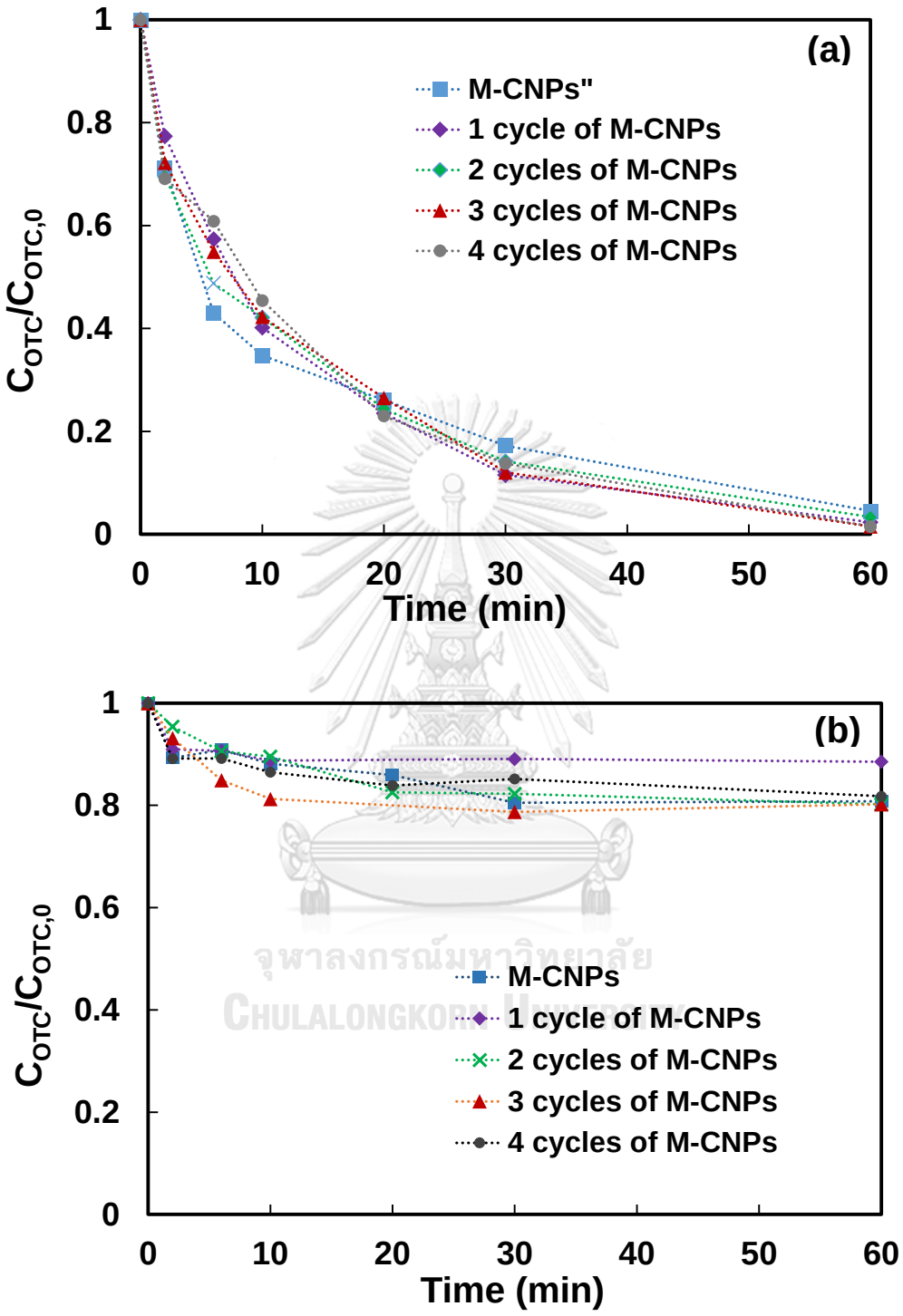

Figure 6.11 (a) Degradation profile of OTC via ozonation and (b) adsorption profile of OTC using fresh and spent M-CNPs for one to three cycles

6.7. Conclusion

M-CNPs could be synthesized using co-pyrolysis of glycerol with ferrocene under a designated temperature of 800 °C and glycerol to ferrocene weight ratio of 3:1. Microscopic analyses confirm that the synthesized M-CNPs possess adsorptive carbonaceous structure with magnetic characteristics due to the presence of Fe nanoparticles. With the presence of carbonaceous materials and ozone in simulated wastewater containing OTC, both adsorption and oxidation would play an integrating role in OTC removal. In addition, M-CNPs could exhibit a superior performance in the removal of OTC by adsorption and catalytic ozonation, resulting in a faster completion of OTC removal within 30 min or 2 times faster when compared with the cases of carbon black and graphite powder as well as ozonation alone. Regeneration of spent M-CNPs by ozone exhibited that OTC removal efficiency of spent M-CNPs was almost same as fresh M-CNPs indicating excellent reusability property of synthesized M-CNPs.

Chapter VII

Conclusion and recommendations

7.1 Conclusion

M-CNPs could be synthesized via co-pyrolysis of nebulized glycerol/ferrocene mixture. The morphology, yield and magnetic susceptibility of M-CNPs synthesized from co-pyrolysis of glycerol and ferrocene were strongly influenced by the synthesizing temperature and initial weight ratio of glycerol to ferrocene. Integration of all experimental confirmation suggests that the synthesizing temperature of 800 °C and initial weight ratio of glycerol to ferrocene at 3:1 was the optimum condition for synthesizing M-CNPs. Under the influence of magnetic induction due to the usage magnetic collectors, M-CNPs with much enhanced yield, higher graphic carbon structure and remarkable magnetic susceptibility could be controlled synthesized.

The OTC adsorption efficiency of synthesized M-CNPs was clearly influenced by the initial pH of OTC solution due to the interaction between OTC molecules and the surface of M-CNPs. Therefore, the adsorption could be promoted under pH in the range of 3-7. The adsorption of OTC on the synthesized M-CNPs preferably obeyed the Langmuir isotherm model.

The catalytic ozonation with the presence of M-CNPs could exhibit a superior performance in the removal of OTC by adsorption and catalytic ozonation, resulting a

faster completion of OTC removal within 30 min or 2 times faster when compared with the cases of carbon black and graphite powder as well as ozonation alone. Moreover, M-CNPs could be easily separated by external permanent magnetic bar.

7.2 Recommendation

Quantitative analyses of such M-CNP self-assembly should be implied with respect to thermodynamics viewpoint. Further theoretical and experimental exploration would probably provide an insight into the selective production of M-CNPs with controllable yield and characteristics. Synthesized M-CNPs should be applied as adsorbent and catalyst for removal various organic compounds and other kinds of antibiotics solution.

REFERENCES

[1] H.W. Kroto, J.R. Heath, S.C. O'Brien, R.F. Curl, R.E. Smalley, Nature 318 (1985) 162-163.

[2] S. Iijima, Nature 354 (1991) 56-58.

[3] S. Iijima, M. Yudasaka, R. Yamada, S. Bandow, K. Suenaga, F. Kokai, K. Takahashi, CPL 309 (1999) 165-170.

[4] J.N. Coleman, U. Khan, W.J. Blau, Y.K. Gun'ko, Carbon 44 (2006) 1624-1652.

[5] Z. Wu, Z. Chen, X. Du, J.M. Logan, J. Sippel, M. Nikolou, K. Kamaras, J.R. Reynolds, D.B. Tanner, A.F. Hebard, A.G. Rinzler, Sci 305 (2004) 1273-1276.

[6] G.M. Mutlu, G.R.S. Budinger, A.A. Green, D. Urich, S. Soberanes, S.E. Chiarella, G.F. Alheid, D.R. McCrimmon, I. Szleifer, M.C. Hersam, Nano Lett. 10 (2010) 1664-1670.

[7] M.F.L. De Volder, S.H. Tawfick, R.H. Baughman, A.J. Hart, Sci 339 (2013) 535-539.

[8] J. Prasek, J. Drbohlavova, J. Chomoucka, J. Hubalek, O. Jasek, V. Adam, R. Kizek, JMCh 21 (2011) 15872-15884.

[9] S.B. Sinnott, R. Andrews, D. Qian, A.M. Rao, Z. Mao, E.C. Dickey, F. Derbyshire, CPL 315 (1999) 25-30.

[10] M. Kumar, Y. Ando, Journal of Nanoscience and Nanotechnology 10 (2010) 3739-3758.

[11] N.J. Morales, S. Goyanes, C. Chiliotte, V. Bekeris, R.J. Candal, G.H. Rubiolo, Carbon 61 (2013) 515-524.

[12] F.C. Dillon, A. Bajpai, A. Koós, S. Downes, Z. Aslam, N. Grobert, Carbon 50 (2012) 3674-3681.

[13] N. Sano, M. Uehara, Chemical Engineering and Processing: Process Intensification 45 (2006) 555-558.

[14] T. Charinpanitkul, N. Sano, P. Puengjinda, J. Klanwan, N. Akrapattangkul, W. Tanthapanichakoon, J. Anal. Appl. Pyrolysis 86 (2009) 386-390.

[15] V.G. Pol, S.V. Pol, A. Gedanken, M.-G. Sung, S. Asai, Carbon 42 (2004) 2738-2741.

[16] L. Hu, R. Zhang, Q. Chen, Nanoscale 6 (2014) 14064-14105.

[17] C. Zhang, Z. Mo, C. Jiang, P. Zhang, R. Guo, CrystEngComm 15 (2013) 6546-6552.

[18] F. Yang, M. Hanna, R. Sun, Biotechnology for Biofuels 5 (2012) 13.

[19] Y. Li, H. Wang, G. Wang, J. Gao, Chem. Eng. J. 211-212 (2012) 255-259.

[20] A. Bazargan, G. McKay, Chem. Eng. J. 195-196 (2012) 377-391.

[21] N. Sano, Y. Hori, S. Yamamoto, H. Tamon, Carbon 50 (2012) 115-122.

[22] M.M.A. Rafique, J. Iqbal, Journal of encapsulation and adsorption sciences 1 (2011) 29.

[23] W. Yang, W.J. Sun, W. Chu, C.F. Jiang, J. Wen, Chin. Chem. Lett. 23 (2012) 363-366.

[24] G. Vijayaraghavan, K.J. Stevenson, Langmuir 23 (2007) 5279-5282.

[25] R.A. Afre, T. Soga, T. Jimbo, M. Kumar, Y. Ando, M. Sharon, P.R. Somani, M. Umeno, Microporous Mesoporous Mater. 96 (2006) 184-190.

[26] X. Liu, Y. Yang, X. Lin, B. Xu, Y. Zhang, Fuel Process. Technol. 87 (2006) 919-925.

[27] A. Szabó, C. Perri, A. Csató, G. Giordano, D. Vuono, J.B. Nagy, Materials 3 (2010) 3092-3140.

[28] N. Sano, M. Naito, T. Kikuchi, Carbon 45 (2007) 78-82.

[29] C. Zhuo, B. Hall, H. Richter, Y. Levendis, Carbon 48 (2010) 4024-4034.

[30] V.N. Popov, Materials Science and Engineering: R: Reports 43 (2004) 61-102.

[31] Y.T. Ong, A.L. Ahmad, S.H.S. Zein, S.H. Tan, Brazilian Journal of Chemical Engineering 27 (2010) 227-242.

[32] K. Kümmerer, Journal of Antimicrobial Chemotherapy 54 (2004) 311-320.

[33] P.H. Serrano, Responsible use of antibiotics in aquaculture, Food & Agriculture Org., 2005.

[34] D.L. Giokas, A.G. Vlessidis, Talanta 71 (2007) 288-295.

[35] L. Zhang, X. Song, X. Liu, L. Yang, F. Pan, J. Lv, Chem. Eng. J. 178 (2011) 26-33.

[36] M. Jafari, S.F. Aghamiri, G. Khaghanic, World Applied Sciences Journal 14 (2011) 1642-1650.

[37] S.A.C. Carabineiro, T. Thavorn-amornsri, M.F.R. Pereira, P. Serp, J.L. Figueiredo, Catal. Today 186 (2012) 29-34.

[38] E.E. Ghadim, F. Manouchehri, G. Soleimani, H. Hosseini, S. Kimiagar, S. Nafisi, PloS one 8 (2013) e79254.

[39] E.K. Putra, R. Pranowo, J. Sunarso, N. Indraswati, S. Ismadji, Water Research 43 (2009) 2419-2430.

[40] J. Radjenović, M. Petrović, F. Ventura, D. Barceló, Water Research 42 (2008) 3601-3610.

[41] J.L. Acero, F.J. Benitez, F.J. Real, G. Roldan, Water Research 44 (2010) 4158-4170.

[42] I. Arslan-Alaton, F. Gurses, J. Photochem. Photobiol. A: Chem. 165 (2004) 165-175.

[43] H. Tekin, O. Bilkay, S.S. Ataberk, T.H. Balta, I.H. Ceribasi, F.D. Sanin, F.B. Dilek, U. Yetis, Journal of Hazardous Materials 136 (2006) 258-265.

[44] D. Klauson, J. Babkina, K. Stepanova, M. Krichevskaya, S. Preis, Catal. Today 151 (2010) 39-45.

[45] G. Saracco, L. Solarino, R. Aigotti, V. Specchia, M. Maja, Electrochimica Acta 46 (2000) 373-380.

[46] K. Li, A. Yediler, M. Yang, S. Schulte-Hostede, M.H. Wong, Chemosphere 72 (2008) 473-478.

[47] N. Sano, T. Yamamoto, H. Shinomiya, A. Endo, A. Eiad-Ua, A. Soottitantawat, T. Charinpanitkul, W. Tanthapanichakoon, T. Ohmori, H. Tamon, JOURNAL OF CHEMICAL ENGINEERING OF JAPAN 42 (2009) s17-s22.

[48] S. Zhang, D. Wang, X. Quan, L. Zhou, X. Zhang, Sep. Purif. Technol. 116 (2013) 351-359.

[49] X. Wang, C. Chen, J. Li, X. Wang, Chem. Eng. J. 262 (2015) 1303-1310.

[50] T.J. Federici, Pharmacological Research 64 (2011) 614-623.

[51] W.-R. Chen, C.-H. Huang, Chemosphere 79 (2010) 779-785.

[52] Y. Gao, Y. Li, L. Zhang, H. Huang, J. Hu, S.M. Shah, X. Su, Journal of Colloid and Interface Science 368 (2012) 540-546.

[53] J.M.M.C. Engineers, Water treatment principles and design, Wiley, 1985.

[54] K.Y. Foo, B.H. Hameed, Chem. Eng. J. 156 (2010) 2-10.

[55] J. Guo, X. Wang, Y. Yao, X. Yang, X. Liu, B. Xu, MCP 105 (2007) 175-178.

[56] K. Kerdnawee, C. Termvidchakorn, P. Yaisanga, J. Pakchamsai, C. Chookiat, A. Eiad-ua, W. Wongwiriyapan, W. Chaiwat, S. Ratchahat, K. Faungnawakij, K. Suttiponparnit, T. Charinpanitkul, KONA Powder and Particle Journal (2017).

[57] M. Kusaba, Y. Tsunawaki, TSF 506–507 (2006) 255-258.

[58] Y. Li, H. Wang, G. Wang, J. Gao, Chem. Eng. J. 211–212 (2012) 255-259.

[59] J. Zhang, J. Li, J. Cao, Y. Qian, MatL 62 (2008) 1839-1842.

[60] C. Quan, A. Li, N. Gao, J. Hazard. Mater. 179 (2010) 911-917.

[61] J.O. Alves, C. Zhuo, Y.A. Levendis, J.A.S. Tenório, Applied Catalysis B: Environmental 106 (2011) 433-444.

[62] T. Altalhi, T. Kumeria, A. Santos, D. Losic, Carbon 63 (2013) 423-433.

[63] J. Gong, J. Feng, J. Liu, Z. Jiang, X. Chen, E. Mijowska, X. Wen, T. Tang, Chem. Eng. J. 248 (2014) 27-40.

[64] G.S. Bajad, S.K. Tiwari, R.P. Vijayakumar, Materials Science and Engineering: B 194 (2015) 68-77.

[65] Y.T. Lee, N.S. Kim, J. Park, J.B. Han, Y.S. Choi, H. Ryu, H.J. Lee, CPL 372 (2003) 853-859.

[66] N.J. Morales, S. Goyanes, C. Chiliotte, V. Bekeris, R.J. Candal, G.H. Rubiolo, Carbon 61 (2013) 515-524.

[67] N. Sano, H. Akazawa, T. Kikuchi, T. Kanki, Carbon 41 (2003) 2159-2162.

[68] Y. Xiao, Y. Liu, L. Cheng, D. Yuan, J. Zhang, Y. Gu, G. Sun, Carbon 44 (2006) 1589-1591.

[69] V. Popov, Materials Science and Engineering: R: Reports 43 (2004) 61-102.

[70] H. Zhang, Y. Ding, C. Wu, Y. Chen, Y. Zhu, Y. He, S. Zhong, Physica B: Condensed Matter 325 (2003) 224-229.

[71] N. Parkansky, R.L. Boxman, B. Alterkop, I. Zontag, Y. Lereah, Z. Barkay, J. Phys. D: Appl. Phys. 37 (2004) 2715.

[72] L.A. Montoro, R.C.Z. Lofrano, J.M. Rosolen, Carbon 43 (2005) 200-203.

[73] Y.Y. Tsai, J.S. Su, C.Y. Su, W.H. He, J. Mater. Process. Technol. 209 (2009) 4413-4416.

[74] L.L. Lebel, B. Aissa, M.A.E. Khakani, D. Therriault, Composites Sci. Technol. 70 (2010) 518-524.

[75] A. Barreiro, D. Selbmann, T. Pichler, K. Biedermann, T. Gemming, M.H. Rümmeli, U. Schwalke, B. Büchner, Appl. Phys. A 82 (2005) 719-725.

[76] P. Puengjinda, N. Sano, W. Tanthapanichakoon, T. Charinpanitkul, Journal of Industrial and Engineering Chemistry 15 (2009) 375-380.

[77] K.-E. Kim, K.-J. Kim, W.S. Jung, S.Y. Bae, J. Park, J. Choi, J. Choo, CPL 401 (2005) 459-464.

[78] J. Qiu, G. Chen, Z. Li, Z. Zhao, Carbon 48 (2010) 1312-1315.

[79] T. Charinpanitkul, N. Sano, P. Muthakarn, W. Tanthapanichakoon, MaRBu 44 (2009) 324-327.

[80] M.A. Nahil, C. Wu, P.T. Williams, Fuel Process. Technol. 130 (2015) 46-53.

[81] C. Zheng, W. Qian, Y. Yu, F. Wei, Particuology 11 (2013) 409-414.

[82] F. Yang, M.A. Hanna, R. Sun, Biotechnology for biofuels 5 (2012) 13.

[83] S.Y. Sawant, R.S. Somani, A.B. Panda, H.C. Bajaj, MatL 94 (2013) 132-135.

[84] V.G. Pol, S.V. Pol, A. Gedanken, M.-G. Sung, S. Asai, Carbon 42 (2004) 2738-2741.

[85] L. Hu, R. Zhang, Q. Chen, Nanoscale 6 (2014) 14064-14105.

[86] M. Paradise, T. Goswami, Materials & Design 28 (2007) 1477-1489.

[87] L. Ji, W. Chen, S. Zheng, Z. Xu, D. Zhu, Langmuir 25 (2009) 11608-11613.

[88] G.M. Mutlu, G.R. Budinger, A.A. Green, D. Urich, S. Soberanes, S.E. Chiarella, G.F. Alheid, D.R. McCrimmon, I. Szleifer, M.C. Hersam, Nano Lett. 10 (2010) 1664-1670.

[89] K. Kuwana, K. Saito, Proceedings of the Combustion Institute 31 (2007) 1857-1864.

[90] N. Sano, D. Himara, H. Tamon, Chem. Eng. J. 271 (2015) 43-49.

[91] H. Liu, Y. Zhang, R. Li, X. Sun, H. Abou-Rachid, Particuology 9 (2011) 465-470.

[92] L. Ma, A. Chen, J. Lu, Z. Zhang, H. He, C. Li, Particuology 14 (2014) 24-32.

[93] W.Z. Li, J.G. Wen, Z.F. Ren, ApPhA 74 (2002) 397-402.

[94] R. Rajarao, B.R. Bhat, Journal of Metals, Materials and Minerals 22 (2012).

[95] R. Soltani, M.A. Faghihi Sani, F. Mohaghegh, Fullerenes, Nanotubes and Carbon Nanostructures 23 (2014) 245-252.

[96] N. Sano, K. Yamada, T. Suntornlohanakul, H. Tamon, Chem. Eng. J. 283 (2016) 978-981.

[97] F. Yu, Y. Li, S. Han, J. Ma, Chemosphere 153 (2016) 365-385.

[98] R. Ocampo-Pérez, R. Leyva-Ramos, J. Rivera-Utrilla, J.V. Flores-Cano, M. Sánchez-Polo, Chem. Eng. Res. Des. 104 (2015) 579-588.

[99] Y. Sun, Q. Yue, B. Gao, Q. Li, L. Huang, F. Yao, X. Xu, J. Colloid Interface Sci. 368 (2012) 521-527.

[100] M.A. Tofighy, T. Mohammadi, MaRBu 68 (2015) 54-59.

[101] Z.I. Kimera, R.H. Mdegela, C.J. Mhaiki, E.D. Karimuribo, F. Mabiki, H.E. Nonga, J. Mwesongo, Onderstepoort J Vet Res 82 (2015) 911.

[102] V. Homem, L. Santos, J Environ Manage 92 (2011) 2304-2347.

[103] Y. Wang, H. Zhang, J. Zhang, C. Lu, Q. Huang, J. Wu, F. Liu, J. Hazard. Mater. 192 (2011) 35-43.

[104] X. Ren, C. Chen, M. Nagatsu, X. Wang, Chem. Eng. J. 170 (2011) 395-410.

[105] W. Ling, Z. Qiang, Y. Shi, T. Zhang, B. Dong, J. Mol. Catal. A: Chem. 342-343 (2011) 23-29.

[106] M. Sanchez-Polo, J. Rivera-Utrilla, U. von Gunten, Water Res 40 (2006) 3375-3384.

[107] Y. Wang, H. Sun, X. Duan, H.M. Ang, M.O. Tadé, S. Wang, Applied Catalysis B: Environmental 172-173 (2015) 73-81.

[108] P. Krawczyk, Chem. Eng. J. 172 (2011) 1096-1102.

[109] A.G.G. M. F. R. Pereira*, J. J.M. Órfão, Bol. Grupo Español Carbón (2014) 18-24.

[110] J.N. Liu, Z. Chen, Q.Y. Wu, A. Li, H.Y. Hu, C. Yang, Sci. Rep. 6 (2016) 31405.

APPENDIX

APPENDIX A

SYNTHESIS OF M-CNPs

A.1 Temperature profile along the axial direction of quartz tube reactor

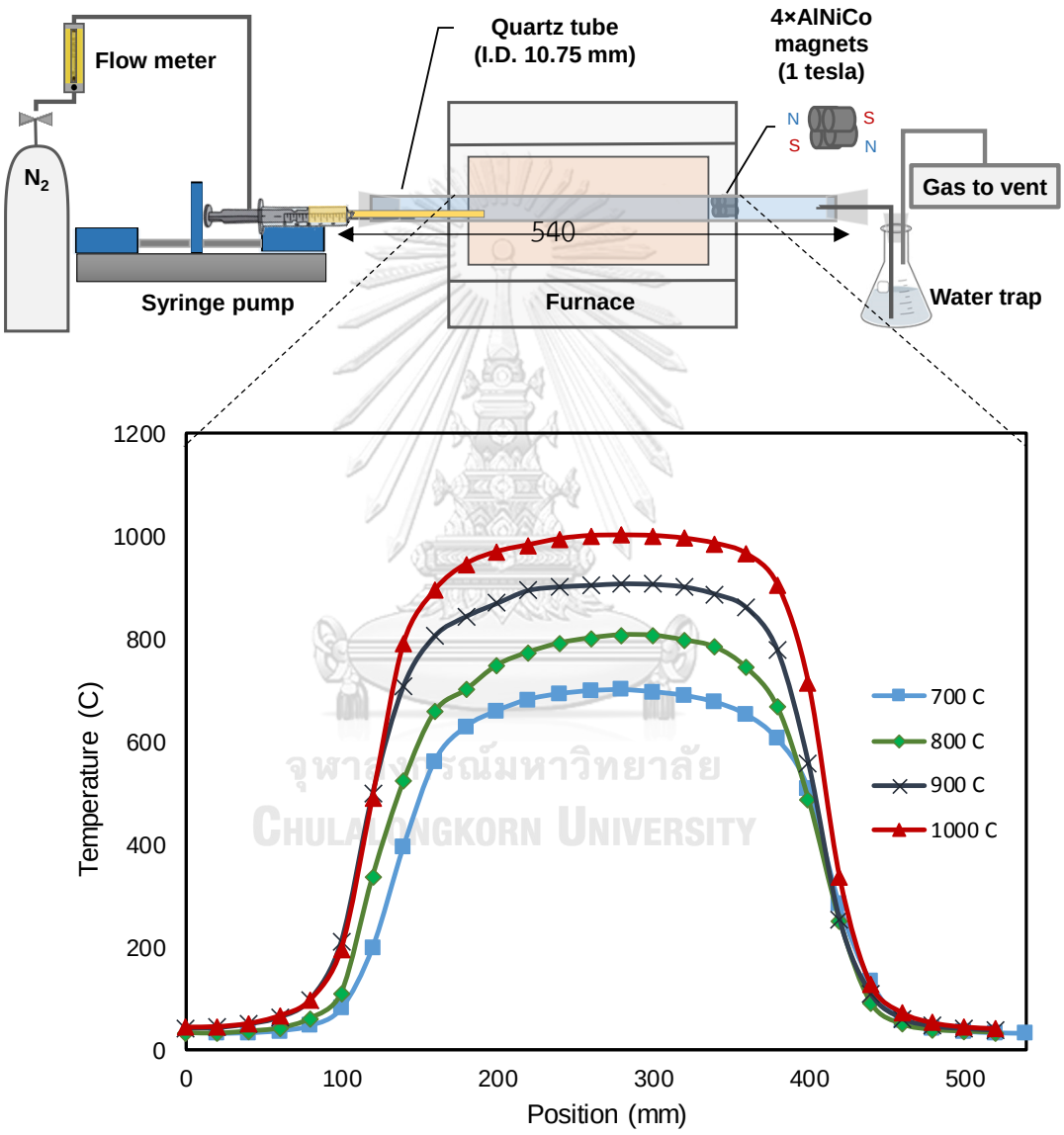

Figure A.1 Temperature profile along the axial direction of quartz tube reactor

A.2 AC magnetic susceptibility of synthesized MCNPs

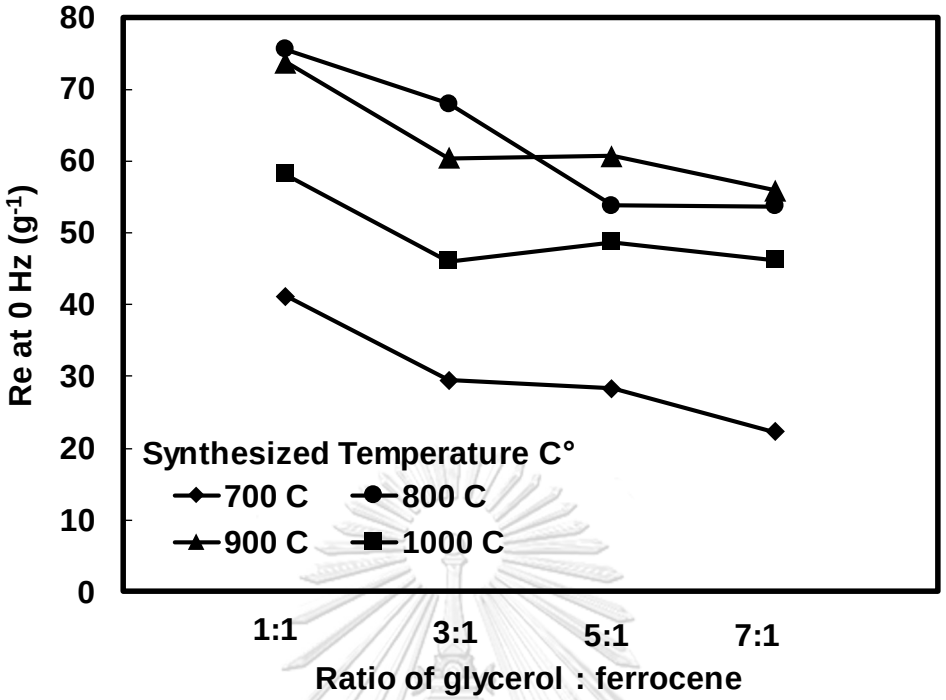

Figure A.2 AC magnetic susceptibility of synthesized M-CNPs which was synthesized with glycerol to ferrocene weight ratio, 1:1, 3:1, 5;1 and 7:1 at 700 -800 °C

A.3 Raman spectroscopic analyses of M-CNPs

Table A.3 I_G to I_D of M-CNPs which was synthesized with glycerol to ferrocene weight ratio, 1:1, 3:1, 5;1 and 7:1 at 700, 900, 800 and 1000 ^{o}C

Glycerol: ferrocene / Synthesized temperature	1:1	3:1	5:1	7:1
700 °C	0.983	0.992	0.985	0.988
800 °C	1.035	1.089	1.065	1.035
900 °C	1.038	1.024	1.028	1.026
1000 °C	1.028	1.005	1.017	0.996

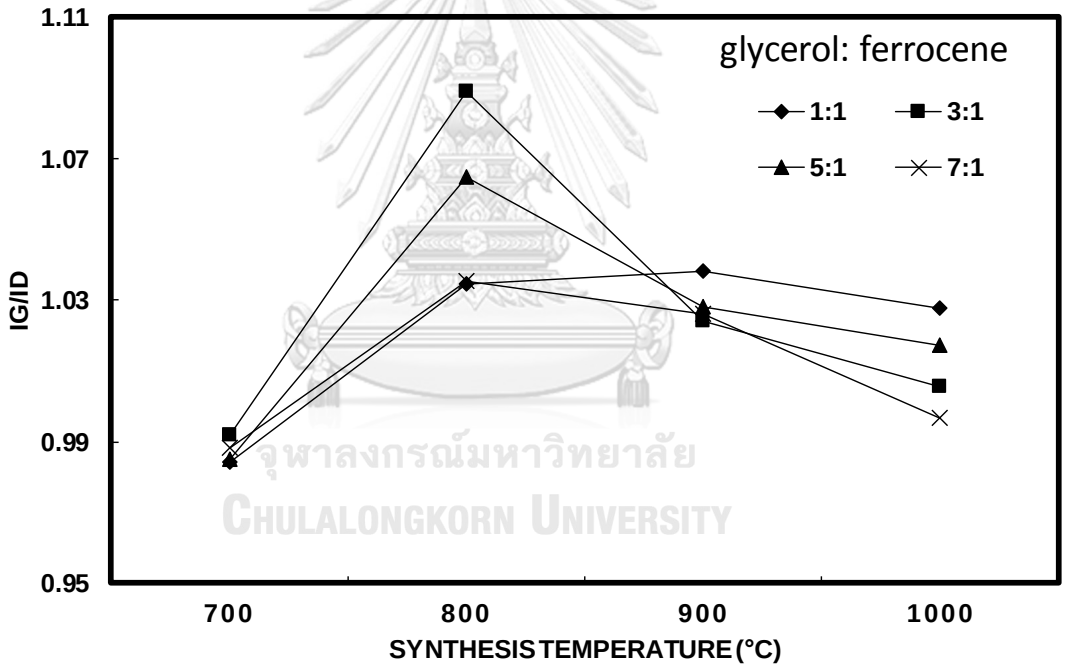

Figure A.3 Raman spectroscopic analyses of M-CNPs which was synthesized with glycerol to ferrocene weight ratio, 1:1, 3:1, 5;1 and 7:1 at 700 -1000 ^{o}C

APPENDIX B

REMOVAL OF OTC

B.1 Standard calibration curve of OTC

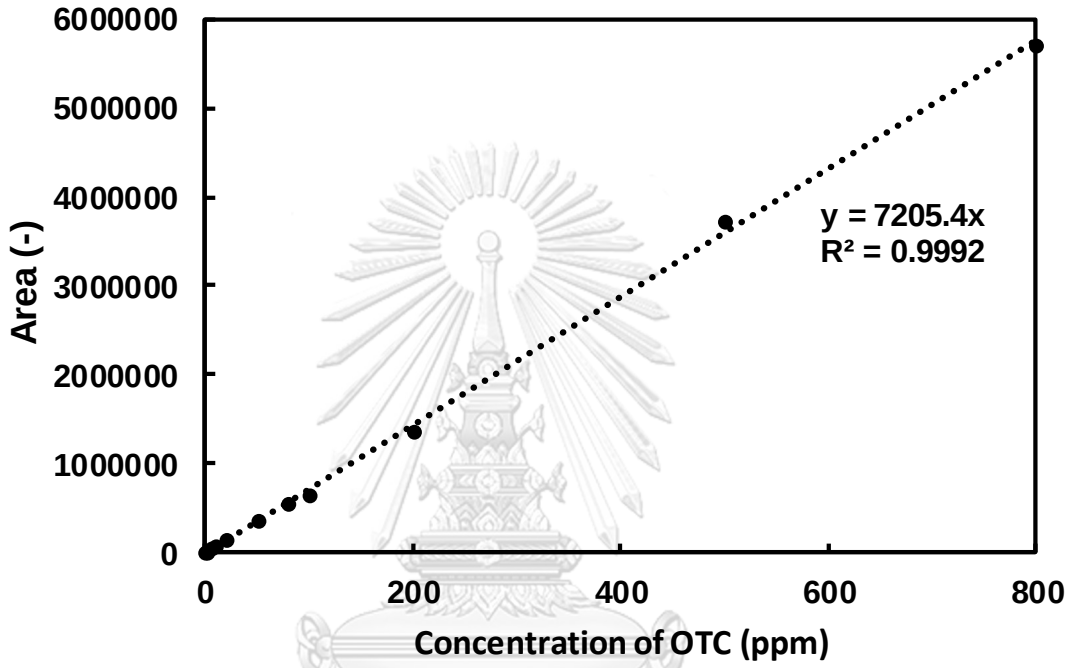

Figure B.1 Calibration curve of OTC

B.2 Influence of ozone concentration on OTC removal

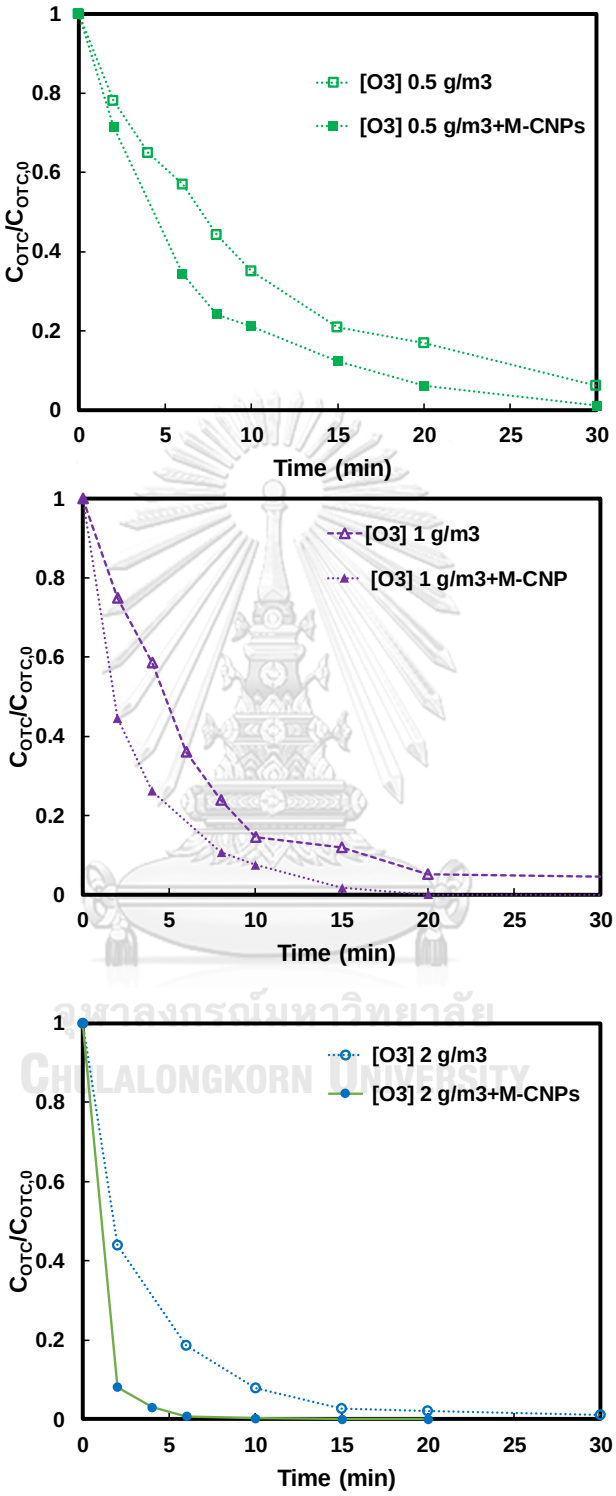

Figure B.2 Influence of ozone concentration (0.5 -2 g/m^3) on OTC removal with M-CNPs and without M-CNPs

B.3 Influence of M-CNPs loading on OTC removal

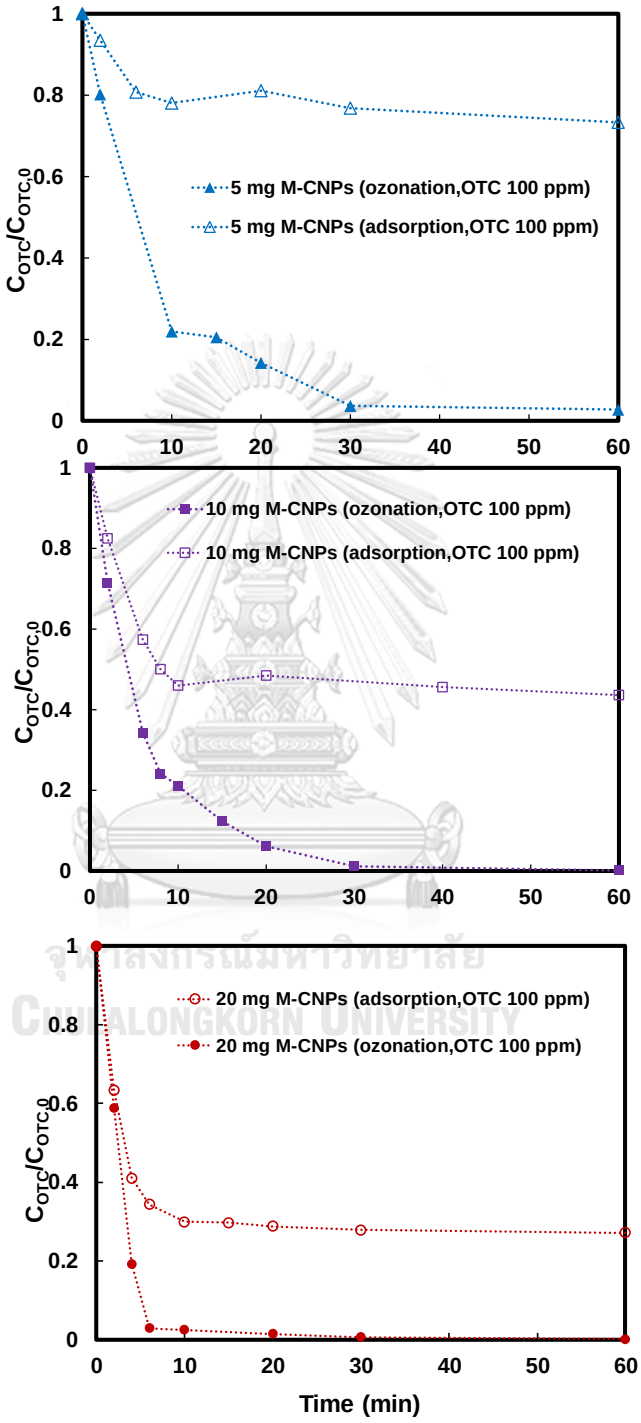

Figure B.3 Influence of M-CNPs loading (5-20 mg) on 100 ppm of OTC adsorption and ozonation

B.4 Influence of initial OTC concentration on OTC removal

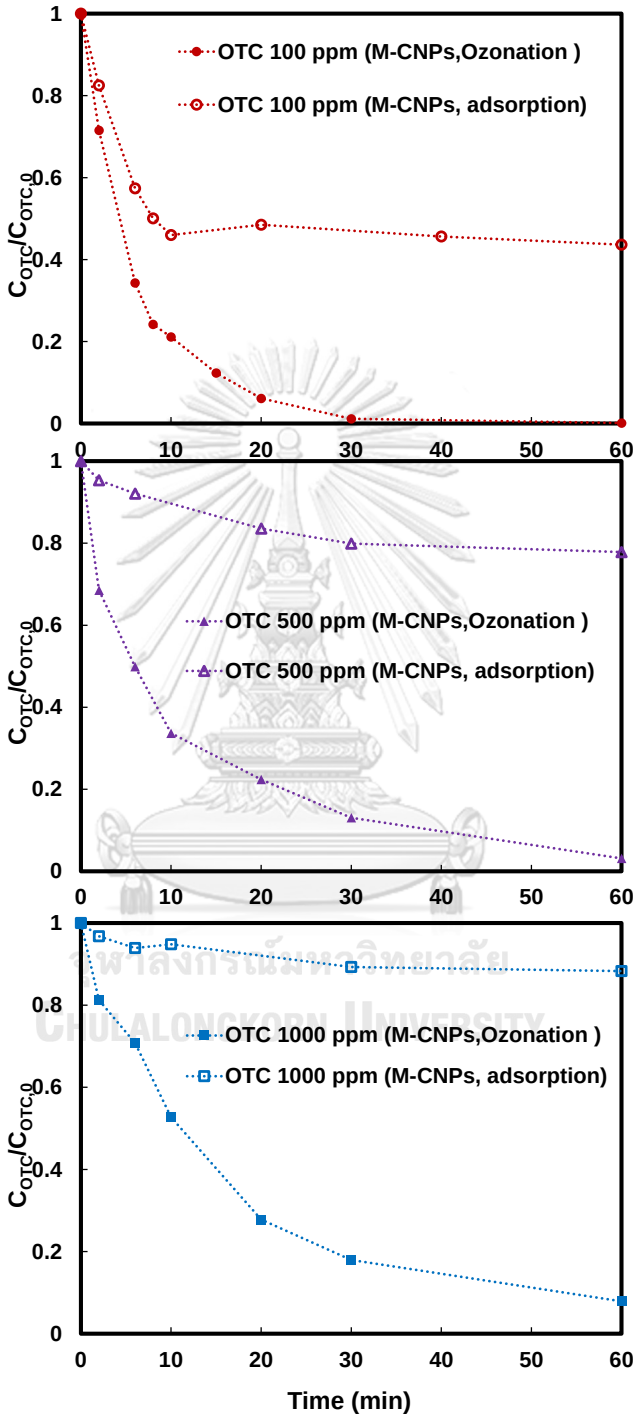

Figure B.4 Influence of initial OTC concentration (100, 500 and 1000 ppm) on OTC adsorption and ozonation

B.5 Influence of catalysts on OTC removal at 100 ppm of OTC

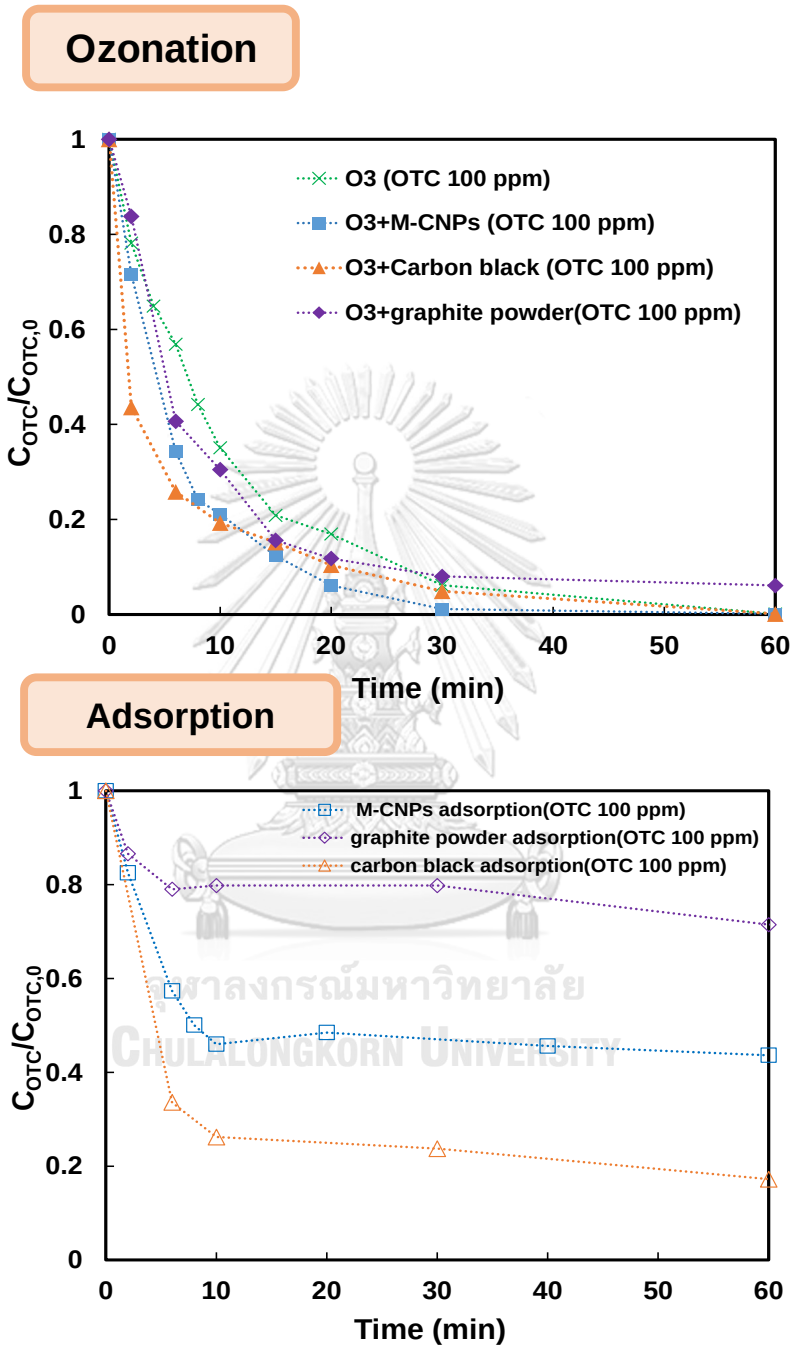

Figure B.5 Influence of catalysts (M-CNPs, carbon black and graphite powder) on OTC removal at 100 ppm of OTC on OTC adsorption and ozonation

B.6 Influence of catalysts on OTC removal at 500 ppm of OTC

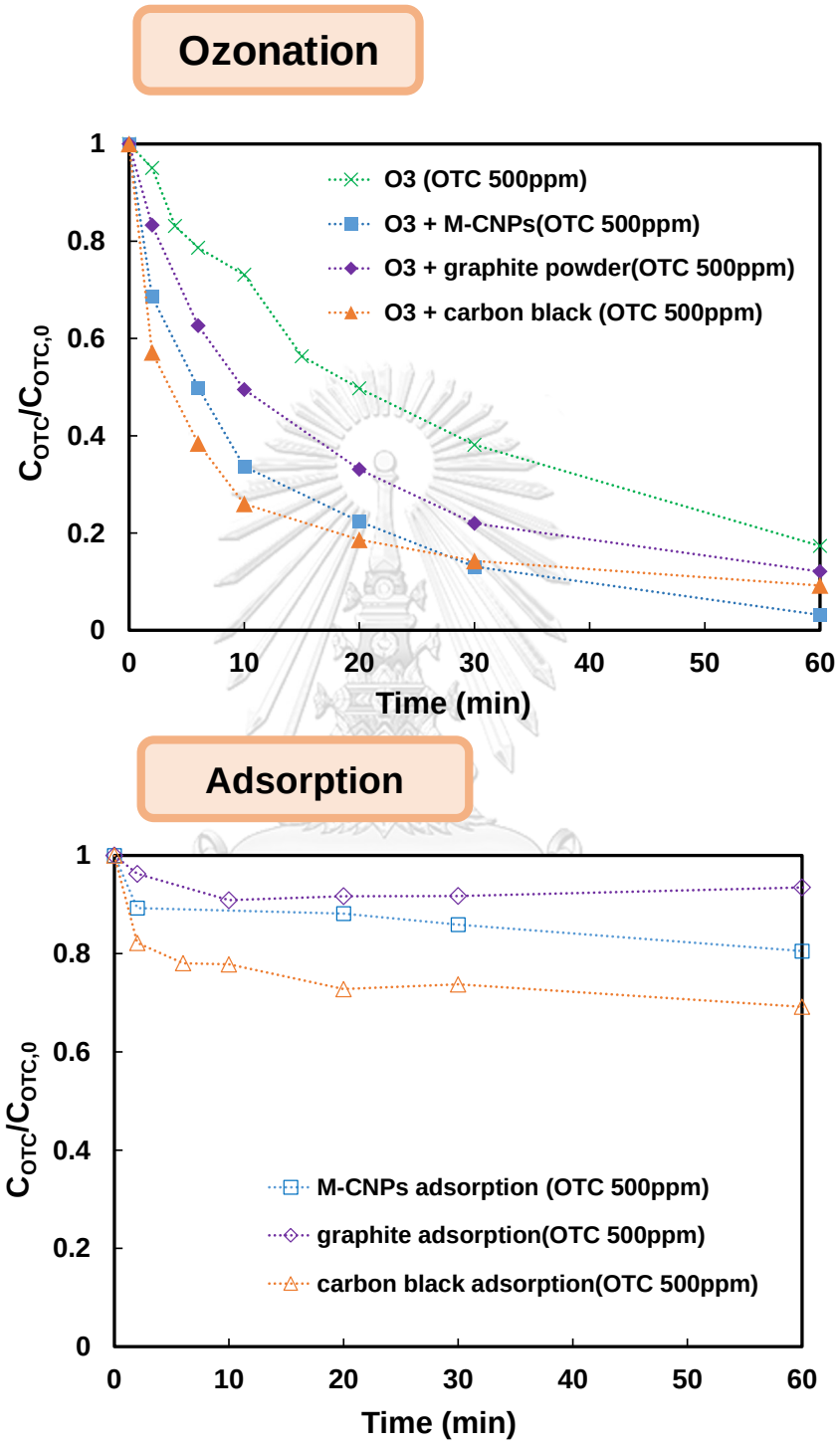

Figure B.6 Influence of catalysts (M-CNPs, carbon black and graphite powder) on OTC removal at 500 ppm of OTC on OTC adsorption and ozonation

B.7 Influence of catalysts on OTC removal at 1000 ppm of OTC

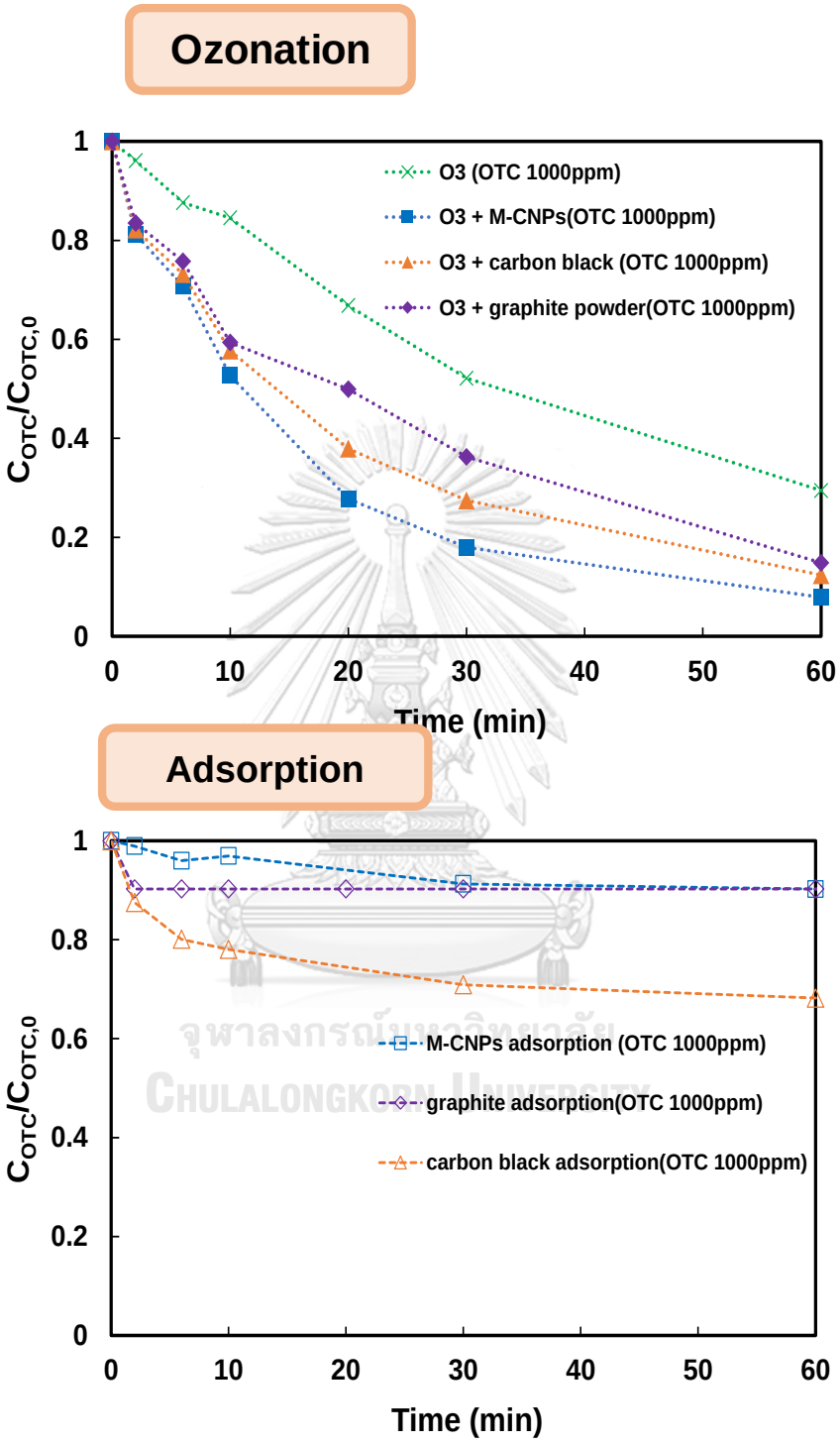

Figure B.7 Influence of catalysts (M-CNPs, carbon black and graphite powder) on OTC removal at 1000 ppm of OTC on OTC adsorption and ozonation

B.8 Comparison of removal efficiency via ozonation of synthesized M-CNPs to those of commercial carbon nanotubes

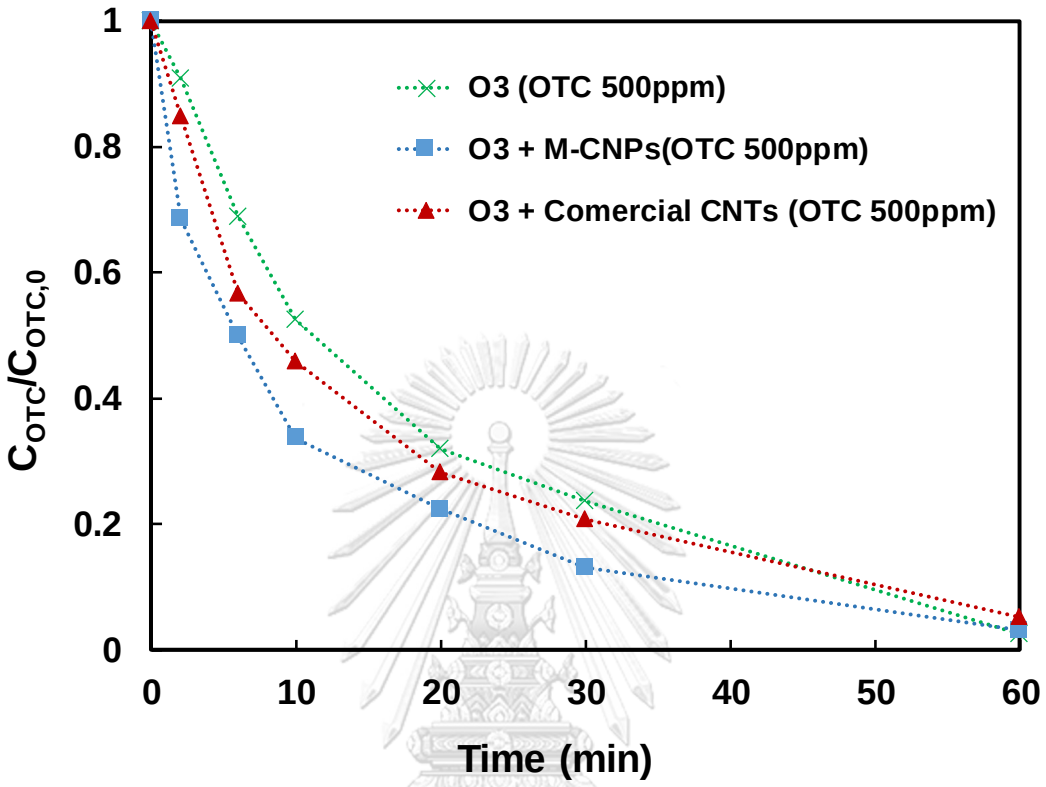

Figure B.8 Comparison of removal efficiency via ozonation of synthesized M-CNPs to those of commercial carbon nanotubes

APPENDIX C
PUBLICATIONS

C.1 International journal

1. Konrat Kerdnawee , Chompoopitch Termvidchakorn , Pacharaporn Yaisanga ,Jirapat Pakchamsai , Cheewapon Chookiat , Apiluck Eiad-ua, Winadda Wongwiriyapan, Weerawut Chaiwat, Sakhon Ratchahat, Kajornsak Faungnawakij, Komkrit Suttiponparnit and Tawatchai Charinpanitkul. “Present advancement in production of carbon nanotubes and their derivatives from industrial waste with promising applications”. KONA Powder and Particle Journal. 2016.

2. Konrat Kerdnawee, Purichaya Kuptajit, Noriaki Sano, Hajime Tamon, Weerawut Chaiwat and Tawatchai Charinpanitkul. “Catalytic ozonation of oxy-tetracycline using magnetic carbon nanoparticles”. Journal of the Japan institute of Energy. 96, p.362-366. 2017.

3. Konrat Kerdnawee, Noriaki Sano, Hajime Tamon, and Tawatchai Charinpanitkul. “Controlled synthesis of magnetic carbon nanoparticles via glycerol/ferrocene co-pyrolysis with magnetic induction”. Particuology. Accepted 8 September 2017.

C.2 International conference

1. Konrat Kerdnawee, Pacharaporn Yaisanga, Thantorn Vanavanichkul, Jirarat Kaewngam, Jirapat Pakchamsai, Cheewapon Chookiat,Thipok Klinpakdee, Weerawut Chaiwat and Tawatchai Charinpanitkul. “Synthesis of magnetic carbon nanotube from glycerol using co-pyrolysis with ferrocene for antibiotic adsorption”, The 3rd Joint Conference in Renewable Energy and Nanotechnology (JCREN 2014), December 22-23, 2014, Kanchanaburi, Thailand

2. Konrat Kerdnawee, Thipok Klinpakdee, Weerawut Chaiwat, Noriaki Sano, Tawatchai Charinpanitkul, “Adsorption of tetracycline using magnetic carbon nanoparticles synthesized by nebulizing pyrolysis of glycerol and ferrocene”, The 4th Joint Conference on Renewable Energy and Nanotechnology (JCREN 2014), December 5-7, 2015, Matsuyama, Japan

3. Konrat Kerdnawee, Noriaki Sano, Hajime Tamon, Weerawut Chaiwat, Tawatchai Charinpanitkul, “Catalytic ozonation of oxy-tetracycline using magnetic carbon nanoparticles”, The 5th Joint Conference in Renewable Energy and Nanotechnology (JCREN 2016), December 8-9, 2016, Kuala Lumpur, Malaysia

4. Konrat Kerdnawee, Noriaki Sano, Hajime Tamon, Tawatchai Charinpanitkul, “Oxy-tetracycline Removal via Ozonation Enhanced with Synthesized Magnetic Carbon Nanoparticles, Carbon 2017, July 23-28, 2017, Melbourne, Australia

5. Konrat Kerdnawee, Noriaki Sano, Hajime Tamon, Tawatchai Charinpanitkul, “Adsorption of oxy-tetracycline antibiotic on magnetic carbon nanoparticles”, The 6th Joint Conference in Renewable Energy and Nanotechnology (JCREN 2017), October 12-14, 2017, Bangkok, Thailand

VITA

Miss Konrat Kerdnawee was born on August 16th, 1989 in Ayutthaya, Thailand. She graduated primary education from Wat Jaojetnok school and secondary education from Sena "Senaprasit" school. She obtained her Bachelor in Chemical Engineering from King Mongkut's University of Technology Thonburi (KMUTT) with second class honors in 2012. She continuously conducted her Ph.D. in Center of Excellence in Particle Technology (CEPT), Department of Chemical Engineering, Faculty of Engineering, Chulalongkorn University. During her Ph.D. study, she got opportunity for research aboard for one year at Kyoto university, Kyoto, Japan. She received financial support from Chulalongkorn University Dutsadi Phiphat Scholarship throughout her doctoral period.